SEPARATING DOLOMITE FROM PHOSPHATE ROCK BY REACTIVE FLOTATION: FUNDAMENTALS AND APPLICATION

By

AYMAN A. EL-MIDANY

A DISSERTATION PRESENTED TO THE GRADUATE SCHOOL
OF THE UNIVERSITY OF FLORIDA IN PARTIAL FULFILLMENT
OF THE REQUIREMENTS FOR THE DEGREE OF
DOCTOR OF PHILOSOPHY

UNIVERSITY OF FLORIDA

2004

To all who made this work possible, and
To all who had parts in shaping the person that I am today.

ACKNOWLEDGMENTS

In the Name of Allah, the Most Gracious, the Most Merciful.
"Oh Allah! Make useful for me what you have taught me, and teach me knowledge that will be useful to me. I entrust you with what I have read and studied. Oh Allah! Bring it back to me when I am in need of it. You are my protector, and the best of aid.". I thank Allah for blessing me with all of the good that I have, and I ask that I will be able to use such gifts to help those in need. Amen.

I have fortunate to be able to study in an excellent institution surrounded by a group of extremely intelligent people. I would like to recognize the amazing staff in Department of Materials Science and Engineering at University of Florida. I would also like to thank everyone who helped me arrive at this point. Special thanks and recognition go to my advisor, Dr. Hassan El-Shall. He gave me the opportunity to do research in his group. His drive and commitment to research have inspired and motivated me through this work. He has been a constant source of ideas and encouragement over the years. Many thanks go to my committee members; especially Dr. Spyros A. Svoronos, who helped me greatly and bore with me in the modeling part of my study. I would also like to thank the other members of my committee (Drs. John J. Mecholsky, Wolfgang Sigmund, and Susan Sinnott from the Department of Materials Science and Engineering, and my external committee member, Dr. Ben Koopman, Department of Environmental Engineering). I would also like to recognize the remarkable past and present members of Dr. El-Shall's research group for their assistance, advice, and support.

Finally, I cannot thank my family enough for all of their love, encouragement, and counsel. To my parents, I owe everything. They have taught me many things. Above all

they taught me that patience, determination, persistence, and faith are the keys to success. I thank my wife for her help and patience over the years.

I thank the Particle Engineering Research Center (PERC) staff for helping me to get started and for providing support and guidance along the way. Much of the experimental work in my study could not have been accomplished without their help, and for that I am extremely grateful.

This work was supported by the Florida Institute of Phosphate Research (FIPR), and the National Science Foundation / Particle Engineering Research Center (NSF/PERC).

TABLE OF CONTENTS

page

ACKNOWLEDGMENTS iv

LIST OF TABLES ix

LIST OF FIGURES xi

ABSTRACT xiv

CHAPTERS

1 LITERATURE REVIEW 1

Introduction 1
Previous Efforts to Separate Dolomite from Phosphate Rock 2
Anionic Flotation 4
Direct flotation 4
Reverse flotation 5
Cationic Flotation 8
Nonconditioning Flotation 9
Two-Stage Conditioning Process 11
The CLDRI Process 12
Acid Leaching 14
Physical Separation Methods 14
Heavy Media Separation 14
Sizing, Attrition Scrubbing, and Desliming 15
Problem Statement 15
Novelty and Scope of Study 15
Goal of Study 16

2 MATERIALS AND METHODS 17

Flotation Study 18
Screening Design (Plackett-Burman Design) 18
Central Composite Design 18
Flotation Procedures for Screening and CCD Designs 21
Factorial Design for Conditioning with PVA before Flotation 21
Flotation Procedure for Conditioning Statistical Designs 21
Density and Surface Area Determination 22

PVA Preparation....23
Spectrophotometric Determination of PVA....23
Static (Equilibrium surface tension)....24
Dynamic Surface Tension (DST)....24
Maximum bubble pressure method....24
Dynamic surface tension setup....26
Contact Angle....26
Measurement of Contact Angle....27
Surface Characterization by FTIR....28
Zeta Potential Measurements....28
Adsorption....28
Dissolution Kinetic Experiments....29
Pilot Scale Experiments....30
The Sluice....30
Sluice Experiments....30

3 TECHNICAL ASPECTS OF REACTIVE FLOTATION: PRELIMINARY TESTS32

Introduction....32
List of Potential Surfactants: Surfactants Screening....33
Initial Screening Tests....33
Specific Tests....34
Acid type....34
Acid dosage....35
Surfactant type....36
Surfactant dosage....37
Particle size....38
Oil-Surfactant Experiments....39
Poly-Vinyl-Alcohol (PVA) Testing....41
Effect of acid concentration....41
Effect of particle size....43
PVA with acid vs. PVA on the particle surface....44
Preliminary Testing Using PVA Coated Particles....45
Flotation of a Representative Sample....45
Fraction of Representative Sample (-4+1.19 mm)....46
Effect of Time on Weight Percentage of Floated Particles....46
Effect of Size on the Flotation....47
Summarizing Remarks....48

4 OPTIMIZATION OF THE REACTIVE FLOTATION PROCESS AND PILOT SCALE TESTING....49

Introduction....49
Optimization of the RF Process....49
Screening Statistical Design....49
Central Composite Design....52

Research to Reduce the PVA Consumption 52
Experimental Design of the PVA Conditioning Step 56
Saturation Experiment 56
Pilot Scale Testing: Sluice Results 57

5 FUNDAMENTAL STUDIES 58

Polyvinyl alcohol-Particle Interaction 58
Introduction 58
Surface Tension 60
Contact Angle 63
Work of Adhesion 64
Zeta Potential 67
Zeta potential of minerals in supernatant solutions 70
Zeta potential in the presence of PVA 71
Infrared (FTIR) 72
Adsorption Study 75
Kinetics of adsorption 76
Adsorption isotherm 79
Calculation of PVA adsorption and parking area 82
Adsorbed layer thickness 84
Effects of pH 84
Adsorption in supernatants 87
Desorption 88
Desorption in Acidic Solution 89
Bubble Formation and Stability 90
Effect of Particle Size 91
Effect of PVA Coating 94
Modeling of Bubble Formation and Dolomite-Particle Separation 96
Blockage of the Acid Model 96
Disappearance of Active Sites Model 99
Empirical Models 101
First-order kinetic model 101
Acid concentration dependence model 103
Estimation of CO_2 Required to Float the Dolomite Particle 106
Bubbles Stability 109
Validation of the Model Using a Different Carbonate Mineral 112
Summarizing Remarks 114

6 CONCLUSIONS AND RECOMMENDATIONS FOR FUTURE WORK 116

Conclusions 116
Recommendations for Future Work 119

LIST OF REFERENCES 120

BIOGRAPHICAL SKETCH 129

LIST OF TABLES

Table page

2-1. Experimental Plackett-Burman design for 11 variables 19

2-2. Rotatable central composite design with 5 levels and 3 variables 20

2-3. Factorial design for conditioning with PVA.....21

3-1. Surface-active agents used in RF tests 33

3-2. Size analysis of the dolomitic phosphate sample 34

3-3. Chemical analyses of the dolomitic phosphate sample 34

3-4. Effect of sulfuric acid concentration 35

3-5. Effect of sulfuric acid concentration on the bubble formation.....36

3-6. Preliminary tests of high dolomitic phosphate with different surfactants.....37

3-7. Effect of surfactant concentration ($SDSO_3$, 2 %).....38

3-8. Effect of particle size on the dolomitic particle floatability 39

3-9. Effect of presence of surfactant and oil layer on particle flotation 40

3-10.Effect of acid concentration.....42

3-11.Effect of acid concentration above 2 %.....43

3-12.Comparison between coating the particle before adding it to acidic solution and adding the particle to acid+PVA solution without coating 45

3-13.Results of representative sample (- 4+1.19 mm particle size).....46

3-14.Effect of time on the flotation of - 4+1.19 mm particle size 47

3-15.Effect of particle size on flotation 47

4-1. The MgO % removal in floated fraction for Plackett-Burman design. 50

4-2. Plackett-Burman calculated t values for different variables.....51
4-3. Effect of saturated acid on the RF 57
4-4. Comparison of two different coating methods and their effects on MgO removal ..57
5-1. Chemical analysis of the samples used in adsorption tests 66
5-2. Fitting parameters of second-order kinetic model.....77
5-3. Chemical analysis of the samples used in kinetic tests 91
5-4. Acid-blockage model parameters 97
5-5. Active sites disappearance parameters 100
5-6. Reaction rate constants of first-order model.....103
5-7. Acid concentration dependence parameters 105
5-8. Active sites disappearance parameters for dissolution of calcite 113

LIST OF FIGURES

Figure page

1-1. Simplified flowsheet for phosphoric acid production 3

1-2. Simplified flowsheet of USBM direct flotation 6

1-3. Flowsheet of TVA's diphosphonic depressant process 8

1-4. Flowsheet for IMCF cationic flotation 9

1-5. University of Alabama pebble processing, simplified flowsheet 10

1-6. Flowsheet for University of Florida two conditioning stages 11

1-7. Simplified flowsheet for CLDRI dolomite flotation 13

2-1. Strategic plan to achieve research goals 17

2-2. Five-level, rotatable central composite design.. 20

2-3. Characteristic bubble-pressure vs. time curve in MBP. 25

2-4. Setup for the measurement of dynamic surface tension by MBP.....26

2-5. Contact angle and its relation with surface tension 27

2-6. Contact angle measuring apparatus 28

2-7. Schematic diagram for separation of dolomite from phosphate in sluice 30

3-1. Effect of acid concentration on bubble formation and flotation time.....36

3-2. Effect of the particle size on the time needed to float the particle 44

4-1. Effect of PVA dosage and acid conc. on MgO recovery % 53

4-2. Effect of PVA dosage and acid concentration on MgO % 54

4-3. Cube graph for MgO % and MgO recovery %.....56

5-1. Contact angle and interfacial surface tension at solid/liquid/gas interface 60

5-2. Structural formula for PVA. 61
5-3. Equilibrium Surface tension for aqueous PVA solutions at 23 °C....61
5-4. PVA crystal structure; the dotted lines indicate hydrogen bonds....62
5-5. Static contact angle variation with the PVA concentration....64
5-6. Work of adhesion as a function of PVA concentration....65
5-7. Cumulative pore size distribution for apatite sample....66
5-8. Cumulative pore size distribution for dolomite sample....67
5-9. Zeta potential of dolomite and apatite samples....68
5-10. Zeta potential of dolomite in absence and presence of polymer....68
5-11. Zeta potential of dolomite in absence and presence of polymer....69
5-12. Effect of polymer on the shear plane position....69
5-13. Zeta potential of apatite and apatite in dolomite supernatant....70
5-14. Zeta potential of dolomite and dolomite in apatite supernatant....71
5-15. Zeta potential of dolomite in apatite supernatant before/after PVA adsorption....72
5-16. Zeta potential of apatite in dolomite supernatant before/after PVA adsorption....72
5-17. Infrared transmittance spectra of poly vinyl alcohol (PVA)....73
5-18. Infrared absorbance spectra of dolomite and dolomite/PVA system. 74
5-19. Infrared absorbance spectra of apatite and apatite/PVA system. 75
5-20. Calibration curve for PVA concentration measurements....76
5-21. Kinetics of PVA adsorption on dolomite and Apatite....78
5-22. Adsorption isotherm of PVA on dolomite at 23°C 81
5-23. Adsorption isotherm of PVA on apatite at 23°C....82
5-24. Polymer-conformation changes with increase the concentration. 83
5-25. Effect of pH on adsorption of PVA on apatite and dolomite 85
5-26. Adsorption isotherm of apatite in dolomite supernatant solution, and dolomite in apatite supernatant solution....87

5-27. Desorption of PVA from apatite surface 88
5-28. Desorption of PVA from dolomite surface.....89
5-29. The bubble formation mechanism 90
5-30. Schematic diagram of reaction kinetics of the RF.....91
5-31. Dissolution kinetic of different particle sizes in terms of calcium ions 92
5-32. Dissolution kinetic of different particle sizes in terms of magnesium ions.....93
5-33. Dolomite particle (1-2 mm) before and after the reaction with 3 % H_2SO_4.....93
5-34. Dissolution kinetics of coated and uncoated 0.2-0.3 mm dolomite particle 94
5-35. Growth of the bubbles with time on the dolomite particle surface, 50 X.....95
5-37. Acid blockage model fitting to 0.25-0.35 mm experimental data 98
5-38. Active sites disappearance model fitting to 1-2 mm data.....100
5-39. Active sites disappearance model fitting to 0.25-0.35 mm data.....100
5-40. First-order model fitting for data of 0.25-0.35 mm particle size.....102
5-41. First-order model fitting for data of 1-2 mm particle size.....102
5-42. Model fitting for data of 0.25-0.35 mm particle size.....104
5-43. Model fitting for data of 1-2 mm particle size.....105
5-44. Sequence of calculating the particle density and membrane elasticity 108
5-45. Density changes for different particle sizes.....109
5-46. Dynamic surface tension of PVA concentration at different CO_2 flowrate 111
5-47. Elasticity of PVA membrane vs. PVA concentration 112
5-48. Calcite dissolution: model vs. experimental data 0.25-0.35 mm particle size 113
5-49. Calcite dissolution: model vs. experimental data for 1-2 mm particle size.....113

Abstract of Dissertation Presented to the Graduate School
of the University of Florida in Partial Fulfillment of the
Requirements for the Degree of Doctor of Philosophy

SEPARATING DOLOMITE FROM PHOSPHATE ROCK
BY REACTIVE FLOTATION: FUNDAMENTALS AND APPLICATION

By

Ayman A. El-Midany

December 2004

Chair: Hassan El-Shall
Major Department: Materials Science and Engineering

Florida is currently one of the largest phosphate producers in the world. Unfortunately, the phosphate industry in Florida is suffering from depletion of the phosphate-rich ore. Dolomite, however, is a major impurity in the ores. The presence of MgO, in dolomite, can cause several problems during production of phosphoric acid and final fertilizers. Efforts to solve the dolomite problem have been reported by several researchers throughout the world. Yet, only heavy media separation process has been applied commercially. However, the process was discontinued because of its low separation efficiency in terms of grade and recovery.

In this study, we tested an innovative idea based on simple fact that dolomite, as a carbonate mineral, generates CO_2 when exposed to a slightly acidic solution, capturing CO_2 bubbles at dolomite particle surface can selectively float the dolomite and separate it from phosphate. Formation of such bubbles requires a surface-active agent(s) at

solution/dolomite interface. Preliminary tests indicated that polyvinyl alcohol (PVA) could serve this function. This process is called the Reactive Flotation, RF.

To develop this process and to scale it up for industrial use, we conducted fundamental and applied research studies. Among these studies were optimizing of RF process by investigating the factors affecting the process (including bench and pilot scale tests) using statistical experimental designs. It was found that the acid concentration, PVA concentration, and particle size are the main factors. The optimum conditions were determined and applied to usage in a gravity separation device, (i.e., a sluice). Using such a device, a concentrate contains 0.65 % MgO with > 94 MgO % removal can be achieved. In addition, fundamental studies revealed that the hydrogen bonding is the adsorption mechanism confirmed by adsorption isotherm of PVA on dolomite and phosphate, adhesion of PVA to dolomite surface (using contact angle and surface tension), Fourier Transform InfraRed (FTIR), and Zeta potential. Moreover, PVA film thickness and polymer film elasticity (using dynamic surface tension) revealed that the optimum conditions could keep the PVA film at its highest elasticity. On the other hand, modeling was developed and used to predict CO_2 formation rate and subsequent particle density change.

CHAPTER 1
LITERATURE REVIEW

Introduction

Traditionally, the Florida phosphate industry has effectively responded to the competitive pressures of the market place by implementing technological improvements to mining and beneficiation methods. With further expansion of fertilizer production capacity worldwide and depletion of Florida's high-grade deposits, competitive pressures are expected to continue. To remain the world leader, Florida must continue to seek environmentally sound technological improvements in all areas of phosphatic fertilizer production.

Gu et al. [1999] estimated that the Bone Valley phosphate reserve in Central Florida (which can be cost effectively processed with available technology) may only last about 20 years at the current mining rate. In the near future, with the depletion of the low-dolomite, easy-to-process Bone Valley siliceous phosphate deposits, phosphate mining will move farther south and southeast. The phosphate matrix in the southern extension is leaner in grade and high in dolomite. Dolomite is the most troublesome, causing higher consumption of sulfuric acid, reducing filtration capacity, and lowering P_2O_5 recovery in fertilizer manufacturing. Therefore, the MgO content of dolomite is an important index in evaluating the quality of phosphate concentrate. In Florida, the MgO content in final concentrate is usually required to be less than 1 %.

Geological and mineralogical data show that about 50 % of the phosphate resource would be wasted if the high dolomitic zones were bypassed in mining, and about 13 % of

the resource would be lost if the dolomite pebbles were discarded. Although heavy media separation (HMS) technology was tried commercially, to process a portion of dolomite pebbles in Florida, in most cases the high-dolomite phosphate has been bypassed during mining operations because no technology is available to process high-dolomite pebbles economically. Technically and economically feasible beneficiation technology for processing dolomite pebbles is needed to recover phosphate value, extend Florida phosphate reserves, and prolong the life of Florida phosphate industry [Geo et al., 2002].

Previous Efforts to Separate Dolomite from Phosphate Rock

Phosphate rock is one of the basic materials for fertilizers. About 90 % of the phosphate rock output in the world is used for fertilizer production. The United States is one of the world's largest producers of phosphate rock and fertilizer. Its phosphate production represents approximately one-third of the world's total [Becker, 1989].

Phosphoric acid is an important intermediate product for production of fertilizers. Current phosphoric acid technology essentially comprises sulfuric acid attack, and separation of the phosphoric acid from the calcium sulfate crystals resulting from the reaction. Both the attack and separation, which are effected by filtration, are considerably influenced by the nature of the ore and its impurities [Becker, 1989]. Figure 1-1 shows the main processes in phosphoric acid production.

As mentioned, the main impurity in Florida phosphate ore is dolomite. Dolomite, $(Ca, Mg)CO_3$, is the main source for calcium and magnesium. As impurities, CaO and MgO affect the phosphoric acid production by increasing sulfuric acid consumption, in addition to the MgO stays with the acid phase, and greatly increases viscosity.

$$Ca_{10}(PO_4)_6F_2 + 10\ H_2SO_4 + 20\ H_2O \rightarrow\ 6\ H_3PO_4 + 10\ CaSO_4.2H_2O + 2\ HF$$

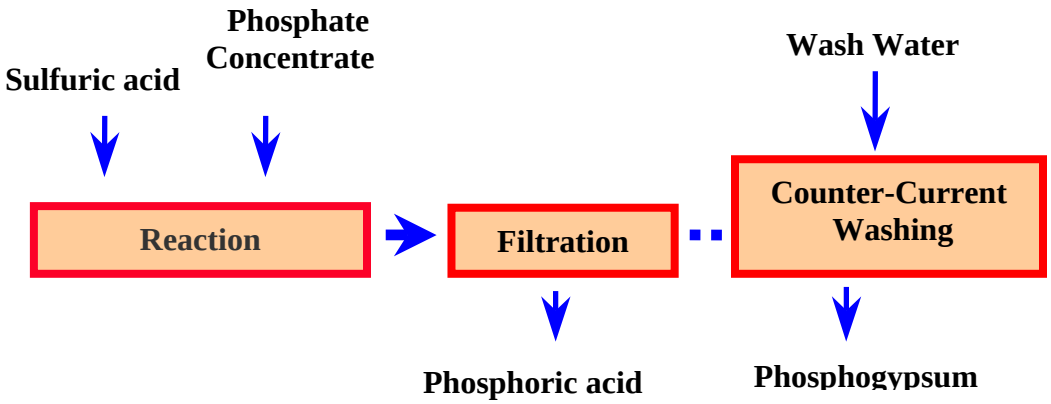

Figure 1-1. Simplified flowsheet for phosphoric acid production

Therefore, because dolomite is the most common impurity, developing an efficient and economical method for separating dolomite from apatite is an effective way to extend phosphate mine life. Generally, acidulation of phosphate rock requires a feed of less than 0.8 % MgO, which has not been achieved at a commercial scale with ores high in MgO. Dolomite is also a worldwide problem. All of the major phosphate-producing countries have faced, or are going to face, the dolomite problem.

Salt-type minerals (such as apatite, calcite, dolomite, barite, fluorite and scheelite) have been successfully separated from oxides and silicates by flotation methods. However, these minerals are often difficult to separate from each other because they contain similar alkaline earth cations that cause them to exhibit similar surface (electrical) behavior. All the zero points of charge (ZPC) of phosphates and carbonates are located in the acid pH range (i.e., 4-5.5) [Smani, 1973; Smani et al., 1975].

Systematic research in carbonate phosphate ore beneficiation started in the early 1950s [El-Shall et al., 2004]. Techniques used include the following:

- Direct flotation of phosphate, using sodium silicate to depress carbonate impurities.

- Reverse flotation of the carbonate impurities by depressing the phosphate using materials such as fluorides, fluosilicic acid, diphosphonic acid, phosphoric acid, aluminum sulfate-tartrate, and inorganic phosphate salts.

- Rapid change of conditioning parameters (such as the University of Florida two-stage conditioning process, Alabama non-conditioning process, the IMC-F process, and the low-pH conditioning process proposed by Minemet research).

- Physical methods: gravity concentration, sizing, desliming, heavy media separation.

- Calcination: although expensive because of its energy requirement, high-temperature destruction of the carbonate followed by leaching has been practiced in North Africa with low –cost energy.

- Acid leaching: carbonates are easily dissolved by acid, and weak acids can be used to dissolve the carbonate, leaving the apatite.

Anionic Flotation

Direct flotation

Sodium silicate is widely used as carbonate depressant [Fuerstenau, 1968; Ananthapadmanabhan and Somasundaran, 1985; Rao, 1988; Dho and Iwasaki, 1990]. Encouraging results were obtained in both batch and continuous pilot tests conducted by the United State Bureau of Mine, USBM, [Davis et al., 1984]. After 1 lb/t sodium silicate was added in each of three cleaning stages, a phosphate rougher was upgraded to about 30.7-31.3 % P_2O_5, 0.6-1.3 % MgO with a P_2O_5 recovery from 55.1 to 89.7. The original matrix contained 5.47-10.2 % P_2O_5, and 1.9-7.6 % MgO.

Rao [1989] studied the effects of major flotation parameters on phosphate grade and recovery using sodium silicate as a calcite depressant. Maximum flotation of apatite occurred at pH 8, and phosphate recovery decreased with increasing pH. Sodium silicate at a concentration below 0.0013 M had no depressive effect on calcite. However, at pH values above 10, calcite depression was observed even in dilute silicate solution. A concentrate with 25.6 % P_2O_5 at 80 % recovery was obtained.

Efforts to concentrate high-dolomite Florida phosphate ores by flotation, using conventional fatty-acid/fuel-oil flotation [Liewellyn, 1982], showed that sodium silicate depression on dolomite was not enough to obtain a concentrate less than 1 % MgO. This may be due to the presence of silica in this ore in addition to dolomite.

Reverse flotation

Depression of phosphate: This method was used when the apatite was more abundant than calcite and dolomite (as in most phosphate ore). Among depressants used are as follow:

Fluosilicic acid: USBM investigated the removal of carbonate from phosphate rock using fluosilicic acid as a depressing agent and tall oil-fatty acid as a collector for carbonate mineral flotation (Figure 1-2) [Rule, 1982;1985]. At collector dosage 0.7 kg/t, 0.45 kg/t depressant, a concentrate of 25.5 % P_2O_5 and 0.84 % MgO with P_2O_5 recovery 89.5 % was obtained from feed with 20.8 % P_2O_5 and 1.1 MgO %.

Abdel Khalek [2000] studied the phosphate depression using fluosilicic acid, but recovery using this process was less than 60 %. Ataly [1985] pointed out that for depressing Turkish ores fluosilicic acid was not efficient as other depressants because of the low recovery (57 %) obtained using fluosilicic acid.

Acid depressants: Orthophosphoric acid was found to decrease adsorption of the fatty acid on apatite because of the increased surfacial solubility of apatite.

Phosphoric acid also was used to depress apatite (by the USBM, in separating dolomite from a southern Florida ore) [Liewellyn, 1982]. The produced concentrate's P_2O_5 % did not exceed 28 %, and the MgO % was not less than 1.9 %.

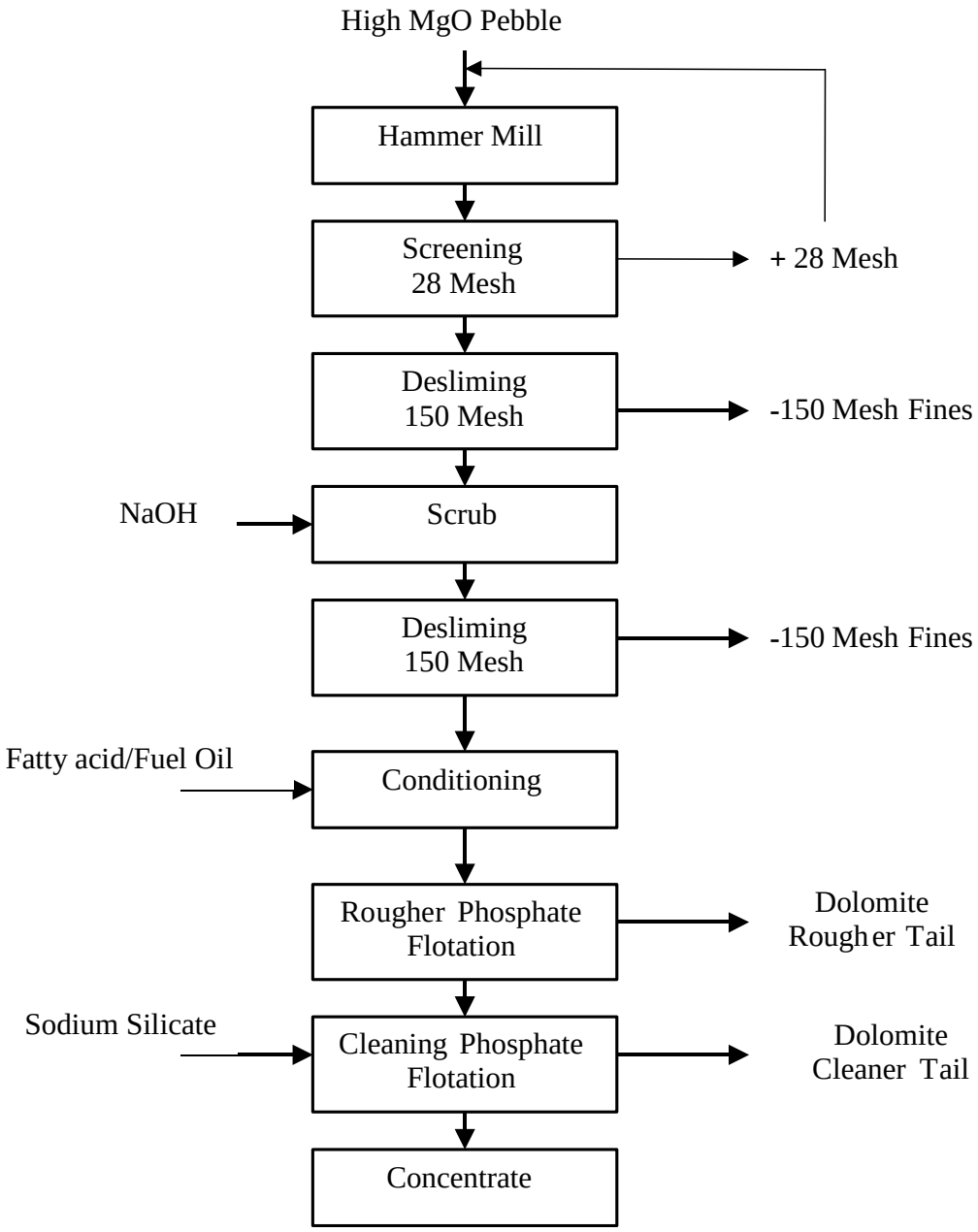

Figure 1-2. Simplified flowsheet of USBM direct flotation

Lawendy [1993] found phosphoric acid to be the best among conventional depressants of phosphate. The concentrate was 32-36 % P_2O_5, 1 % MgO at 70-75 % overall P_2O_5 recovery from feed 16-25 % P_2O_5 and 4-11 % MgO. In other study [Hsieh and Lehr, 1985], diphosphonic acid was used to depress phosphate (TVA process), (Figure 1-3), with fatty acid collectors for beneficiating an ore containing 72 % SiO_2, 1.05 % MgO and 6.3 % P_2O_5. The resulted concentrate contained 73.3 % SiO_2, 0.7 % MgO and 6.4 % P_2O_5.

Although sulfuric acid is a phosphate depressant, its ability to attack phosphate and its high need for pH control limits its usage [Elgilani and Abouzeid, 1993]. Jacob Engineering [Gruber et al., 1987] used sulfuric acid as a pH regulator to completely depress phosphate at pH 5.5.

Phosphates: Rao [1979] found that the depressing action of dipotassium hydrogen phosphate is pH dependent. Phosphate can be depressed at pH 5-8, while carbonate can be depressed only at alkaline pH; which means that selective flotation can be obtained. However, the concentrate produced by this process contained no more than 24 % P_2O_5.

Sodium chloride: The effect of sodium chloride and other salt addition on dolomite and apatite flotation has been studied [Rao, 1985]. It was shown that sodium chloride acts as apatite depressant during flotation at acidic pH values with oleic acid, while dolomite flotation is not affected. It was, however, observed that dolomite particles larger than 48-mesh are difficult to float and they tend to remain in the sink fraction. Trends observed during Hallimond cell tests of single and mixed minerals were confirmed with mixtures of minerals and a natural ore at bench-scale level. Under more

favorable conditions in the bench-scale tests, MgO content of the mineral mixtures was reduced from 5 % to 1 % or less, with at least 90 % recovery of P_2O_5 in the sink fraction.

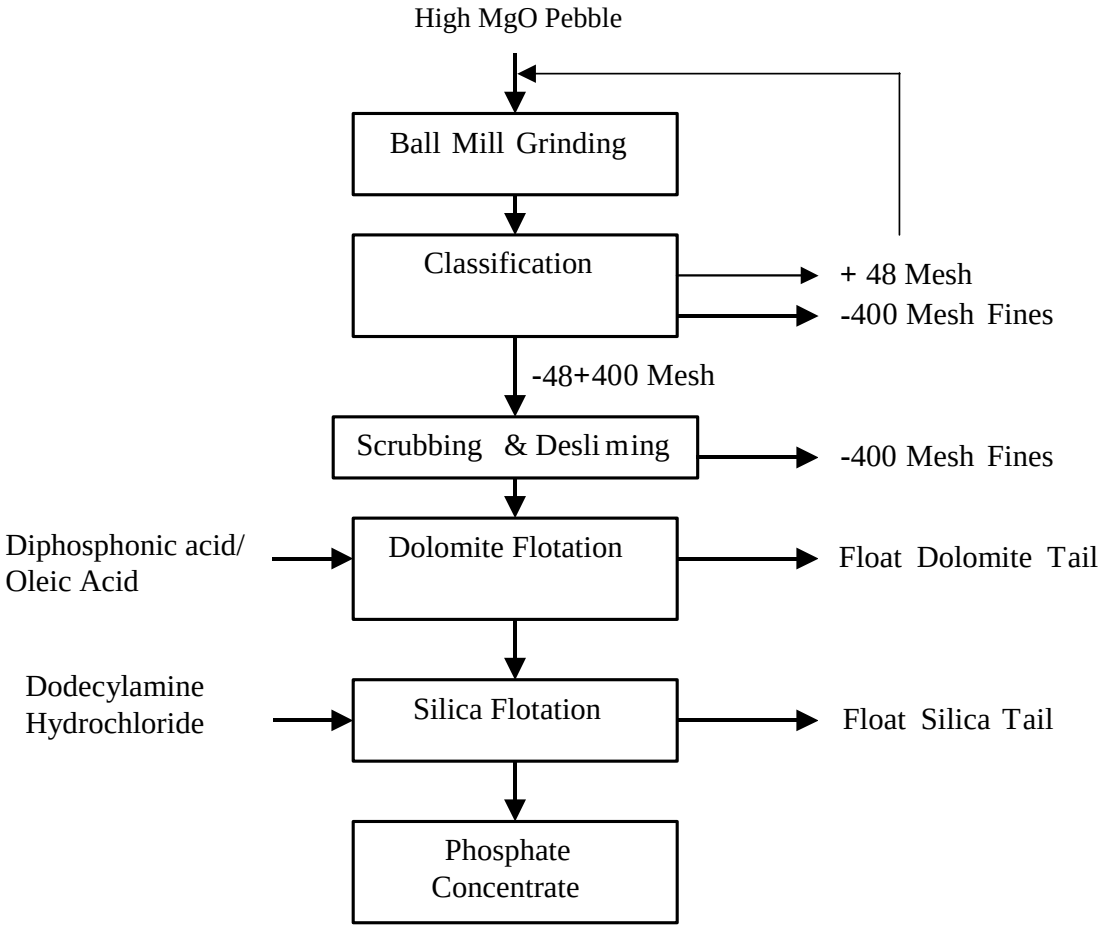

Figure 1-3. Flowsheet of TVA's diphosphonic depressant process

Alizarin Red S (ARS): ARS is an organic depressant. It is used to depress either phosphate or carbonate, depending on pH. ARS can depress calcite impurities at a pH 8-10, while apatite can be depressed at a pH below 6 [Fu and Somasundaran, 1986; Xiao and Somasundaran, 1989].

Cationic Flotation

The IMC-F process (Figure 1-4) is a cationic-flotation process for silica-free ores. The ore is reagentized with a cationic collector (amines or their salts) and the dolomite

separated from phosphate at a rougher stage followed by one or two phosphate-cleaning steps [Snow, 1979; 1982; Lawver and Snow, 1980]. By using IMC-F process, a concentrate of 31 % P_2O_5, 0.86 % MgO from feed of 2 % MgO with 83 % P_2O_5 recovery can be obtained.

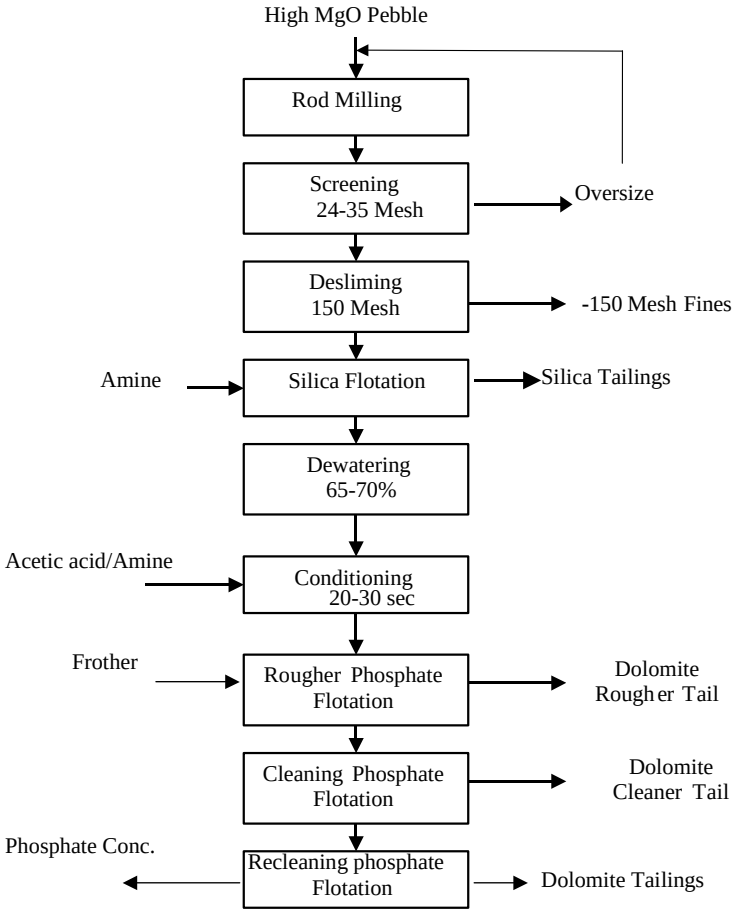

Figure 1-4. Flowsheet for IMCF cationic flotation

Nonconditioning Flotation

A research contract between FIPR and Mineral Resources Institute (MRI) at the University of Alabama aimed to develop a selective flotation process (Figure 1-5) to separate dolomitic limestone from Florida phosphate ore [Hanna and Anazia 1990]. This process depends on the difference in adsorption rate of fatty acids on both phosphate and

carbonates. Fatty acids adsorb more rapidly on carbonate surfaces than on phosphate surfaces. At slightly acidic pH (5.5-6.0), carbonates floated immediately on addition of collector and frother. After carbonate froth collection, the pulp is conditioned briefly to float phosphate thereafter with no more addition of collector.

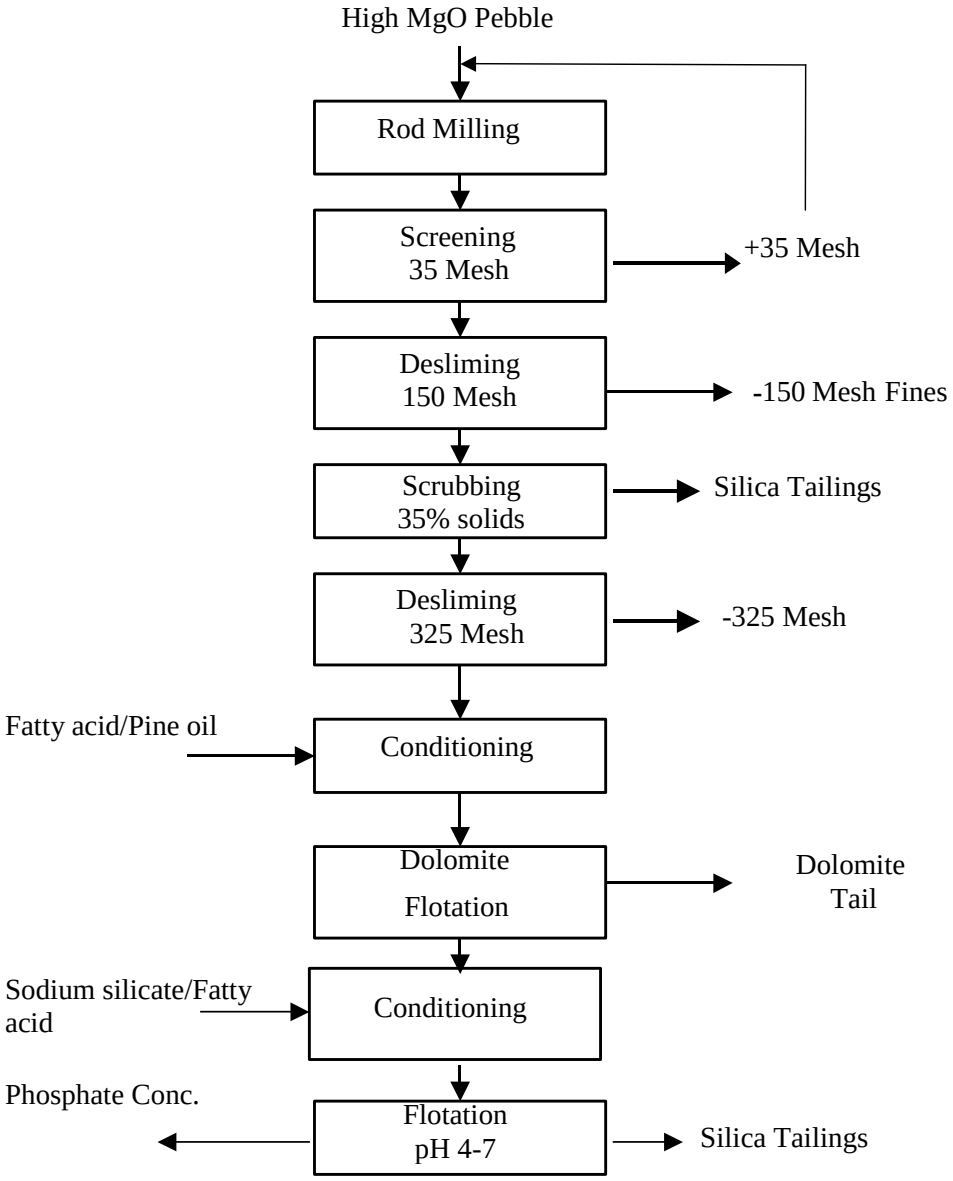

Figure 1-5. University of Alabama pebble processing, simplified flowsheet

Two-Stage Conditioning Process

This process was investigated through FIRP – university of Florida project, in 1983 [Moudgil, 1988]. The process involves conditioning the feed at pH 10, followed by reconditioning at a lower pH before flotation, Figure 1-6. Selective flotation of dolomite from apatite was observed for both single and mixed minerals, by reconditioning at pH 4.

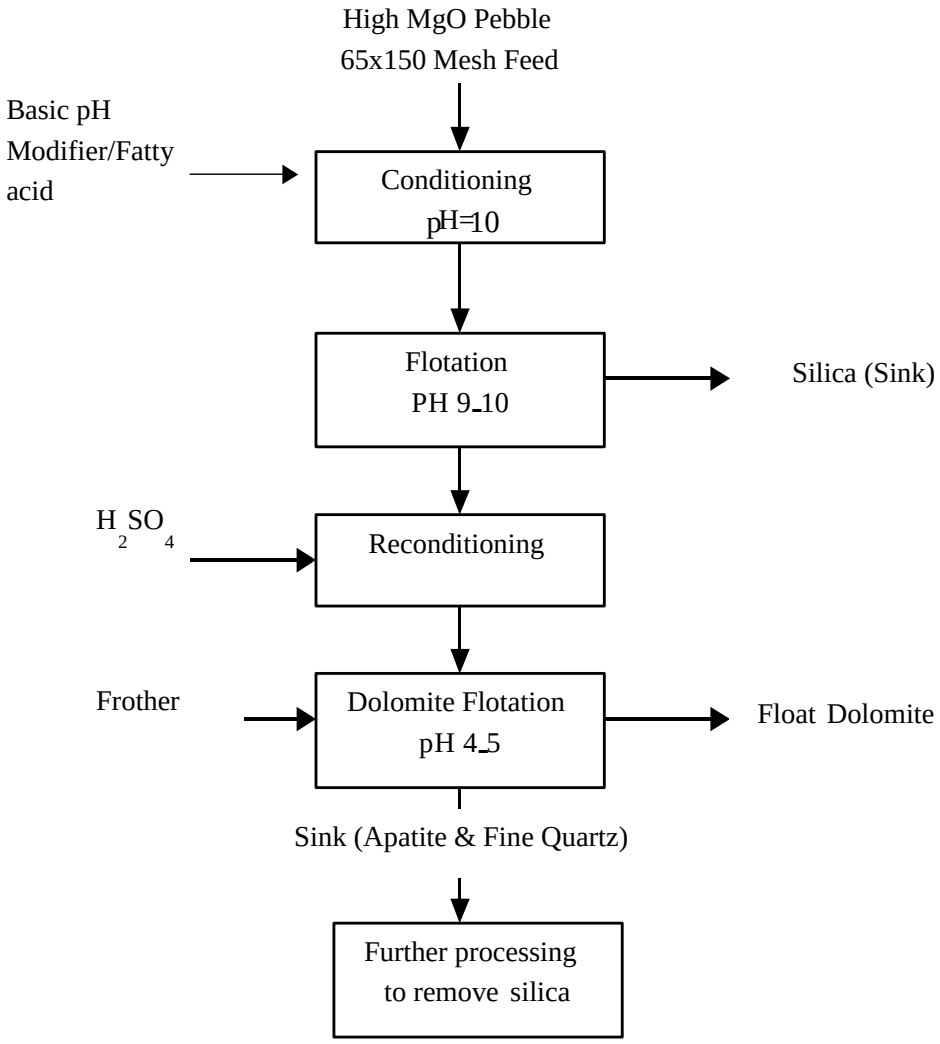

Figure 1-6. Flowsheet for University of Florida two conditioning stages

To understand the mechanisms of observed selective flotation, further studies were conducted involving electrokinetic behavior, oleate adsorption, infrared spectroscopy,

and solubility of the minerals. Selective flotation of dolomite, by reconditioning at pH 4, is attributed to the combined effect of higher oleate adsorption on dolomite and hydrolysis of the adsorbed oleate molecules to oleic acid at lower pH values.

The method has been tested in the laboratory with several dolomite-apatite mixtures and natural magnesium phosphate samples from the Florida phosphate field. Reductions of the MgO content of the samples from 1.8-4.0 % MgO to below 1 % MgO at recoveries of about 90 % P_2O_5 in the sink fraction have been obtained in bench-scale flotation tests. Reconditioning pH was determined to be one of the most important parameters in this process.

The CLDRI Process

In China, over 90 % of the phosphate resources are dolomitic, with MgO content ranging from 2 % to over 10 %. For economical and rational use of domestic phosphate resources, China Lianyungang Design and Research Institute (CLDRI) has conducted studies for many years and developed some flotation technologies for removing MgO impurity from phosphate ore. These flotation technologies have successful industrial applications [El-Shall et al., 1996].

Since 1997, CLDRI has conducted extensive studies on Florida high dolomitic pebble with the objective of using CLDRI's fine particle flotation technology to recover phosphate (Figure 1-7). In 2000, pilot scale testing (400 lb/h) was carried out jointly by CLDRI, Jacobs engineering group, and IMC phosphate's company at Jacob's pilot plant facility. Preliminary economic and technical analysis by Jacob's engineering (based on pilot plant test results) showed that CLDRI's fine-particle flotation technology could be used economically and technically for processing Florida's dolomitic phosphate pebbles [Geo et al., 2002].

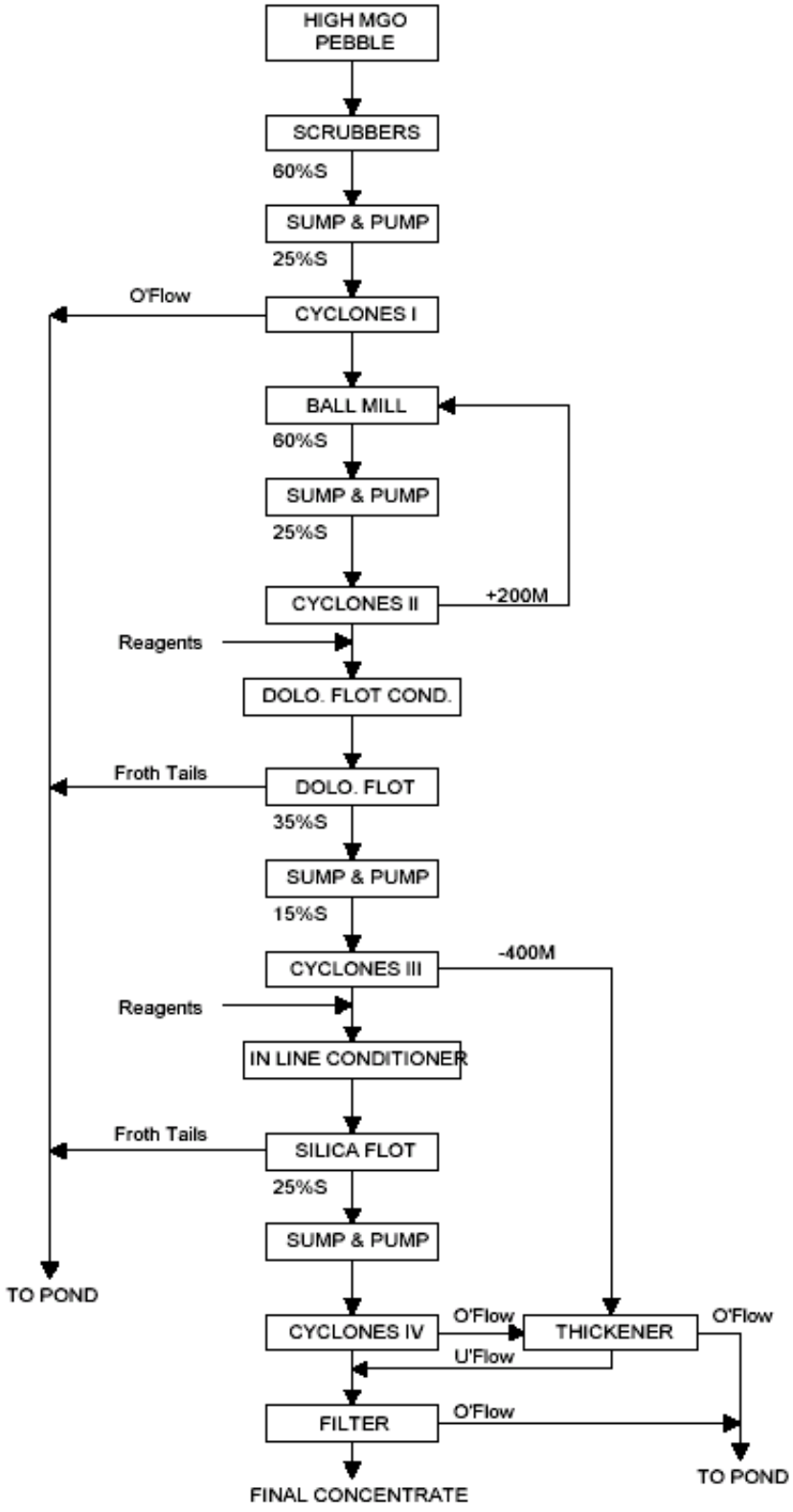

Figure 1-7. Simplified flowsheet for CLDRI dolomite flotation

The CLDRI‘s fine-particle flotation technology (Figure 1-7) utilized for processing Florida high-dolomitic phosphate pebbles has two steps. The first step is grinding for liberation and second nondesliming after grinding, which improves flotation recovery and use of Florida resources, and lowers production cost.

Acid Leaching

Strong and weak acids were used in the acid leaching process. In strong-acid leaching processes, sulfuric acid was used to completely dissolve the dolomite from phosphate ore.

In the early 1970s, the USBM investigated magnesium impurity removal from phosphate concentrates by acid leaching [Rule, 1970]. The MgO level was reduced to less than 0.1 % by using dilute sulfuric acid, but the phosphate loss was about 6 % P_2O_5.

Weak-acid leaching, using weak organic acids, was also studied. Pilot plant studies [Abu El-shah, 1991] using 6.7 % acetic acid solution could remove more than 80 % MgO. The advantage of using weak organic acids is that (unlike strong acids), they do not attack other minerals. The overall disadvantage is that acid leaching, in general, needs fine particle sizes produced by crushing and grinding which means more expenses.

Physical Separation Methods

Heavy Media Separation

The only commercial process to separate dolomite from phosphate is heavy media separation [Wiegel and Hwang, 1984]. Heavy media cyclones are used in IMCF mines for processing the high-dolomite portion of the ore. The concentrate with 1.2 % MgO was obtained from feed that has 3 % MgO.

Sizing, Attrition Scrubbing, and Desliming

The dolomite is more friable than phosphate rock. Thus, dolomite can be separated from phosphate by discarding the fine fraction (mainly dolomite) by scrubbing or sizing [El-Shall and Bogan, 1990].

Problem Statement

The various beneficiating techniques discussed have various limitations or disadvantages. In acid leaching, strong acids can attack phosphate as well as dolomite and can be associated with environmental problems associated with this process.
In flotation processes for high dolomitic phosphate, because they could not reduce the MgO % below 1 % are not applied commercially.

In CLDRI fine flotation process, by which the MgO % could be reduced to less than 1 %, concerns are as follows: handling of fine concentrate (dewatering and transport), capital cost (grinding and multiple process steps), and operating cost: increasing the MgO % in the phosphate rock increases reagent consumption, and requires grinding, thus increasing energy consumption and plant operating cost. The only process with commercial application was heavy media separation (HMS), which also suffers from high MgO % (more than 1 %) in the concentrate in addition to about 50 % phosphate loss.

Novelty and Scope of Study

We sought a process that separates dolomite from phosphate pebbles resulting in a phosphate concentrate with less than 1 % MgO. Since the dolomite is mostly in the pebble fraction and not attached to phosphate, the idea came from well-known reaction between carbonates and acid producing carbon dioxide gas. Dolomite, as a carbonate

mineral, generates CO_2 when exposed to a slightly acidic solution, as shown in the following chemical reaction:

$$\text{Dolomite} + \text{Acid} \rightarrow \text{salt} + CO_2$$

Capturing the generated CO_2, at the dolomite particle surface, into bubbles using coating agent (which is a kind of surfactant or polymer) can selectively float dolomite, and separate it from phosphate rock. Since this process depends on chemical reaction between dolomite and acidic medium to form a stable bubble at the particle surface and then to float it, this process is called the Reactive Flotation (RF) process.

The RF has the following requirements (1) presence of acidic medium at low percentage, and (2) Presence of surfactant that: attaches to the dolomite, is permeable by acid, allows formation of stable bubbles at the particle surface, is impermeable to CO_2 gas, and is stable enough to float the particle to the surface.

Goal of Study

The goal of this study is to develop and to optimize a novel and an effective process to separate the dolomite from phosphate rock. This process will not only reduce the MgO % to less than 1 % but also increase the efficiency of the subsequent processes in phosphoric acid production such as filtration and consequently reduce the phosphate losses. In addition to develop this novel process, a fundamental study needs to be done to elucidate Mechanism(s) involved in this novel process.

CHAPTER 2
MATERIALS AND METHODS

To achieve the goals of this research different measurements and techniques are needed to elucidate polyvinyl alcohol (PVA)/ particle interactions, and bubbles formation and stability as well as its modeling the following strategy will be followed, Figure 2-1.

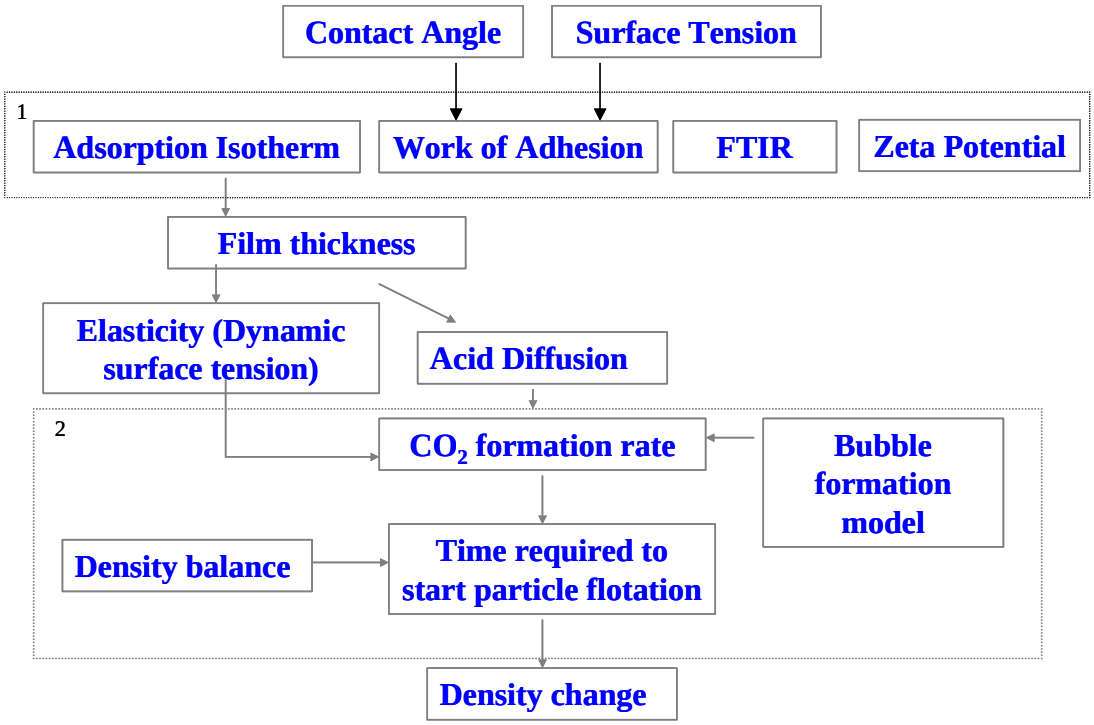

Figure 2-1. Strategic plan to achieve research goals

As it can be seen form Figure 2-1, the first block represents the required techniques and measurements to elucidate polyvinyl alcohol (PVA)/ particle interactions. On the other hand, the second block represents another part of our goal which is bubble formation and stability as well as its modeling.

Flotation Study

In this study, screening and central composite statistical experimental designs are used to determine the effect of various factors on the removal of MgO and its recovery. The Plackett-Burman design was used to screen out which of the 7 factors being considered were the most statistically significant. In other words, it is a tool that helps determine which factors made the greatest impact on the MgO removal. A central composite design was used to determine if there were any interactions between the three most significant factors determined from the Plackett-Burman design.

Screening Design (Plackett-Burman Design)

The variables examined in the screening stage were acid concentration (1% and 3 %), Polyvinyl alcohol concentration in the coating solution (1 % and 3 %), the PVA molecular weight (60,000 and 150,000), the degree of hydrolysis (88 %-99 %) of the PVA, particle size (-0.5 mm and 5-9 mm), and drying time of the coating (0 and 2 hrs). The levels were chosen according to the exploratory test results from phase I of this project. The Plackett-Burman design used for this study had 11 factors and 12 experimental runs (Table 2-1). MgO % was determined using chemical analysis. Chemical analyses were performed using wet chemical methods, acid attack (digestion) method as described below.

Central Composite Design

A central composite design was used to further investigate the three most significant factors (acid concentration, PVA concentration, and particle size) determined from the screening design. Five levels were used. The central composite experimental design had 17 experimental runs (Table 2-2 and Figure 2-2). For each run, the products are chemically analyzed as above-mentioned and the MgO % and MgO removal % were

calculated for all the experimental runs. The computer program, Design expert® (SAS Institute, Inc.), was used to perform the statistical analysis for the central composite design. The data was analyzed by fitting the response variables to a second-order polynomial model.

Table 2-1. Experimental Plackett-Burman design for 11 variables

Run No.	Variable Levels										
	1	2	3	4	5	6	7	8	9	10	11
1	-	-	+	+	+	-	+	+	-	+	-
2	+	-	+	-	-	-	+	+	+	-	+
3	-	-	-	-	-	-	-	-	-	-	-
4	+	+	+	-	+	+	-	+	-	-	-
5	+	-	+	+	-	+	-	-	-	+	+
6	+	-	-	-	+	+	+	-	+	+	-
7	+	+	-	+	-	-	-	+	+	+	-
8	+	+	-	+	+	-	+	-	-	-	+
9	-	+	+	+	-	+	+	-	+	-	-
10	-	-	-	+	+	+	-	+	+	-	+
11	-	+	-	-	-	+	+	+	-	+	+
12	-	+	+	-	+	-	-	-	+	+	+

Plackett-Burman Variables Used in the Reactive Flotation Study

Variables	Low Level (-)	High Level (+)
1) Acid conc	1 %	3 %
2) PVA conc	1 %	3 %
3) dummy ♣		
4) dummy		
5) PVA M.W	60,000	150,000
6) Degree of hydrolysis	88 %	99 %
7) Time of drying	0	2 h
8) dummy		
9) Particle size	-0.5mm	5-9 mm
10) dummy		
11) dummy		

♣ dummy variables are used to calculate the variance of the experimental runs

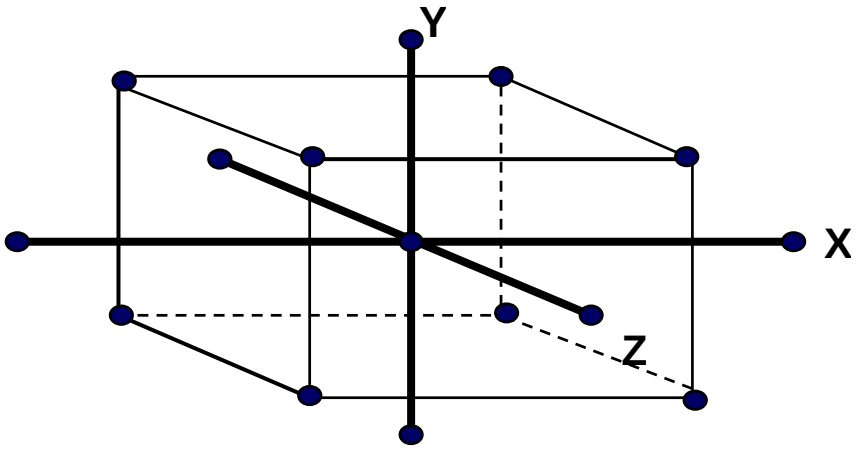

Figure 2-2. Five-level, rotatable central composite design. The X, Y, and Z axes represent the 3 variables, sulfuric acid concentration, PVA concentration, and particle size. The circles represent each experimental run.

Table 2-2. Rotatable central composite design with 5 levels and 3 variables

Run No.	Acid conc	PVA %	Particle Size
1	-1	-1	-1
2	-1	-1	+1
3	-1	+1	-1
4	-1	+1	+1
5	+1	-1	-1
6	+1	-1	+1
7	+1	+1	-1
8	+1	+1	+1
9	-1.68	0	0
10	+1.68	0	0
11	0	-1.68	0
12	0	+1.68	0
13	0	0	-1.68
14	0	0	+1.68
15	0	0	0
16	0	0	0
17	0	0	0

Levels					
Variables	-1.68	-1	0	+1	+1.68
Acid conc. (%)	0.32	1	2	3	3.68
PVA, (lb/t)	0.6	2	4	6	7.4
Particle size, mm	-0.5	0.5-1	1-2	2-5	5-9

Flotation Procedures for Screening and CCD Designs

Using 300 ml (3 % H_2SO_4) in 400 ml beaker, particles were pre-coated by spraying 3 % PVA solution (using a mist delivery nozzle) then added to the acidic solution. The experiment was left for 5 min. Dolomite floats to the surface, which was separated by decantation on a screen. The products (floated and unfloated fractions) were dried, weighed, and chemically analyzed.

Factorial Design for Conditioning with PVA before Flotation

This design was used to study the factors affecting the conditioning step with PVA, which is a promising step for reducing PVA consumption. Table 2-3 shows the design and levels used.

Table 2-3. Factorial design for conditioning with PVA

Run No.	PVA concentration, %	Pulp density (S/L ratio)	Conditioning time, min
1	-1	-1	-1
2	-1	-1	+1
3	-1	+1	-1
4	-1	+1	+1
5	+1	-1	-1
6	+1	-1	+1
7	+1	+1	-1
8	+1	+1	+1
9	0	0	0
10	0	0	0
11	0	0	0

Levels			
Variables	-1	0	+1
PVA concentration, %	0.25	0.625	1
Pulp density	30 %	50 %	70 %
Conditioning time, min	2	11	20

Flotation Procedure for Conditioning Statistical Designs

50 gm of ore were added to 1 % PVA solution in a 600 mL beaker according to specific solid/liquid ratio. The slurry was mixed for required time at 300 rpm (using 2.5

cm magnetic bar). After the conditioning time is elapsed the solids were screened, the solids were used for flotation in acidic solution and the filtrate solution was taken to PVA analysis to determine the PVA residual concentration.

Chemical analysis: About 0.5 gm of the dried and ground representative sample were digested in 50 ml of aqua regia by boiling on hotplate until the reaction complete. After cooling, this solution was filtered through a Whatman 42 filter paper into 1000 ml volumetric flask. The filter paper and residue were then washed at least five times to remove all the traces of dissolved salts and acid. The filtrate was diluted with distilled water and thoroughly mixed and the concentrations were measured using Inductively Coupled Plasma, ICP, emission spectrometer, (Perkin Elmer Optima 3200RL Optical Emission Spectroscopy, Norwalk, CT). ICP was calibrated using AFPC rock check No.22.

Standard sample concentrations were measured from time to time in the course of the analyses to check the accuracy of the calibration curve. Five replicates were taken and averaged for each element. The following wavelengths were used:

Element	Wave lengths, nm
Ca	315.887, 317.933, 393.366, and 396.847
Mg	279.077, 285.213, and 279.553
P	213.617, and 214.914
Fe	238.204, 239.562, 259.939, and 234.349
Al	308.215

Density and Surface Area Determination

Densities of powders were measured using a Quanta Chrome ultrapycnometer. The specific surface area (m^2/g) of dolomite and apatite particles was determined using Quanta Chrome NOVA 1200 instrument. (Quantachrome Corp., Boynton Beach, FL).

The analysis was performed using a five-point BET (0.10, 0.15, 0.20, 0.25, 0.30) using Nitrogen gas. The particles were outgased at 60°C for 24 hours before analysis.

PVA Preparation

PVA was kindly supplied by Celanese chemicals Co., USA. Different PVA types with various ranges of molecular weights and degree of hydrolysis are used in screening factorial design, namely:

Type	Average Molecular Wt.	Degree of Hydrolysis, %
Celvol 165	150000	99
Celvol 540	150000	88
Celvol 305	60000	99
Celvol 203	60000	88

In the rest of the study, PVA, Celvol 165, was used. PVA flakes were gradually dissolved in deionized water at 90 ^{o}C with continuous mixing by magnetic stirrer and heated at 90 °C for 2 h to produce different PVA concentrations (0.5, 1, 2, 3, and 4 %).

Spectrophotometric Determination of PVA

PVA solution of certain concentration treated with 25 ml of 4 % boric acid solution and 2 ml of iodine solution (prepared from 1.27g of iodine and 25 g of KI/l), in that order. The resulting solution is diluted to 100 ml and kept at 25°C and its absorbance measured at 690 nm against a blank solution containing the same amount of boric acid and iodine solution. Beer's law applies in the concentration range of 0-40 mg of PVA/l of solution [Finch, 1973; 1992]. Absorbance spectra were taken using ultraviolet/visible spectrophotometer (UV-Vis spectrophotometer, Perkin-Elmer Lambda 800). All spectra were taken at room temperature.

Static (Equilibrium surface tension)

Equilibrium surface tensions were measured for freshly prepared solutions by the Wilhelmy plate method at room temperature. The platinum plate was always cleaned and heated to a red/orange color with a Bunsen burner before use.

Dynamic Surface Tension (DST)

Maximum bubble pressure method

The dynamic surface tension (DST) measurement is important in the dynamic interfacial processes where the equilibrium surface tension is hard to be achieved. The DST can be measured by different methods such as: the drop weight [Jho and Burke, 1983; Miller et al., 1993], oscillating jet [Thomas and Hall, 1975], capillary wave [Kelvin, 1871], growing drop technique [Macleod and Radke 1993], and the maximum bubble pressure method [Mysels, 1986; Ross et al., 1992]. The maximum bubble pressure (MBP) technique is the most commonly used technique for the measurement of DST, and has been applied to a variety of surfactant and polymer solutions [Fainerman et al., 1994; Tamura et al., 1995]. The physical principle behind the MBP measurement is the Laplace pressure; the pressure inside a curved liquid interface is higher than the ambient. This excess pressure (P) can be calculated from the Laplace equation [Adamson and Gast, 1997].

$$P = \frac{2\gamma}{r} + \rho gh$$

Where γ is the surface tension, r is the radius of curvature of the bubble, ρ is the liquid density, g is the gravitational constant and h is the depth of the bubble in the liquid. The first term expresses the Laplace pressure due to the curved gas/liquid interface, and the second term is the hydrostatic pressure due to the liquid height above the forming

bubble. The first term will vary during the life cycle of the bubble, while the second term will remain constant. Figure 2-3 shows a typical cycle of a bubble and the resulting pressure within the capillary. After a bubble breaks off from the capillary tip, the pressure is the lowest. As more gas flows into the capillary, the pressure builds up as the gas is pushed out of the capillary and the radius of curvature at the tip decreases. During this expansion process, surfactant is populating the new interface and acting to lower the surface tension. At the point of minimum interface radius of curvature, where a hemisphere of gas is formed at the capillary tip, the pressure reaches maximum.

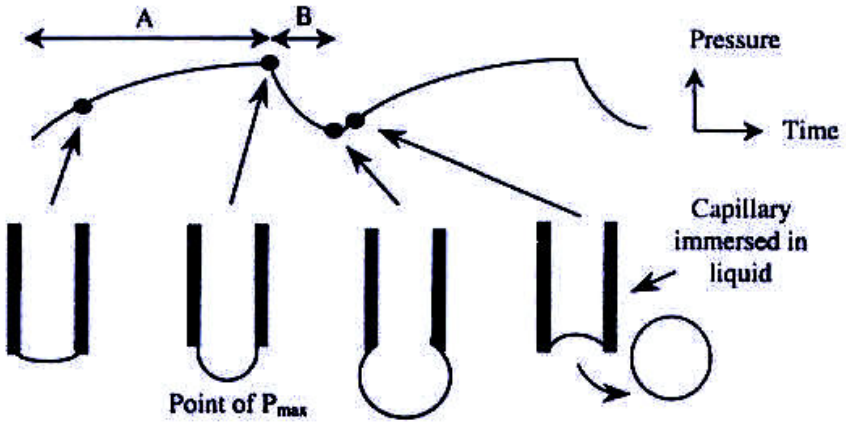

Figure 2-3. Characteristic bubble-pressure vs. time curve in MBP.

Both the minimum radius of curvature and the surface tension, as described by the Laplace equation, govern the maximum pressure experienced. On the incremental addition of gas, the bubble expands out of the capillary tip and the radius of curvature gradually increases. This results in a drop in the Laplace pressure, and a resulting rapid expansion of the bubble. At some point, the bubble breaks off from the capillary tip and the whole process starts again.

Dynamic surface tension setup

The maximum bubble pressure apparatus was constructed using a differential pressure transducer purchased from Omega Engineering, Inc. (Stanford, CT), with a sensitivity of 0 to 10 in. (25 cm) H_2O (0 to 2500 Pa). A #23 steel needle was used as a capillary, with nominal 0.025 in. (0.64 mm) external diameter, 0.013 in (0.33mm) internal diameter, and a flush cut tip. The capillary diameter was chosen so that the various resistance of water to bubble growth could be ignored. Such internal and viscous effects are a potential source of error in these measurements that need to be taken into consideration [Garrett and Ward, 1989]. All measurements were conducted with the capillary tip 1 cm beneath the liquid surface. CO_2 gas was used as the bubbling gas to simulate the gas produced in the reaction of acid with dolomite and an oscilloscope connected to the pressure transducer was used to determine the bubble frequency and the dynamic surface tension (Figure 2-4).

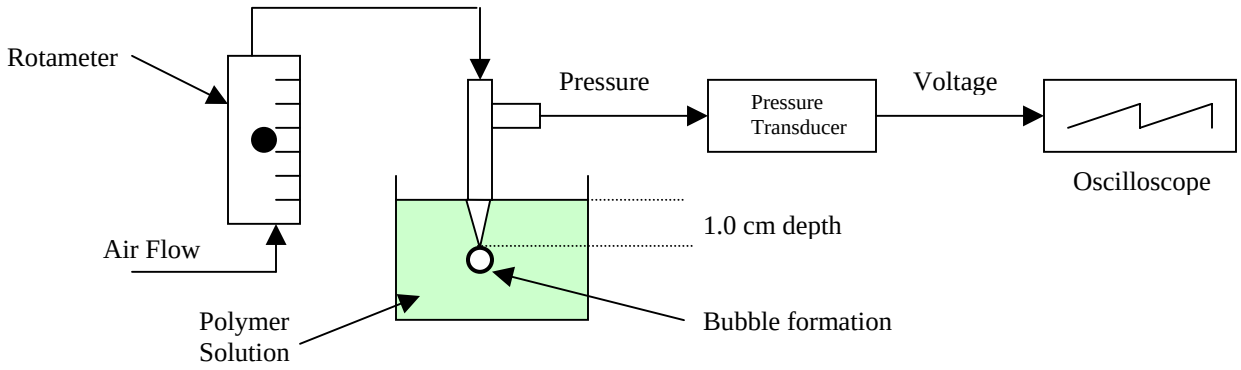

Figure 2-4. Setup for the measurement of dynamic surface tension by maximum bubble pressure method.

Contact Angle

The angle formed at a point on the line of contact of three phases, of which at least two are condensed phases, by the tangents to the curves obtained by intersecting a plane

perpendicular to the line of contact with each of three phases. One of the phases must be a liquid, another phase may be solid or liquid and the third phase may be gas or liquid.

In other words, it is the angle included between the tangent plane to the surface of the liquid and the tangent plane to the surface of the solid, at any point along their line of contact. The surface tension of the solid will favor spreading of the liquid, but this is opposed by the solid-liquid interfacial tension and the vector of the surface tension of the liquid in the plane of the solid surface.

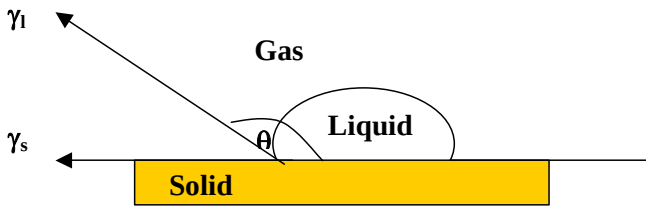

Figure 2-5. Contact angle and its relation with surface tension

Equilibrium wetting properties of liquids and solutions can be interpreted in terms of the balance of surface tensions (Figure 2-5).

$$\gamma_{sg} - \gamma_{sl} = \gamma_{lg} \cos \theta$$

Measurement of Contact Angle

The contact angle goniometer, Figure 2-6, is a device mounted on the optical bench to examine a single liquid drop or gas bubble resting on the smooth, planar, solid substrate. The drop/bubble is illuminated from the rear to form a silhouette, which is viewed through a telescope connected to computer. The image of the drop/bubble appears on the computer monitor by which the brightness and contrast, focusing and amount of illumination can be adjusted. After adjusting the image the contact angle can be measured.

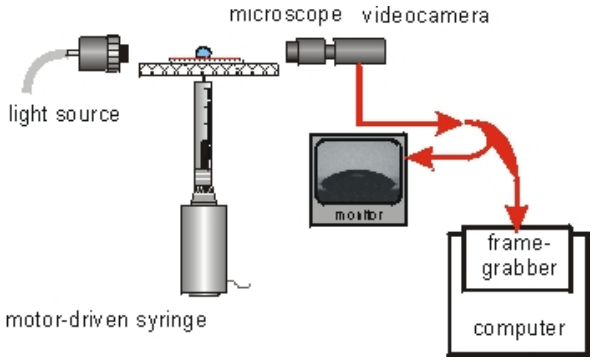

Figure 2-6. Contact angle measuring apparatus

Surface Characterization by FTIR

The spectorometer used for FTIR was a Magna-IR760 spectrometer by Nicolet in transmission setting. As for the spectra recorded in transmission mode, KBr pellets were prepared for the background measurements. Another pellets were prepared by mixing about 1 mg of filtered powder with 50 mg of KBr. Transmission spectra were recorded using a DTGS detector, with 128 scans and 4 cm^{-1} resolution.

Zeta Potential Measurements

In the zeta potential measurement tests, 1 g of ground mineral samples was added into a 250 ml beaker in which 100 ml 0.003 M KNO^3 solutions were added. The suspension was conditioned for 3 min during which the pH was adjusted, followed by 5 min of conditioning after adding the polymer. It was then allowed to settle for 3 min, and about 10 ml of the supernatant was transferred into a standard cuvette for zeta potential measurement using a Brookhaven ZetaPlus Zeta Potential Analyzer. Solution temperature was maintained at 25 °C. Ten measurements were taken and the average was reported as the measured zeta potential.

Adsorption

These studies were carried out at 25°C using 0.5gm mineral sample in 50 ml solution having the desired PVA concentration and the ionic strength fixed at $3X10^{-3}$ M

using KNO_3. One set of experiments was performed first to determine the effect of conditioning time at a fixed pH (pH 7) and PVA concentration was 100 ppm ($3.33X10^{-8}$ M). Then set of experiments was also carried out as a function of pH at the same PVA concentration. Adsorption isotherm was also determined for PVA/dolomite, PVA/apatite, PVA/dolomite/apatite supernatant, PVA/apatite/dolomite supernatant systems at pH 7 and $3X10^{-3}$ M KNO_3 as an ionic strength. After the conditioning step, the suspension was centrifuged at 3000 rpm for 5 min using an IEC-Medispin centrifuge (Model 120). Then a volume of the clear solution was withdrawn for measurement of the PVA residual concentration.

In adsorption kinetic experiments, a 0.5 gm of dolomite or apatite were added to 100 ppm ($3.33X10^{-8}$ M) PVA solution a 30 ml screw-capped bottle and was shaken at room temperature using Wrist hand shaker for a given recorded time (0.05, 0.083, 0.0166, 0.25, 0.5, 1, 2, 4, 6, 8, 10, 16, 20, 24 h). After that the contents of each bottle were allowed to settle, followed by centrifugation step using an IEC-Medispin centrifuge (Model 120). The amount of PVA adsorbed was determined by difference between the initial and final concentrations measured spectrophotometrically with a Uv-vis spectrophotometer (UV-Vis spectrophotometer, Perkin-Elmer Lambda 800). These experiments were used to establish the equilibrium time for adsorption of PVA on dolomite and apatite. This equilibrium time was used as contact time in adsorption isotherm experiments.

Dissolution Kinetic Experiments

Dolomite specimens (1-2 mm and 0.2-0.3 mm), uncoated and coated with PVA, were added to 2000 ml aqueous medium (3 % H_2SO_4) at 23 ± 0.5°C to carry out 120 min static dissolution tests. After a definite time interval, solution samples were collected

periodically and concentrations of Mg^{2+} and Ca^{2+} were determined with ICP. The relations of concentration, C, with time, t was plotted to explore the dissolution kinetics of the dissolution process.

Pilot Scale Experiments

The Sluice

The pre-conditioned material is introduced into a feed box, which contains 3 % sulfuric acid. The reaction of sulfuric acid with particles starts in the feed box forming bubbles around dolomite particles and creating the required density difference for the separation in that device. The particles soon enter the moving stream and, because of the bubbles on dolomite particles, they settle at lower rate and float to the surface when the enough bubbles formed and carried away till they reach the lip of the trough and discharged with liquid overflow. Since phosphate particles do not produce CO_2, and have no bubbles at their surfaces, they are collected at the bottom of the trough (Figure 2-7).

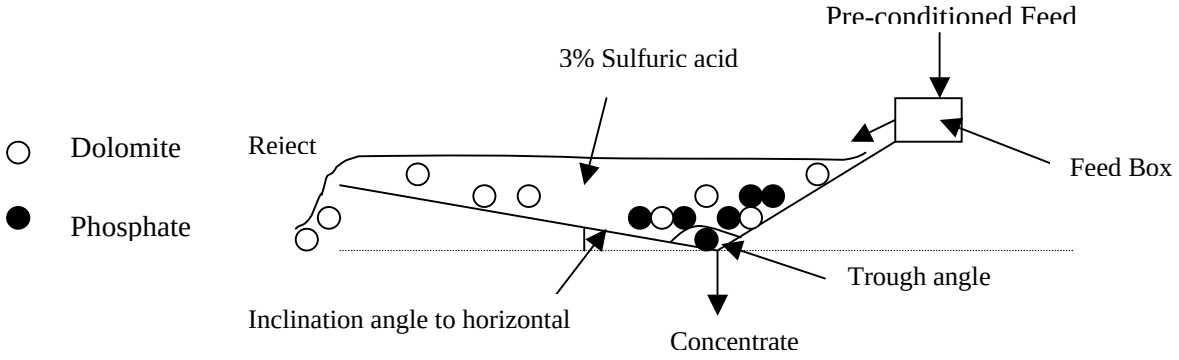

Figure 2-7. Schematic diagram for separation of dolomite from phosphate in sluice

Sluice Experiments

250 gm of ore (a mixture of dolomite and phosphate), with particle size 1-2 mm, were conditioned in 1 % polyvinyl alcohol solution for 5 minutes, then screened to separate the solids from PVA solution. The screened solution was analyzed to determine the actual PVA consumption by depletion method. Or the material was sprayed with the

equivalent amount of PVA and was tumbled to attain a good coating. After that, the coated solids were poured into sluice feed box which the sulfuric acid and the reaction starts to generate CO_2 bubbles. The particles move through the sluice at flow rate 125 ml/sec (2 GPM). The floated fraction, dolomite, was collected on 0.5 mm screen and the sink fraction, phosphate, was collected in the sluice trough. The floated and sink products were analyzed for MgO, P_2O_5, CaO, and insoluble residue (I.R.).

CHAPTER 3
TECHNICAL ASPECTS OF REACTIVE FLOTATION: PRELIMINARY TESTS

Introduction

The reactive flotation process, as mentioned earlier, requires certain conditions to give good results and separate dolomite from phosphate rock. The main requirements for RF to work properly are the acidic medium and surfactant or polymer, which attaches to the dolomite, to allow the acid to diffuse through but at the same time remain impermeable to the CO_2 gas produced by the reaction. Moreover, the formation of CO_2 will lead to stretching of the membrane-like surfactant layers, which requires an elastic behavior of that membrane. The elasticity of the membrane formed around the particle will then allow the formation of stable bubbles. The stable bubbles are the main criterion in RF to float the dolomite particles and separate them from others.

At the starting point of this process, the most well behaved acids and surfactants, under RF conditions, were not known. Different acids and surfactants can be used but it was unknown which one would best fulfill the previously mentioned requirements for the RF process. For that reason, in the current study, preliminary tests were conducted using different acid types (sulfuric, hydrochloric, nitric, acetic) within a particular concentration range (0.5 - 4 % v/v) as well as different types of surfactants (anionic, cationic, and non-ionic), which were prepared as 1-2 % surfactant solution and used in two different ways: (1) surfactant was added to acidic solution and/or (2) surfactant was used to coat the particle before adding the particle to the acidic solution. Also, poly-vinyl-

alcohol (PVA) was used in this study. Vegetable and corn oil were used at the acidic solution/ air interface and oil height was 0.5-0.6 cm.

List of Potential Surfactants: Surfactants Screening

A list of potential surfactants used in this study, are given in Table 3-1. The list contains different types of surfactants, (i.e., cationic, anionic, and non-ionic, as well as polymers).

Table 3-1. Surface-active agents used in RF tests

Surfactant	Chemical Name	Type
Arquad 12-50	Dodecanaminium+isopropyl alcohol	Cationic
Lilamine	N-3-aminopropyl-N-tallow alkyltrimethylenedi-	Cationic
Armac HT	Amines, hydrogenated tallow alkyl acetates	Cationic
Armid HT	Amides	Cationic
Armeen 12 D	dodecanamine	Cationic
Ethofat	Tall Oil	Anionic
$SDSO_3$	Sodium dodecyl-sulphonate	Anionic
$SDSO_4$	Sodium dodecyl-sulphate	Anionic
Oleic acid	Oleic acid	Anionic
Arlacel	Sorbitan sesquioleate	Non-ionic
Span-20	Sorbitan monolautrate	Non-ionic
G-1096	Polyoxyethelene-sorbitol hexaoleate	Non-ionic
Brij-97	Polyoxyethelene oleyl ether	Non-ionic
Arlatone T	Polyoxyethelene polyofatty acid ester	Non-ionic
Tween-21	Polyoxyethelene Sorbitan monolautrate	Non-ionic
Tween-85	Trioleate	Non-ionic
PVA	Poly-Vinyl-Alcohol	Non-ionic

Initial Screening Tests

A 100-pound sample of high-dolomitic phosphate oversize pebble was obtained from the IMC Four Corner's mine. This is not "normal" high MgO rock, but the oversized high MgO rock that is removed from pebble. As such, neither the screen weight fractions nor the chemical analyses are representative of pebble. However, the rock is representative of the high-dolomitic rock that needs to be separated. The rock was screened, and each fraction is chemically analyzed in Tables 3-2 and 3-3.

Table 3-2. Size analysis of the dolomitic phosphate sample

Size, mesh	Size, mm	Wt. %	% Cumulative (passed)	% Cumulative (retained)
+ 3/8 in	+ 9.5	11.62	100.00	11.62
- 3/8 in +3.5	- 9.5+5.6	65.36	88.38	76.98
- 3.5+6	- 5.6+3.36	18.14	23.02	95.12
- 6+9	- 3.36+2	2.05	4.88	97.17
- 9+16	- 2+1	1.6	2.83	98.77
- 16	- 1	1.23	1.23	100
		100.00		

Table 3-3. Chemical analyses of the dolomitic phosphate sample

Size, mesh	P_2O_5 %	CaO %	MgO %	Fe_2O_3 %	Al_2O_3 %
+3/8 in	19.86	32.23	4.02	0.93	0.52
-3/8 in +3.5	21.25	36.34	3.43	1.15	0.84
-3.5+6	17.09	27.92	2.34	1.32	0.86
-6+9	24.32	38.90	2.75	1.08	1.17
-9+16	20.42	28.71	2.12	1.27	1.07
-16	13.62	22.75	2.44	1.13	0.95

Since most of the rock was relatively coarse, a portion of it was crushed and re-screened to obtain smaller fractions that could be used in the tests.

Specific Tests

The results of some preliminary testing are shown in the following paragraphs in terms of acid type and dosage, surfactant type and dosage, particle size, and using of oil layer at the water/acidic solution interface.

Acid type

Different acids (H_2SO_4, HCl, HNO_3, and Acetic acid) were used. Inorganic acids: HCl, HNO_3, and H_2SO_4 gave the same results at 2 % acid concentration. On the other hand, the acetic acid (RCOOH) formed a very small number of bubbles at 2 % acid concentration. Increasing the concentration of acetic acid to 5 % gave no significant variation in bubble formation, which means that the organic acids are weak acids. Consequently, a large amount of organic acids is needed relative to inorganic ones.

Acid dosage

Since all the inorganic acids behave in the same manner, sulfuric acid was used in the rest of the experiments. Table 3-4 shows the effect of acid concentration on the bubble formation rate, amount of bubbles formed, and particle floatability that were taken as a criterion to compare the results. The surfactant used for coating the dolomitic particle was dodycyl sulphonate ($SDSO_3$).

Table 3-4. Effect of sulfuric acid concentration

	Sulfuric acid concentration, %				
	0	0.25	0.5	1	2
Bubble formation rate	Very slow →		Slow →	Fast →	Rapid
Amount of bubbles formed	Very small number of bubbles (about 5 bubbles for 10 minutes then no bubbles formed)	The interval between formation of two bubbles was about 30 seconds	Increasing the rate and number of bubbles formed	Continuous formation of bubbles but at rate higher than 0.5 %	Continuous and quick formation of many bubbles
Flotation of dolomite particle		No flotation		Float after 5-10 minutes	Float after 1 minute

From Table 3-4, we notice that the reaction between dolomite and acid to produce CO_2 decreases noticeably with decreasing acid concentration and the flotation of dolomite particle takes longer time (5-10 min) in 1 % acid than in 2 % acid. Consequently, the 2 % sulfuric acid concentration is the most suitable acid concentration for bubble formation in terms of both bubble formation rate and amount of bubble formed. Because of the wide gap between 1 % and 2 % acid concentration another set of experiments were conducted as shown in Table 3-5 to get the optimum acid concentration.

Table 3-5. Effect of sulfuric acid concentration on the bubble formation

	Sulfuric acid concentration, %					
	1	1.2	1.4	1.6	1.8	2
Bubble formation rate	Increases →					
Amount of bubbles formed	Continuous and small No. of tiny bubbles → Continuous & large No. of tiny bubbles					
Flotation of dolomite particle	Takes 20 minutes to float, not stable (particle goes up and down)	Floats and stays at water/oil (W/O) interface for 5 min. Then oscillates within 2 min intervals		Floats and stays at (W/O) interface		

Table 3-5 shows that the flotation at 1 % & 1.2 % is not stable and flotation occurs after the particle loses part of its weight due to reaction with acid. Accordingly, this concentration deals with a small particles (smaller than 1mm) rather than large particles. The bubble formation rate is decreased with the acid percentage from 2 % to 1 %, but as the difference was narrower between 1.6-2 %, 1.6 % acid concentration was found to be optimal. The effect of acid concentration on the RF criterion was schematically summarized in Figure 3-1.

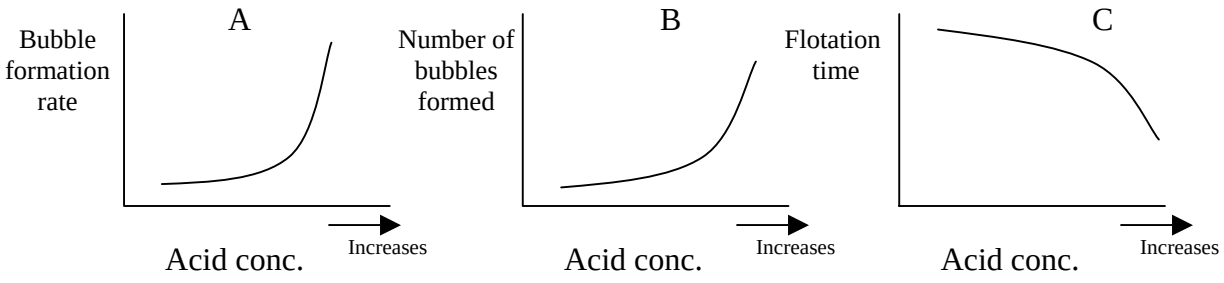

Figure 3-1. Effect of acid concentration on: A) Bubble formation rate, B) Number of bubbles formed, C) Flotation time.

Surfactant type

Table 3-6 shows the anionic, cationic and non-ionic surfactants used. According to RF criterion, the performance of Anionic surfactant was superior to Non-ionic, which was superior to Cationic. Anionic surfactants, especially $SDSO_3$, formed stable

"membranes" that captured CO_2 and persisted for 10 minutes. This may be due to its ability to work at low pH. Therefore, $SDSO_3$ was used in the next experiments.

Table 3-6. Preliminary tests of high dolomitic phosphate with different surfactants

Surfactant Name	Remarks
Arquad 12-50 (1%)	stable bubbles for 20-30 sec, particle 2-3 mm can float
Lilamine (1%)	less stable bubbles, stay 10 s, particle does not reach to surface of the solution (air-water interface)
Armac HT (1%)	surfactant precipitated in the solution
Armid HT (1%)	
Armeen 12 D (1%)	
Ethofat (1%)	Formation of bubbles on the particle surface then particle floats
$SDSO_3$ (1%)	Bubbles form and go up to solution surface, but particle doesn't float
(2%)	Particle takes 2-3 sec to float
$SDSO_4$ (1%)	Bubbles form and go up to solution surface, but particle doesn't float
(2%)	Flotation rate in case of $SDSO_4$ < Flot.rate in case of $SDSO_3$
Oleic acid	Added as it is, particle stays at surface of the solution (air-water interface) with formation of many small bubbles.
Arlacel Span-20 G-1096 Brij-97 Arlatone T Tween-21	Common observations for non-ionic surfactants: No significant change in behaviour of different non-ionic surfactants used The flotation of high dolomitic particle after 3-5 seconds and stay at the surface, while the low dolomitic does not float.
Tween-85	Formation of stable bubbles on the floated particle surface

Surfactant dosage

The results of different dosages of surfactant sodium dedocyl sulfonate (SDS) are shown in Table 3-7 in terms of bare and coated particles. It is indicated from Table 3-7 that bare particles, without coating, forms bubbles quickly and in large quantity due to rapid dolomite/acid reaction but the bubbles are not stable at the interface where they can be collected.

Table 3-7. Effect of surfactant concentration ($SDSO_3$, 2%)

	$SDSO_3$ (2 %)		
	2 %	4 %	6 %
Particle without coating	▪ Many bubbles formed ▪ Small particle (1-2 mm) floats ▪ Large particle (3-4 mm) goes up and down	▪ Many bubbles formed ▪ Particles (1-2 mm) and (3-4 mm) float	▪ Many bubbles formed ▪ Particles (1-2 mm) and (3-4 mm) float
Particle coated with $SDSO_3$	Many bubbles formed -small particle floats-large particle does not float		

On the other hand, the coated particles take more time to float due to the diffusion of acid through the surfactant layer around each particle. Also, a greater number of bubbles are formed when no coating is used. Finally, when coating is not used each bubble forms as a separate bubble, while formation of bubbles clusters occurs when with a coating with SDS is used.

Increasing the surfactant concentration increases the flotability of the particles and large particles (3-4 mm) can float at high surfactant concentrations of up to 4 %; after that, there is no noticeable change in floatability—(i.e., 6 % is very much similar to 4 %). The oscillated motion of large particles (3-4 mm) for short period of time (3-5 sec) was noticed at 2 % surfactant concentration; however, the same size floats without oscillation at 4 % and 6 %. This means more surfactant is needed.

Particle size

The particle size effect on the RF process was studied for coated and uncoated particles. The observations of different size ranges were recorded in Table 3-8 which indicates that the coating affects the stability of the bubbles on the particle surface as well as the stability of the floated particle at the interface; however, even uncoated particles

release many bubbles and float quickly for very short time due to their rapid reaction with acid.

Table 3-8. Effect of particle size on the dolomitic particle floatability

	Particle Size, mm			
	0.5-1	1-2	2-4	4-6
Without treatment	Particle floats and stays at water/air interface	Particle floats for few seconds then oscillates	No flotation -the particle oscillates without reaching the interface	
With treatment	Floats and stays at interface	Floats after 30 sec and stays at (w/a) interface	Oscillates and finally stays at w/a interface	Floats after 1 min then oscillates for 5 min

This rapid rate of reaction causes rapid reduction in particle weight. In addition, it causes the production of many bubbles at a faster rate than bubbles-particle detachment, leading to presence of uncoated particle at the interface, although for shorter time than coated ones. But once the uncoated particle reaches the interface, the bubbles will not be stable anymore due to high surface tension, which is the reverse of coated particles.

Large size particles need more bubbles; the bubbles formed were not enough to lift the particle causing the particle to oscillate up and down. On the contrary, the small particles 1-2 mm and smaller do not oscillate and float directly to the interface.

To improve the stability of the floated particles at the interface, the reduction of the surface tension is required. Therefore, the oil layer was used at the interface for that purpose.

Oil-Surfactant Experiments

Addition of an oil layer, either vegetable or corn oil, to the acidic solution/ air interface was attempted with different types of surfactants to enhance the bubble stability at the interface, as shown in Table 3-9. The selected surfactants for this set of

experiments were the best ones from Table 3-6. The particle was coated with the surfactant before its addition to acidic medium.

Table 3-9. Effect of presence of surfactant and oil layer on particle flotation

	Surfactant	Type	Observations
2 % sulfuric acid solution + oil layer	Arquad Lilamin Ethofat	Cationic	Formation of bubbles due to dissolution of dolomite, but no flotation. Bubble formation,
	$SDSO_3$ $SDSO_4$	Anionic	Particle floats to water/oil interface for 10 min and then comes back to acidic solution.
2 % sulfuric acid solution + 1 % surfactant	Arquad Lilamin Ethofat	Cationic	Formation of cluster of bubbles on particle surface, but no flotation. Bubble formation and particle oscillates and
	$SDSO_3$ $SDSO_4$	Anionic	the bubble bursts at water/air interface.
2 % sulfuric acid solution + 1 % surfactant + oil layer	Arquad Lilamin Ethofat	Cationic	The same as before Bubbles form - No flotation
	$SDSO_3$ $SDSO_4$	Anionic	Bubbles form on particle surface and particle floats to water/oil interface then to oil/air interface

It is clear that, as can be seen in Table 3-9, the oil layer enhance the bubbles' stability on the particle and at the interface. When the particle floats to the acidic medium/oil interface, the floated particle stays at the interface for up to 10 min. The presence of oil layer may add another layer, an oil layer, in addition to the surfactant layer on the particle surface, although this would depend on the adsorption of the surfactant to the particle as well as the type of the surfactant and its interaction with oil.

From Table 3-9, it was observed that the presence of a low percentage of surfactant (1 %) in the acidic solution slightly increases the stability of bubbles in the absence of an oil layer. The presence of 1 % surfactant in the solution may reduce the fast detachment of surfactant molecules from the particle surface through reduction of the diffusion of surfactant molecule to bulk solution.

By using acidic solution in combination with 1 % surfactant and an oil layer (Table 3-9), it was found that the oil layer causes more stable formation of bubbles on the particle when the particle floats to oil/air interface. The particle does not go back into the acid solution but stay at oil/ air interface. Consequently, large particles of up to 3 mm can float in the presence of the surfactant and oil layer.

SDS is a good surfactant under these experimental conditions. However, Ethofat and cationic surfactants did not work well in the presence of surfactant mixed with acidic solution. This may be due to the interaction between the oil layer on the particle and those surfactants possibly causing the formation of a non-flexible surfactant layer, which cannot capture the CO_2 gas and cannot form the bubbles required for flotation.

Poly-Vinyl-Alcohol (PVA) Testing

PVA was used as a viscous polymer to coat and to float the dolomite particles. The effect of acid concentration, particle size, and different PVA concentration were studied.

Effect of acid concentration

PVA forms a membrane on the particle. This membrane needs a high acid concentration to penetrate it and to perform the reaction between the acid and particle surface. It was observed that there were a very small number of bubbles generated. However, most of the bubbles formed a cluster on the particle surface, which increased the volume of the bubbles at the surface and floated the particle. The floated particles were not stable at the beginning, going up and down at interface, but ultimately staying at the interface for long time (sometimes more than 2 days).

On the other hand, PVA also floated the low dolomite-content particles, which were able to form bubbles. This observation is due to PVA's very low permeability by CO_2, which makes it the best among the surfactants used. By increasing the PVA

concentration, longer time was taken to form a bubble and to float the particle, which requires high acid concentration, but in this case it became possible to float large particle sizes (up to 8 mm).

Table 3-10. Effect of acid concentration

	Acid concentration, %			
	0.5	1	1.5	2
Particle coated with PVA	Formation of cluster of bubbles Very low bubble formation rate No particle flotation (up and down at 1.5 %)			Cluster of bubbles formed Low bubble formation rate Particle floats

From Table 3-10, it is evident that the findings were that the PVA forms a membrane on the particle. This membrane needs a high acid concentration to penetrate it and to perform the reaction between the acid and particle surface to release the gas, which is responsible for floating the particle. No quick release of bubbles was observed at low acid concentrations, but rather only a very small number of bubbles at the beginning; furthermore, the rate of bubble formation and particle flotation was very slow. After a while, an increasing number of bubbles appeared and clustered on the particle surface, which then caused the particle to float.

Moreover, at low acid concentrations, the floated particles were not stable, going up and down at the interface due to absence of surfactant. Even at high acid concentrations, the acid takes time to penetrate the PVA membrane and react with particle surface. For that reason, the bubble formation rate was low. But after the formation of bubbles began to cover the particle surface with clusters of bubbles, the particles started to float.

The acid concentrations of less than 2 % were not effective due to the high viscosity of PVA membranes, which requires a high concentration difference to permeate

the membrane and the reach the particles' surface. Because the previous set indicated that the 2 % acid concentration was optimal, another set of experiments was conducted at higher acid concentration (> 2 %) under the premise that a concentration higher than 2 % would be even better. Therefore, additional experiments were conducted using 2.5-4 % acid concentrations. Table 3-11 shows the results of those experiments.

Table 3-11. Effect of acid concentration above 2 %

	Sulfuric acid concentration, %			
	2.5	3	3.5	4
Bubble formation rate	Increases with increasing acid conc. %			
Amount of bubbles formed	Cluster of bubbles formed on the particle surface			Rapid reaction no stable bubbles are seen on the surface (bubbles released in high rate from particle surface)
Flotation of dolomite particle	Particle Floats Is more stable than higher acid conc.		Particle floats Less stable than 2.5-3 %	Particle oscillates and finally goes down

There was no flotation at acid concentrations above 3 % due to the high bubble formation rate and absence of stable bubbles that can attach to the surface of the particle and float it. The bubble formation rate increases with increasing acid concentration, 4 % > 3.5 % > 3 % > 2.5 %; however, 2.5-3 % resulted in the most stable bubbles.

Different PVA concentrations (2 %, 3 %, and 4 %) were also used and the experiments indicated that 3-4 % concentration is most suitable for dolomite flotation. However, increasing PVA concentration increased the time it takes each particle to float.

Effect of particle size

Increasing the particle size increased the time needed to float the particle. This can be explained by variation of surface area to weight of the particle ratio, which decreases with increasing particle size. The results of these tests are shown in Figure 3-2.

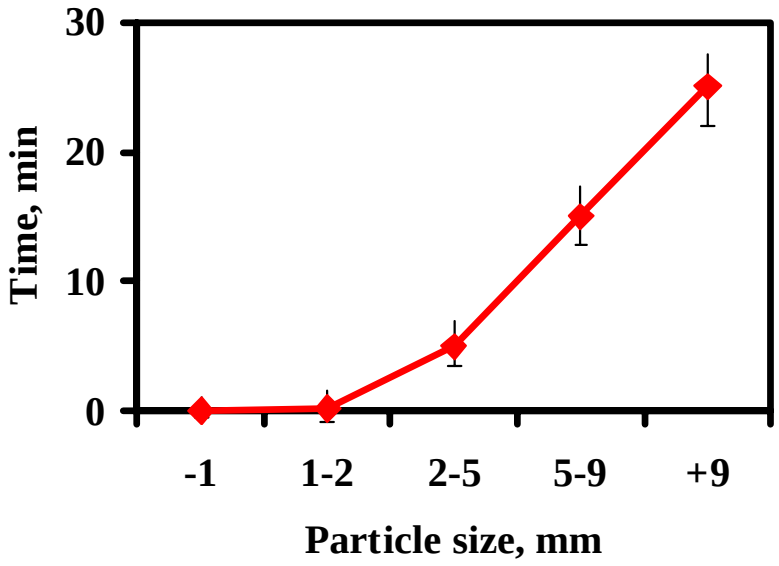

Figure 3-2. Effect of the particle size on the time needed to float the particle in 3 % H_2SO_4 when the particle is pre-coated with 3 % PVA

PVA with acid vs. PVA on the particle surface

By using two beakers, one of them containing uncoated particles added to 3 % PVA + 3 % acid solution and the other containing PVA coated particles added to 3 % acidic solution, the comparison between the performance of different application of PVA was obtained. Table 3-12 shows the results in terms of bubble formation, rate of formation, and particle flotation.

When uncoated particles were added to the PVA+acid solution, the acid attacked the particle surface. Consequently, the dissolution of dolomite is higher than in case of coating the particle with PVA before adding it to the acidic solution. Presence of micro-bubbles (cotton shape) at the particle surface indicated the dissolution of dolomite.

Bubbles were vertically distributed rather than horizontally in first beaker, while the bubble distribution was horizontally uniform (spreading on the particle surface) in the second beaker. The bubble formation rate is higher in the first case than in the second.

The flotation of the particles was better in the second case due to the presence of relatively large bubbles and uniform bubble distribution. Despite rapid dissolution of dolomite particles in the first case, flotation of the particles took a long time due to the small size of the bubbles. In both cases, the particles floated stay at interface for a long period of time (days).

Table 3-12. Comparison between coating the particle before adding it to acidic solution and adding the particle to acid+PVA solution without coating

	First beaker PVA + acidic solution in the beaker and the particle added without coating	Second beaker Particle was pre-coated with PVA before adding it to acidic solution
Bubble formation rate	Tiny bubbles were formed	Relatively large bubbles were formed
Amount of bubbles formed	Cluster of the bubbles grows vertically and cover parts of the particle surface— no uniform distribution of the bubbles on the particle surface.	Cluster of the bubbles grows almost horizontally and uniformly distributed on the particle surface.
Flotation of dolomite particle	Takes long time (hours) to float	Takes short time (min) to float

Preliminary Testing Using PVA Coated Particles

In the following preliminary tests, all particles were pre-coated with PVA

Flotation of a Representative Sample

Flotation of a representative sample, a mixture of phosphate and dolomite, was attempted in a one-liter beaker. The percentage of floated fraction by weight obtained after 6 hours was about 22 % and un-floated fraction was about 78 %. It was noticed that the smaller particle sizes (less than 1mm) floated immediately. It was then determined that using small size fractions of about 1 mm coated with PVA would reduce the flotation time with very low chance to dissolve the particle; it appears that good PVA coating

prevented rapid acid-attack to the particle. On other hand, we should take into account that the PVA consumption will increase due to increased surface area.

Fraction of Representative Sample (-4+1.19 mm)

A bucket (11 in diameter and 15 in height) was filled with a solution of 15 liters of water containing 3 % sulfuric acid and 3 % PVA. The water height in the bucket was about 1 foot. Most of the particles were in monolayer form to avoid mechanical entrapment of the particles.

After applying the finalized procedure, the MgO percentage in the representative sample was reduced to less than 1 % of the sink fraction; P_2O_5 percentage was reduced to less than 4 % (Table 3-13).

Table 3-13. Results of representative sample (- 4+1.19 mm particle size)

Sample	Chemical analysis, %				Recovery, %			
	Wt%	MgO	CaO	P_2O_5	I.R.	MgO	CaO	P_2O_5	I.R.
Float	14.55	13.21	32.56	2.71	6.89	75.1	13.73	2.33	10.01
Sink	85.45	0.75	34.83	19.35	10.55	24.9	86.27	97.67	89.99
Balance	100	2.56	34.50	16.93	10.02	100	100	100	100
Feed	100	2.6	34.78	16.84	10.32	100	100	100	100

Effect of Time on Weight Percentage of Floated Particles

Two samples of - 4+1.19 mm size were gathered at different flotation time (30 min and 60 min). The samples were immersed in a beaker containing a solution of 3 % PVA and mixed to ensure the coating of all particles with PVA before adding the sample to acidic water (3 % sulfuric acid). The same bucket as in the previous test was used and at the same conditions. Each experiment was observed for two days and the floated fraction was collected. Most of the particles (about 90 %) floated within 30 minutes and about 10 % in the remaining two days of the experiment. The results are shown in Table 3-14.

Table 3-14. Effect of time on the flotation of - 4+1.19 mm particle size

Time, min		Wt%	Chemical Analysis MgO%	CaO%	P_2O_5%	Recovery MgO%	CaO%	P_2O_5%
30	Float	16.75	13.62	24.25	0.76	77.84	13.55	0.8
	Sink	83.25	0.78	31.12	18.89	22.16	86.45	99.2
	Balance	100	2.93	29.97	15.73	100	100	100
	Feed	100	3.03	30.38	15.76	100	100	100
60	Float	17.44	13.6	26.17	0.94	78	15.22	1.03
	Sink	82.56	0.81	30.8	19.06	22	84.78	98.97
	Balance	100	3.04	29.99	15.90	100	100	100
	Feed	100	3.03	30.38	15.76	100	100	100

The percentage of MgO was reduced to about 0.8 %; the percentage of P_2O_5 was reduced to less than 1 % in the float fraction, which indicates that using PVA in a pre-coating solution is a promising process for separation of dolomite from phosphate pebbles.

Effect of Size on the Flotation

Two samples were crushed in a closed circuit to obtain the following sizes: -4+1.19 mm and -3.36 +1.19 mm. The conditions were the same as in the previous two tests. The results of these tests are shown in Table 3-15 within 5 minutes flotation time. The percentage of MgO was reduced to less than 1 % (0.6 % of the un-floated fraction in first experiment and 0.95 % in the second).

Table 3-15. Effect of particle size on flotation

Size, mm	Sample	Wt%	Chemical analysis, % MgO	CaO	P_2O_5	I.R.	Recovery, % MgO	CaO	P_2O_5	I.R.
-4+1.19	Float	20.5	12.13	30.34	3.31	8.1	83.9	20.55	4.27	17.87
	Sink	79.5	0.6	30.24	19.13	9.6	16.1	79.45	95.73	82.13
	Balance	100	2.96	30.26	15.89	9.29	100	100	100	100
	Feed	100	3.03	30.38	15.76	9.46	100	100	100	100
-3.36+1.19	Float	17.8	11.84	34.53	3.86	7.04	72.96	16.43	4	12.84
	Sink	82.2	0.95	38.02	20.07	10.35	27.04	83.57	96	87.16
	Balance	100	2.89	37.40	17.18	9.76	100	100	100	100
	Feed	100	2.95	37.07	17.41	9.93	100	100	100	100

Summarizing Remarks

Separation of dolomite from apatite using CO_2 generated in the chemical reaction between dolomitic particles and slightly acidic media was explored by testing different parameters effecting this process, including: acid type and concentration, surfactant type and concentration, particle size, and use of polymer (PVA). The results were promising with anionic surfactants, especially $SDSO_3$, and Mr. Bubble solution with a concentration of 1.6 % sulfuric acid; however, low dolomite-content particles did not float.

The most encouraging results were obtained with PVA, which floats the low dolomite-content particles, in addition to floatation of large particle sizes. Additional testing with a representative sample of ore mixture (phosphate and dolomite) showed the ability to reduce the MgO content to less than 1 % by using a PVA concentration of 3 % in an acidic medium concentration of 3 %. The next step will be the optimization of the RF process using PVA as well as performance of this process under dynamic conditions.

CHAPTER 4
OPTIMIZATION OF THE REACTIVE FLOTATION PROCESS AND PILOT SCALE TESTING

Introduction

In previous chapter, it was demonstrated that when PVA coated high MgO phosphate rock is immersed in a 3 % sulfuric acid solution, effectively all the high MgO particles will float to the surface leaving a sink phosphate rock phase that is a low in MgO. In this chapter, the optimization of separation process using PVA as well as development of a separation continuous process is discussed.

In this chapter, the RF is optimized using statistical designs (i.e., screening statistical design and central composite design (CCD)). Also, the reduction of PVA consumption was studied using statistical design, (i.e., factorial design). The tests show that as little as less than one pound of PVA per ton of feed rock can be effective in floating the dolomite. The tests also show that there is no significant adverse effect of having the sulfuric acid solution saturated with calcium sulfate. Furthermore, pilot scale testing of a simple sluice was carried out and demonstrated the effectiveness of this approach in giving a good separation between the phosphate and dolomite particles.

Optimization of the RF Process

Screening Statistical Design

The MgO % removal in floated fraction, Table 4-1, was used as the response in calculating the statistical effect of variables. The effect of variables are calculated as follows:

Table 4-1. The MgO % removal in floated fraction for Plackett-Burman design.

Runs	Response (MgO % removal)
1	3
2	3
3	3
4	3
5	86
6	90
7	3
8	12
9	3
10	20
11	3
12	3

$$E_i = \frac{\sum \mathrm{Re}sponse_{(+)} - \sum \mathrm{Re}sponse_{(-)}}{6} \quad (4.1)$$

The variance is estimated by evaluating the effect of dummy variables and using this equation:

$$\sigma^2 = V_{eff} = \frac{\sum E_d^2}{n} \quad (4.2)$$

where Ed = effect of dummy variable and n = number of dummy variables = 5. The statistical significance of the effects is evaluated using the student t-test as calculated using:

$$t = \frac{E_i}{\sqrt{\sigma^2}} \quad (4.3)$$

where the degrees of freedom = 5, confidence level = 95 % and $t_{5,0.05} = 2.015$. Comparing the absolute t-values to 2.015 led to acceptance of variables with a higher t-value and rejecting the variables with lower t-values. In other words, the variables accepted were significant within 95 % confidence level. This comparison of the Plackett-Burman design is presented in Table 4-2. The PVA molecular weight t-value is 2.761,

which is higher than 2.015. Nevertheless, the higher PVA molecular weight was used because of its significance. From the Plackett-Burman design, the most significant variables are acid concentration, PVA concentration, and particle size.

From the screening design, a model relating the MgO % removal to the different variables could be represented by:

$$y = -91.75 + 14.83X_1 + 12X_2 - 3.2X_3, \quad (4.4)$$

where y represents MgO % removal and X_1, X_2, and X_3 represent acid concentration, PVA concentration, and particle size, respectively. All coefficients are statistically significant close to 95 % confidence level. The negative sign for particle size coefficient indicates that increase the particle size can lead to a decrease in the MgO % removal. On the other hand, the positive acid concentration and PVA concentration values indicate that an increase in both concentrations lead to higher MgO % removal. In order to further investigate the interaction among these three significant variables with respect to their effect on MgO % removal, a central composite design focusing on these three variables with five levels was used.

Table 4-2. Plackett-Burman calculated t values for different variables. The decisions to accept or reject the significance of variables on the bases of comparing t-value to critical value at 95 % confidence level.

Factors	Effect on MgO % removal (t-value)♣	Significant Variable
Sulfuric acid concentration	2.69697♦	Accept
PVA concentration	2.181818♦	Accept
PVA Molecular Weight (MW)	2.969697♦	Accept
PVA degree of hydrolysis (D.H.)	0.181818	Reject
Particle size	- 2.45455♦	Accept
Drying time	0.333333	Reject

♦Statistically significant (95 % confidence level)
♣(+ ve) sign indicates more MgO % removal
♣♣(- ve) sign indicates less MgO % removal

Central Composite Design

Central composite design (CDD) results of dolomite flotation experiments are given in Figures 4-1 and 4-2 in terms of MgO removal % in floated fraction and MgO % in sink (nonfloat) fraction respectively. The confidence interval is within 95 %. In other words, the effects are statistically significant at the 95 % level. The standard deviation and R-Squared for both of them are 13, 0.9287 and 0.36, 0.9287 respectively.

It was indicated, from these figures, that the % MgO recovery and MgO % in concentrate are greatly and positively affected by increasing either acid concentration or PVA dosage, (i.e., % MgO recovery increases from 30 to more than 90 % and MgO % in the concentrate decreases from more than 2.1 to 0.6 respectively). However, particle size negatively affects the % MgO recovery and MgO % in concentrate. With increasing particle size the % MgO recovery decreases. At the maximum acid concentration and PVA dosage, it decreases from 90 to 75 % and % MgO concentration in the concentrate increases from 0.6 to 1.1 %.

As it can be seen from these results that the PVA consumption is high (about 4.5 lb/t), which is economically unfeasible, to get a concentrate contains < 1 % MgO with high recovery > 90 %. Therefore, further study is needed to reduce that consumption, which is discussed in next section.

Research to Reduce the PVA Consumption

From the results obtained from the experimental designs following the screening the main factors, then studying the main factors, unfortunately, the PVA consumption was about 4-6 lb/t (calculated according to used amount of PVA to certain weight of rock including the losses on the coating device), which threaten the success of this process economically. At this point, it was necessary to find a method to reduce the consumption.

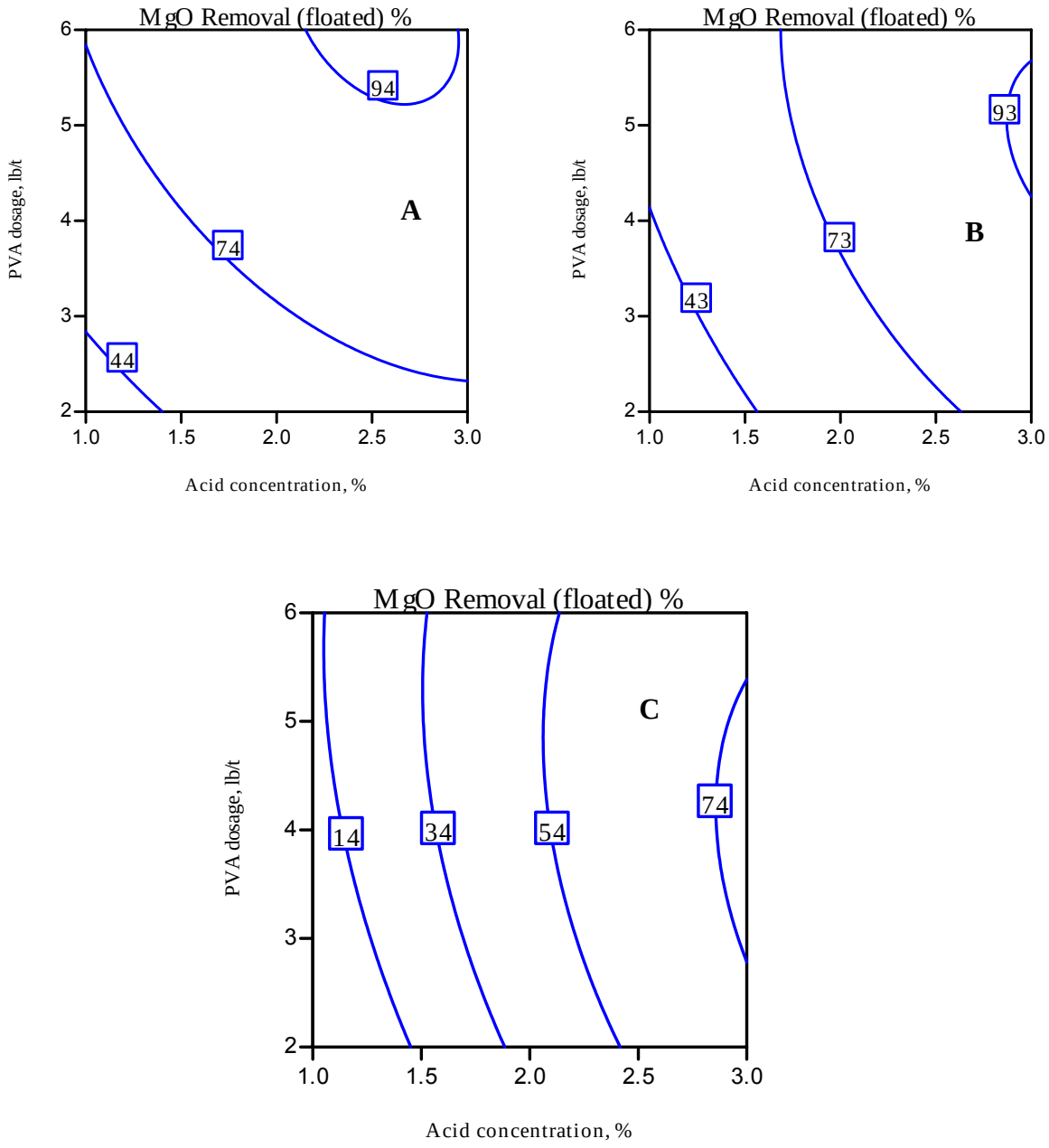

Figure 4-1. Effect of PVA dosage and acid conc. on MgO recovery % in floated fraction at different particle size

A) Particle size = -0.5 mm

B) Particle size = 1-2 mm

C) Particle size = 5-9 mm

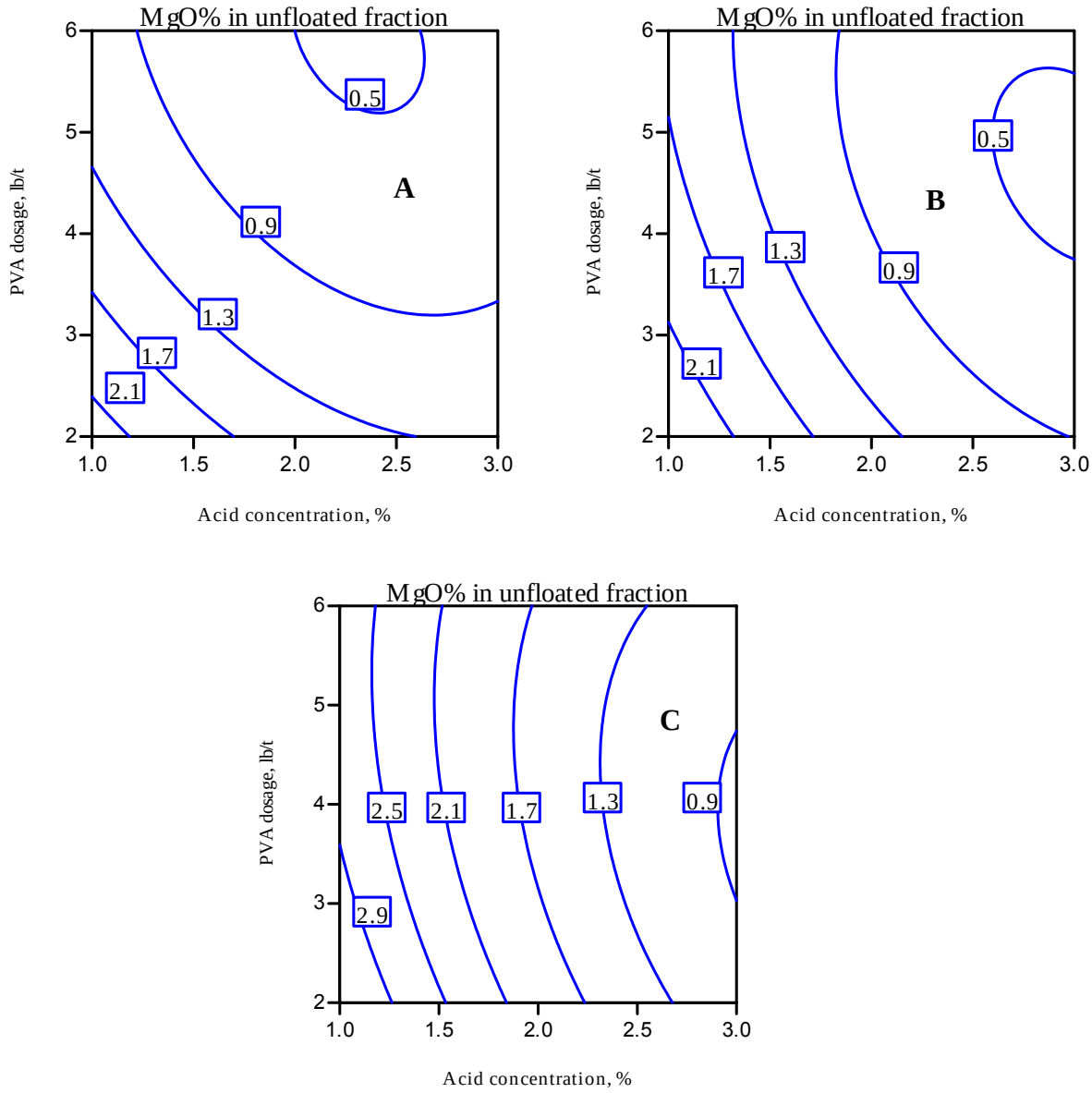

Figure 4-2. Effect of PVA dosage and acid concentration on MgO % in Unfloated fraction at different particle size

A) Particle size = -0.5 mm

B) Particle size = 1-2 mm

C) Particle size = 5-9 mm

In this regard many tests were conducted among these tests were:

- Using compatible compounds with PVA like starch and cellulose. It was found that the presence of these compounds negatively affected the stability of the bubbles at the interface.

- Using fine particles (- 40 mesh) with different PVA (1, 2, 3 %) and acid conc.(1, 2, 3 %). It was found that the 3 % PVA and 3 % acid were needed which is the same condition as before and in addition the reaction was too fast due to the high surface area of the small particles.

- PVA + Drimax (spreading agent): to spread the PVA on the particle surface and then reduce the amount needed to cover the particles. The results of these experiments indicates that there is an interaction between the PVA and Drimax in such a way that prevented the formation of stable bubble at the particle / solution interface, probably by interfering with the crosslinking of the polymer layers that is necessary for the formation of a membrane and consequently stable bubbles.

- PVA + Boric acid: as it is in the literature [Finch, 1973; 1992], the boric acid and borax are used in PVA crosslinking. Using the boric acid (5 % of PVA) helps in reducing the PVA consumption due to polymer crosslinking but we did not go further in these experiments because of toxicity of boric acid and environmental reasons.

- PVA + Na_2SO_4: sulfate ions lead to coagulation of the PVA according to literature [Finch, 1973; 1992]. It was found that the coagulation is not enough to float the dolomite particle at low PVA concentration.

- Conditioning of the rock particles with PVA and screening it (or filtering it) to recover the excess PVA. Actually, this step was a most promising one in which the consumption of PVA was reduced to 1 lb/t instead of 4-6 lb/t in previous coating procedure. The conditioning step (with about 1 % PVA) in the same manner as a regular flotation is followed by a filtration step and calculation of the actual PVA consumption.

  On the other hand, it was found that the full coverage of the particle with PVA is not needed since the formation of some bubbles may be enough to create the density difference and by using sluice or spiral in which the dolomite particles will be lighter and follow the liquid stream. In this manner, the dolomite particle can be separated from the phosphate.

Experimental Design of the PVA Conditioning Step

Due to the high PVA consumption as indicated from experimental designs, different methods were tested as mentioned before, the conditioning step as in regular flotation circuits was tested since this step can reduce the consumption to one-fourth or more (The PVA consumption was reduced to 1-2 lb/t from 4-6 lb/t). For that reason statistical design with three factors, (i.e., conditioning time, PVA concentration, and pulp density) was used. It is indicated, from Figure 4-3, that the PVA concentration is the main factor and then the conditioning time while the pulp density (solid liquid ratio) has a very slightly effect on the % MgO in the concentrate and % MgO recovery in floated fraction.

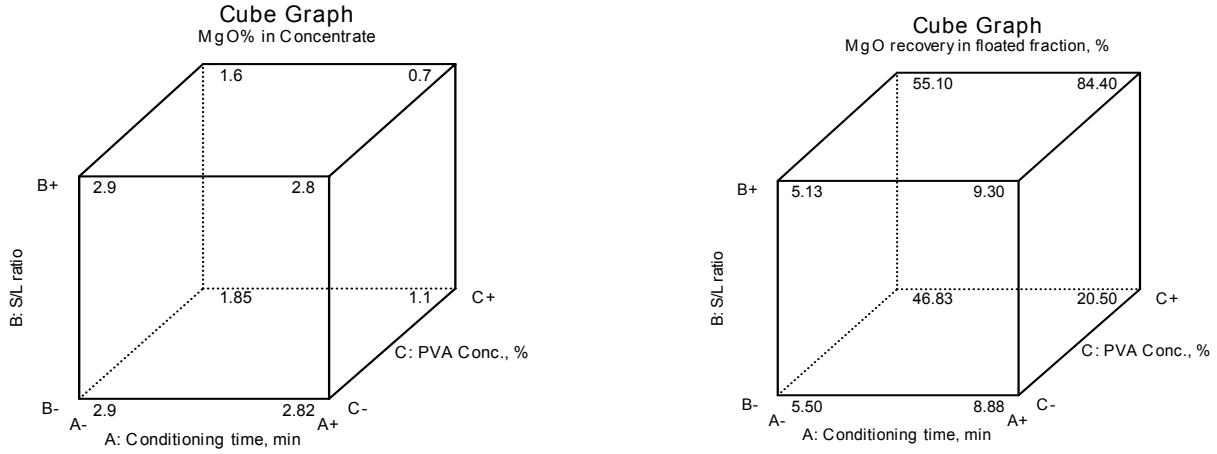

Figure 4-3. Cube graph for MgO % and MgO recovery %

Saturation Experiment

The $CaCO_3$ was used to saturate the solution with calcium sulfate by adding $CaCO_3$ to 3 % sulfuric-acid solution. The formation of the precipitate of $CaSO_4$ indicated that the solution was saturated. It was found that 1.78gm/l of $CaCO_3$ would cause the precipitate to form. After the formation of the $CaSO_4$ precipitate, the flotation test was run as an indication of the acid performance after its saturation. Table 4-3 shows the results of these experiments before and after the saturation is reached.

Table 4-3. Effect of saturated acid on the RF

	Before saturation			After saturation		
	Wt%	MgO%	P_2O_5%	Wt%	MgO%	P_2O_5%
Float	22.1	11.1	4.2	21.3	10.95	4.15
Sink	77.9	0.8	21.1	78.7	0.85	21.2

Pilot Scale Testing: Sluice Results

It was shown that the PVA consumption could be reduced to 1 lb/t on lab scale. Testing of the reactive flotation process using a simple sluice was conducted on pilot scale. Starting from the point that the formation of the bubbles on the dolomite surface creates a density difference between dolomite and phosphate particles. Therefore, the gravity separators are the promising techniques to do this separation.

In that regard, two tests were run using the sluice under two different coating conditions. The first was spraying the particles with 3 % PVA solution before adding the particles to the sluice and the second was conditioning the particles in 1 % PVA solution and screening the particles to remove the excess PVA solution to reuse it (the PVA consumption is estimated to be 0.8 lb/t), then adding the particles to the sluice. The results of these two tests are given in Table 4-4. From these results, it can be seen that by applying the optimum conditions, the reactive flotation process can reduce the MgO % to less than 1 % with high recovery. In the rest of this work, the fundamental interpretations of what are observed experimentally were carried out.

Table 4-4. Comparison of two different coating methods and their effects on MgO removal

Sample	Coating					Conditioning				
	Wt%	MgO%	P_2O_5%	CaO%	I.R%	Wt%	MgO%	P_2O_5%	CaO%	I.R%
Float	20.74	12.3	2.9	32.82	9.8	20	12.41	2.85	33.55	10.01
Sink	79.26	0.65	22.3	38.33	11.22	80	0.68	21.90	37.93	11.14
Calc. Feed	100	3.06	18.27	37.19	10.97	100	3.03	18.09	37.05	10.93
Feed	100	3.04	18.13	37.45	11.05	100	3.04	18.13	37.45	11.05

CHAPTER 5
FUNDAMENTAL STUDIES

Polyvinyl alcohol-Particle Interaction

Introduction

Generally, adsorption of a polymer is utilized in many applications, such as: dispersion of particles, flotation, flocculation processes, treatment of surfaces, etc. If a solvent is a poor solvent (i.e., the interaction energy between the polymer segment and the solvent molecules is unfavorable when compared to polymer-polymer or solvent – solvent molecular interaction energy), then the effective polymer –surface interaction can be strongly attractive and the polymer will seek any opportunity to minimize the contact points with the solvent. Hence, in cases where a poor solvent is used, adsorption will increase on almost any surface, even the liquid-air interface. Adsorption is, therefore, always accentuated before precipitation will occur. The surfaces will act as a nucleation sites for polymer precipitation. This means, the poorer the solvent, the higher the adsorption and vice versa. In addition to the solvent quality, there are other factors that can affect the polymer adsorption and change its conformation, including: polymer molecular weight, polymer concentration, pH, and ionic strength.

Previous studies of polymer adsorption suggest a number of qualitative trends that have been noticed in most polymer adsorption systems. The most important of them are as follows: many polymers adsorb on a variety of surfaces, Reach a plateau at few mg/m^2, a sharp isotherm sometimes is obtained, and molecular weight is a main factor, especially in a poor solvent.

In this work, the polymer (PVA) is used as a membrane-forming agent to capture produced CO_2 gas on dolomite particles and makes them lighter than other particles leading to their flotation and separation from non-carbonate (apatite) particle.

To understand this process and to elucidate the interaction mechanism between polyvinyl alcohol (PVA) and dolomite and apatite surfaces in the reactive flotation process, different techniques were used, such as: estimation of work of adhesion using surface tension and contact angle measurements, adsorption/desorption isotherms, Zeta potential, and surfaces characterization using Fourier Transform InfraRed (FTIR), etc.; the details of each one of these techniques are discussed in this chapter.

The strength of adhesion to a solid surface can be estimated from the value of the thermodynamic 'work of adhesion' or W_a, a concept first introduced by [Harkins, 1928]. In a simple system where a liquid *L* adheres to a solid *S,* Figure 5-1, the work of adhesion is defined as:

$$W_a = \gamma_l + \gamma_s - \gamma_{sl} \quad \text{..... (5.1)}$$

where γ_s , γ_l and γ_{sl} are the interfacial tensions of the solid/air, liquid/air and solid/liquid interfaces respectively.

The problem with using Equation 5.1 is that, of the three interfacial tensions, only γ_l can be measured with fluid phases, in this case the liquid and air. Those tensions involving the solid cannot be measured independently. Another approach, then, is to combine Equation 1 with the Young-Dupre equation (Equation 5.2), to provide a more useful expression for the work of adhesion [Adamson and Gast, 1997]:

$$\gamma_s - \gamma_{sl} = \gamma_l \cos\theta \quad \text{..... (5.2)}$$

where θ is the contact angle that the liquid makes with the solid surface. Provided that γ_l and θ can be measured experimentally, it is then possible to use Equation 5.3 to calculate the work of adhesion.

$$W_a = \gamma_l (1 + \cos\theta) \quad \text{……..……..……..(5.3)}$$

Therefore, the measurements of surface tension and contact angle are essential towards the calculation of the work of adhesion of the polymer (PVA) with solid surfaces, which will be discussed in the following sections.

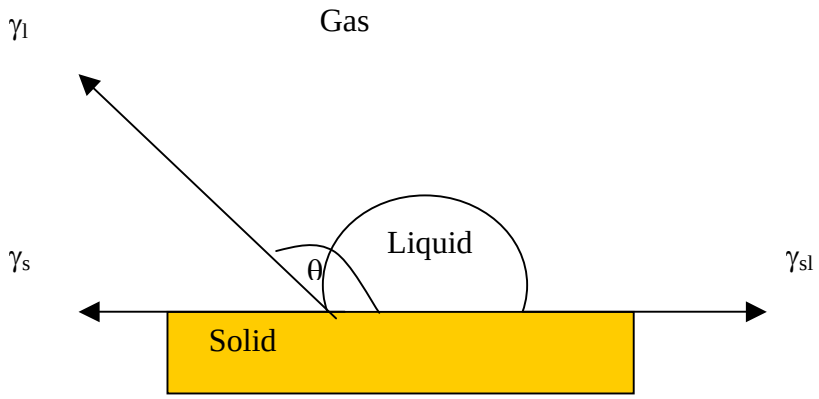

Figure 5-1. Contact angle and interfacial surface tension at solid/liquid/gas interface

Surface Tension

The equilibrium surface tension values of fully hydrolyzed PVA solutions (average Mw =150000) as a function of the initial bulk concentration at room temperature (23 °C) are shown in Figure 5-3. The surface tension of PVA decreases with increasing concentration of PVA until it reaches a region where the surface tension (59 – 60 dyne/cm) no longer decreases with increasing the polymer concentration. The critical concentration at which the surface tension starts to be constant is 1 % PVA in aqueous solution. These results coincide with the literature concerning the surface tension of fully hydrolyzed polyvinyl alcohol (PVA). The fully hydrolyzed polymer has less effect on

surface tension than partly hydrolyzed PVA [Fbiehn and Erusberger, 1951; Kim and Luckham, 1991]. The chemical structure of both is shown in Figure 5-2.

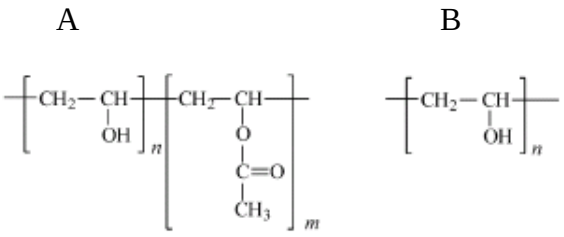

Figure 5-2. Structural formula for PVA: A) partially hydrolyzed; B) fully hydrolyzed.

It is reported that the surface tension reaches a constant level at 1-3 % PVA depending on the PVA molecular weight and degree of hydrolysis [Finch 1973; 1992]. These results are similar to several findings reported in the literature regarding polymer systems; the stabilization of the surface tension of high-*Mw* PEO (> 100000) solutions was associated with the saturation of the air/water interface by the polymer chains [Zeno et al., 2004].

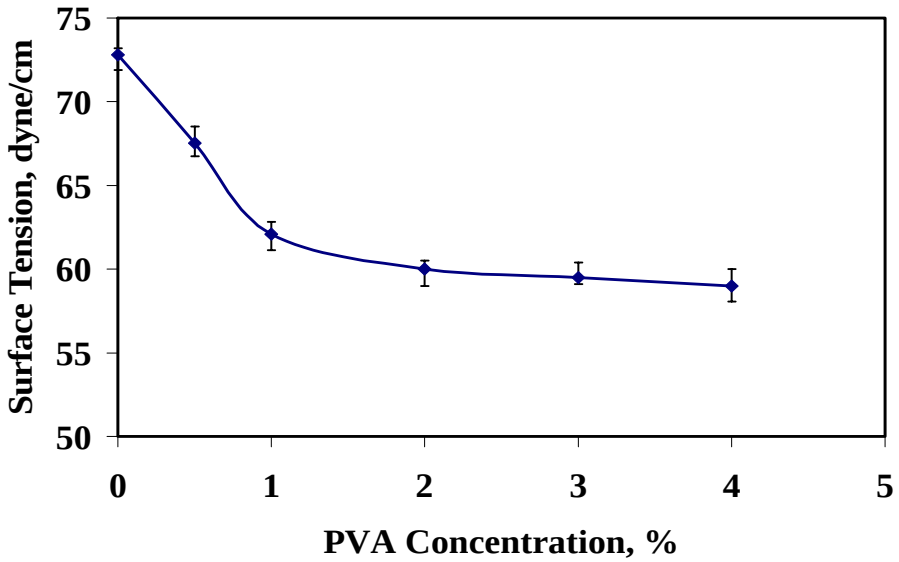

Figure 5-3. Equilibrium Surface tension for aqueous PVA solutions at 23 °C

An explanation of this phenomenon is that the surface activity of a polymer mainly relies on its conformation in the aqueous solution, whereas the conformation of macromolecule depends on its chemical structure and composition, etc. At low concentrations, the chains of macromolecule are stretched in the water due to the formation of hydrogen bonding with water molecules. These long chains lying on the liquid/air interface can dramatically decrease the surface tension of water, even though the adsorbed amount on the liquid/air interface is very small. With the increase of concentration, the polymer's molecules that adsorb on the surface increase and a tight macromolecular film is formed, which makes the surface tension decrease. When the polymers occupy all the surface of solution, the adsorption reaches a level of saturation corresponding to the lowest value of surface tension. As this concentration further increases, the polymers in the solution begin to aggregate and form micelle-like clusters; at this point, the surface tension shows no more changes. In the case of PVA, it may also be related to degree of crystallinity due to formation of hydrogen bonding as indicated in Figure 5-4 [Finch 1973].

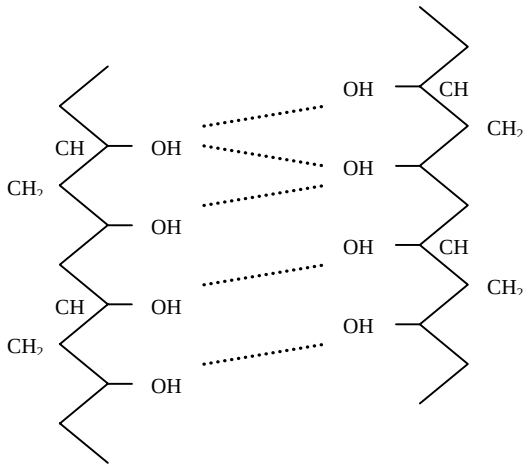

Figure 5-4. PVA crystal structure; the dotted lines indicate hydrogen bonds.

It is expected that the surface tension will have higher values in the presence of the acidic media since the $SO4^{-2}$ ions increases the surface tension, affects the polymer solubility, and enhances the formation of polymer aggregates at even a slightly high acid concentration [Sun, 1994].

Contact Angle

The phenomenon of wetting or non-wetting of a solid by a liquid is better understood by studying contact angle, which is the most universally applied method of quantifying wettability. Contact angle methods have been developed extensively over the past four decades. The contact angles of dolomite and apatite surfaces with PVA aqueous solutions at different concentrations are shown in Figure 5-5. From the figure, it can be seen that the contact angle increases with the increase of PVA concentration for both minerals' surfaces. This phenomenon can be explained by the structure of PVA in the solution shown in Figure 5-4. When a droplet of PVA placed on the surface of dolomite or apatite, the PVA adsorbs to the surface by hydrogen bond. As the PVA concentration increases, more and more hydrogen bonds form; as a result of hydrogen bonds among its molecules, the PVA begins to form clusters. These clusters result in a local viscosity increase, which controls the droplet shape as well as its tendency to spread. This, in turn, increases the contact angle accordingly.

The dynamic behavior of the molecules, their conformation at solid-liquid interface, and diffusion of macromolecules will affect the adsorption of more molecules, with a subsequent increase in contact angle. The increase in contact angle is proposed to result from polymer cluster formation and preferential coverage of the hydrophilic sites by polymer molecules. This phenomenon is observed for PVA and also for some modified PVA end groups [Finch 1992].

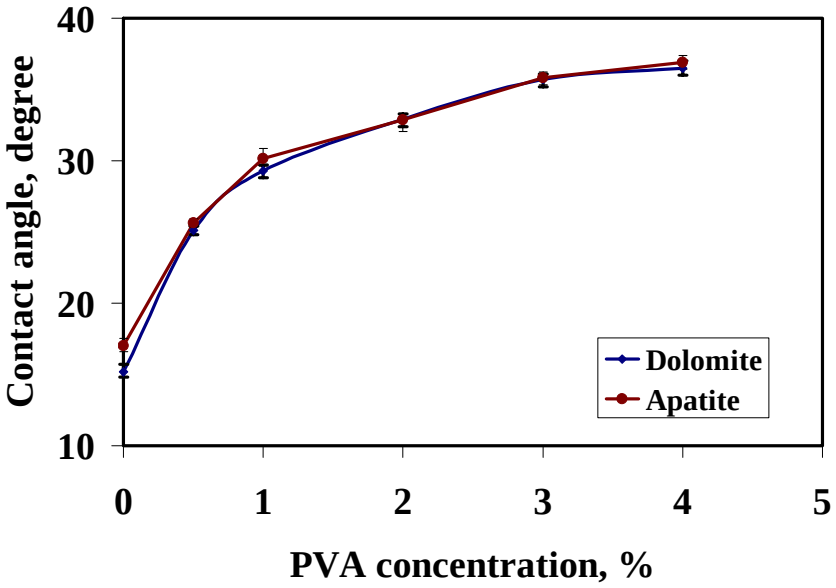

Figure 5-5. Static contact angle variation with the PVA concentration

All measurements shown in Figure 5-5 were conducted immediately after application of the drop. Evaporation of water caused the drop to contract and a consequent change in the contact angle.

Work of Adhesion

Figure 5-6 shows the dependence of work of adhesion, W_a, on the PVA concentration. The work of adhesion decreases with increasing PVA concentration (increase in ΔG, where $W_a = -\Delta G$ [Lloyd, 1994]). The increase in ΔG reflects the formation of polymer clusters and increase of its crystallinity. This is due to the formation of OH-group bonds between PVA molecules causing them to favor adhesion to a solid surface. Additionally, the polymer's diffusivity decreases with higher concentrations.

With increasing PVA concentration, the PVA molecules not only adsorb to the surface but also form hydrogen bonds among themselves. This behavior affects the

conformation of the molecules at the solid-liquid interface till they reach the saturation stage, when the work of adhesion becomes constant. It appears that this saturation stage is the same region of PVA concentration, 1-3 %, at which constant surface tension and contact angle are achieved.

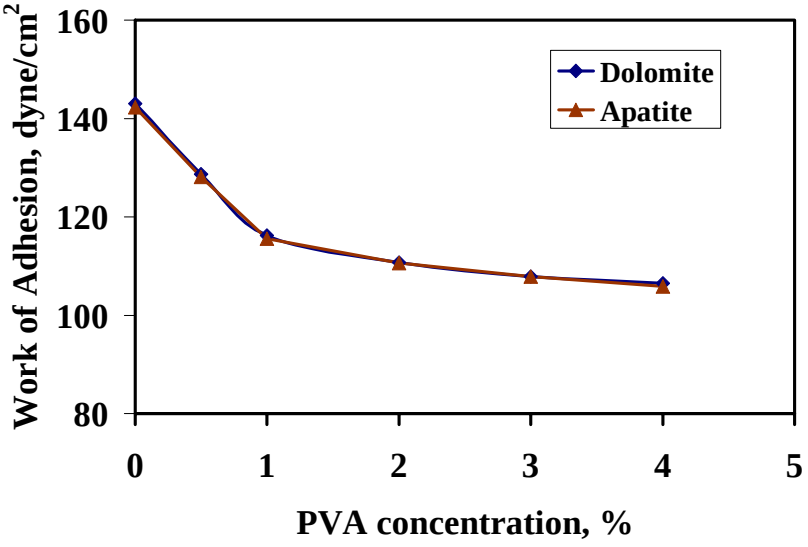

Figure 5-6. Work of adhesion as a function of PVA concentration on dolomite and apatite substrates

Additional Studies

To substantiate the presence of hydrogen bonding hypothesis and to establish an adsorption mechanism additional studies were conducted and their results are discussed in the paragraphs that follow.

Adsorption study: Research grade samples were purchased from Wards Natural Science and used to conduct the adsorption study. These samples were chemically analyzed by the wet chemical method and the results are listed in Table 5-1.

Table 5-1. Chemical analysis of the samples used in adsorption tests

	MgO%	P_2O_5%	CaO%	Al_2O_3%	Fe_2O_3%	I.R.%	L.O.I. %
Dolomite	20.39	0.58	31.6	0.97	0.10	2.52	42.6
Apatite	-	31.73	49.50	2.64	1.04	4.95	5.0

Specific surface area measurements (BET method): The specific surface area of dolomite and apatite particles was determined by the BET in order to be used in adsorption isotherm calculations (applied in the next section). Using nitrogen as the adsorbate, the measured surface areas for dolomite and apatite were 0.9 and 1.48 m^2/g respectively.

Pore size distribution: The results of cumulative pore size distribution for apatite and dolomite are shown in Figures 5-7 and 5-8. It is clear that the apatite has a higher cumulative pore area, 9 m^2/g, than the dolomite, 1.8 m^2/g. Mean pore sizes for apatite and dolomite are 28 $\mathring{A}$ and 42.5 $\mathring{A}$ respectively.

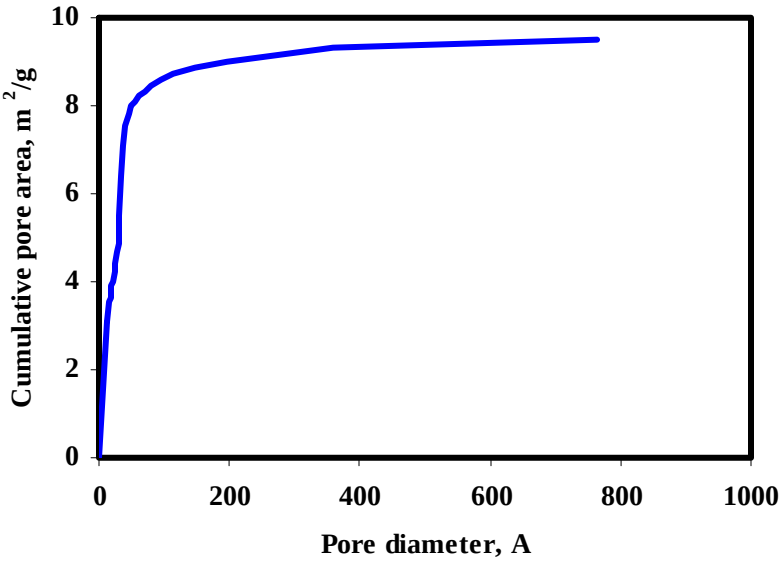

Figure 5-7. Cumulative pore size distribution for apatite sample

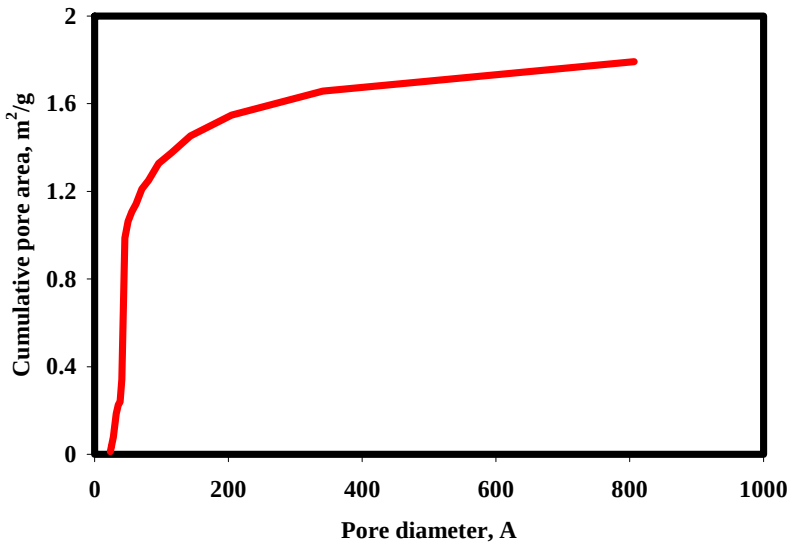

Figure 5-8. Cumulative pore size distribution for dolomite sample

Zeta Potential

In order to obtain a more detailed description of the adsorption and electrical properties of the solid–solution interface, measurements of the zeta potential were taken. The tendency of zeta potential to vary with nonionic polymer adsorption may be caused by one of two different factors: 1) the shift of the position of the shear plane, or 2) the blocking of the active sites on the surface by adsorbing polymer chains. The participation of these effects was estimated by the determining the difference in the values of the zeta potential with no polymer and with polymer present. The use of a KNO_3 solution ($3X10^{-3}$ M) acted as a control in these experiments.

The results of measuring the zeta potential of apatite and dolomite in $3X10^{-3}$ KNO_3 solution as function of pH are presented in Figure 5-9. It can be seen that the iso-electric points (IEP) of apatite and dolomite are about 6.8 and 9, respectively. This is in agreement with the results reported in the literature [Amankonah and Somasundaran, 1985; Chander and Furestenau, 1982; Pugh and Stenius, 1985].

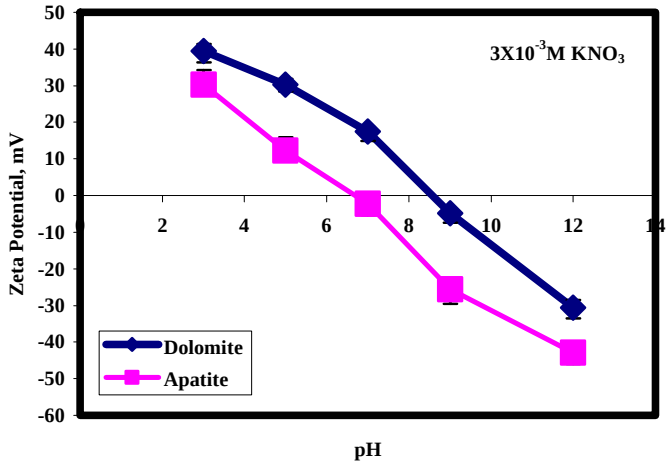

Figure 5-9. Zeta potential of dolomite and apatite samples

Zeta potential in the presence of PVA was determined as well. Figures 5-10 and 5-11 show the results of measuring the zeta potential in the presence of a PVA solution. It is evident that the presence of PVA does not change the IEP of the apatite or dolomite. It does, however, cause compression in the electrical double layer.

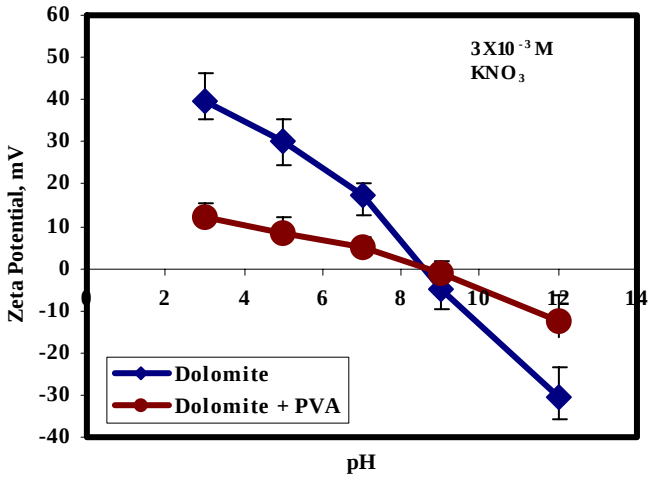

Figure 5-10. Zeta potential of dolomite in absence and presence of polymer

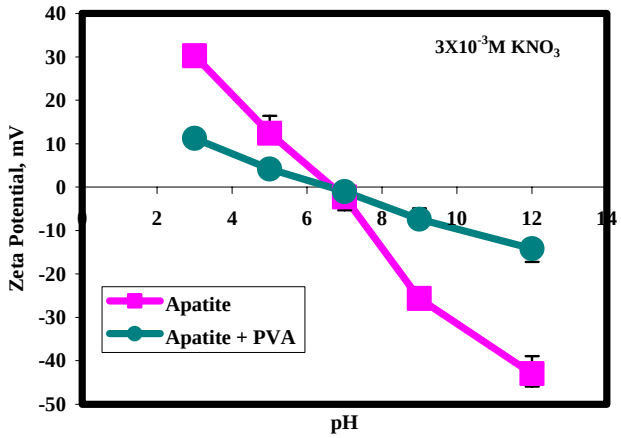

Figure 5-11. Zeta potential of dolomite in absence and presence of polymer

The results indicate that the surface sites remain accessible to potential determining ions (H^+ and OH^-) and the IEP remains unchanged during PVA adsorption, thus implying that the polymer does not alter the surface potential. It can be considered, as other investigators asserted [Ottewill, 1967; M'pandou and Siffert, 1984;1987; Luckham et al., 1983] that the decrease in zeta potential relating to adsorption of PVA is not due to a decrease in charge and surface potential, but rather to a shift of the shear plane (Figure 5-12).

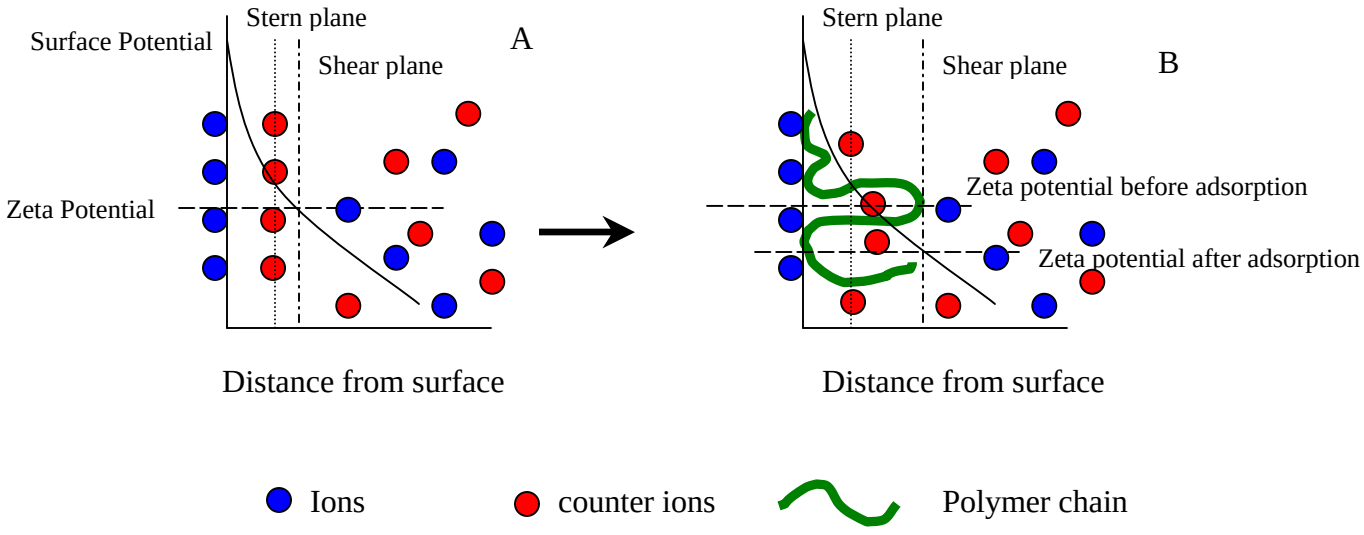

Figure 5-12. Effect of polymer on the shear plane position, A) without polymer, B) after polymer adsorption

In short, the changes of the zeta potential produced by the adsorption of substances with high molecular weight, result from blocking of the active sites on the minerals' surface and as well as from the shift of the shear plane.

Zeta potential of minerals in supernatant solutions

In natural ores, the dolomite and apatite form a mixture. Their presence together may affect the adsorption of the polymer on both of the minerals' surfaces. Therefore, the adsorption on the dolomite in presence of apatite supernatant and apatite in presence of dolomite supernatant were studied.

The effect of the supernatant of dolomite on the zeta potential of apatite is shown in Figure 5-13. The results show that the apatite surface becomes more positive over the entire pH range and that the IEP has shifted from 6.8 to 8.6. Both effects are hypothesized to be due to the presence of calcium and magnesium ions in the solution.

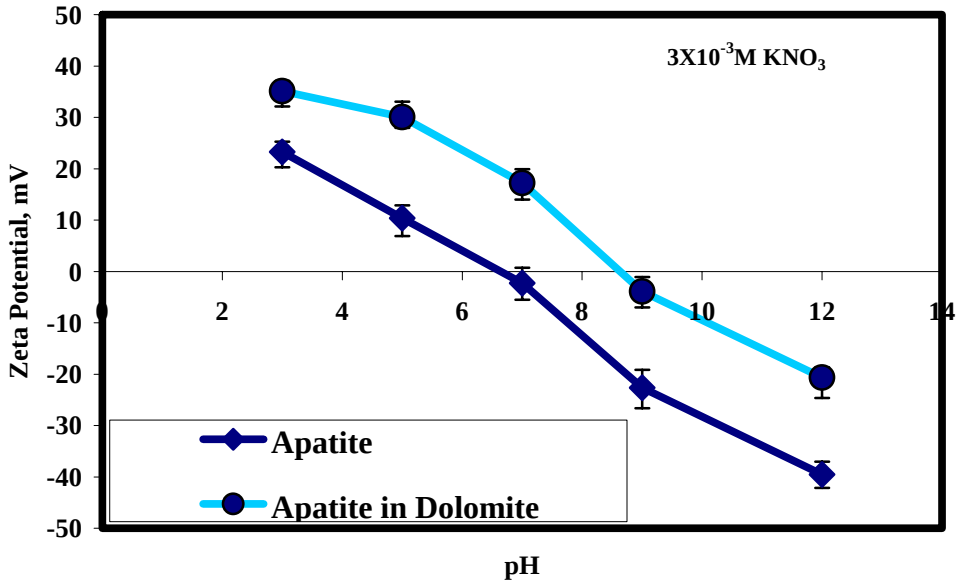

Figure 5-13. Zeta potential of apatite and apatite in dolomite supernatant

Similarly, the zeta potential of dolomite in an apatite supernatant was measured as a function of pH. The results, given in Figure 5-14, show the zeta potential of dolomite to be reduced drastically in presence of apatite supernatant. The IEP shifts from 9 to 6.5.

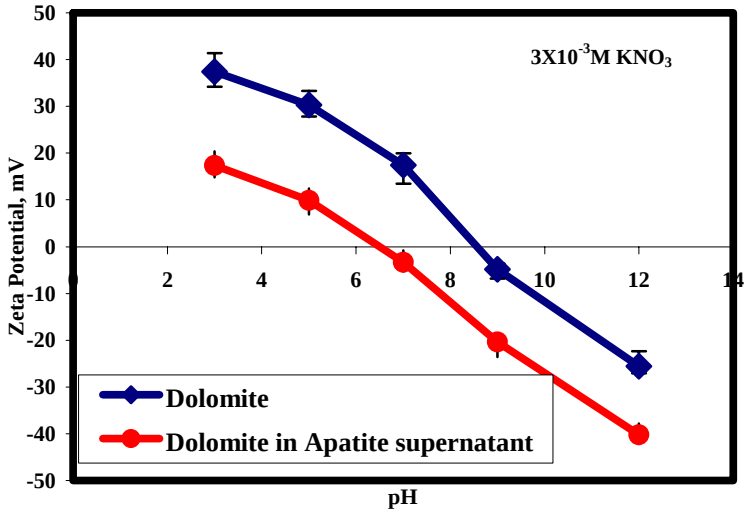

Figure 5-14. Zeta potential of dolomite and dolomite in apatite supernatant

Zeta potential in the presence of PVA

Moreover, the zeta potential of dolomite in apatite supernatant in presence of PVA was determined. The results in Figure 5-15 indicate that the PVA deals with surface of dolomite, when suspended in an apatite supernatant, as an apatite surface. This is due to the faster diffusion of small ions and molecules from the solution to the dolomite surface, which converts it to surface similar to apatite. As can be expected, the movement and diffusion of these ions is quite faster than that of polymer molecules. Consequently, The polymer's role is applied after the surface changing and the adsorption of the polymer appears as if it is on apatite surface.

The same argument mentioned in the previous paragraph can be applied in the case of PVA present with apatite in a dolomite supernatant. The results of the zeta potential of this system are shown in Figure 5-16.

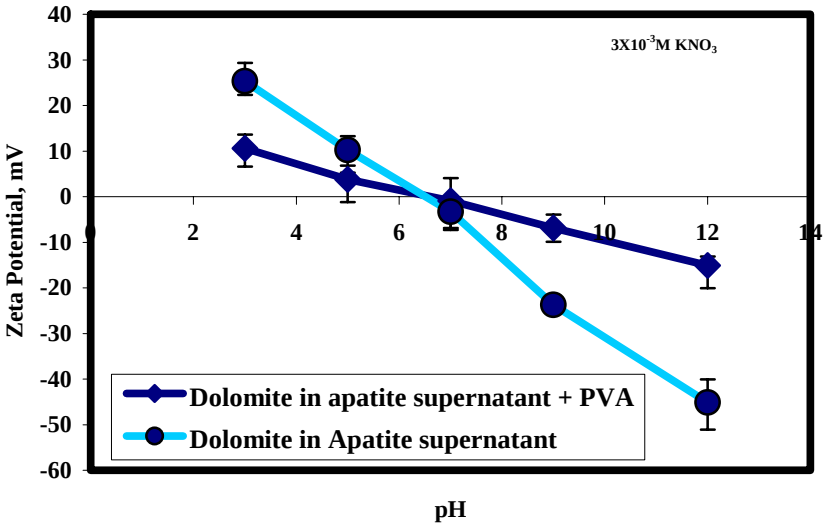

Figure 5-15. Zeta potential of dolomite in apatite supernatant before and after PVA adsorption

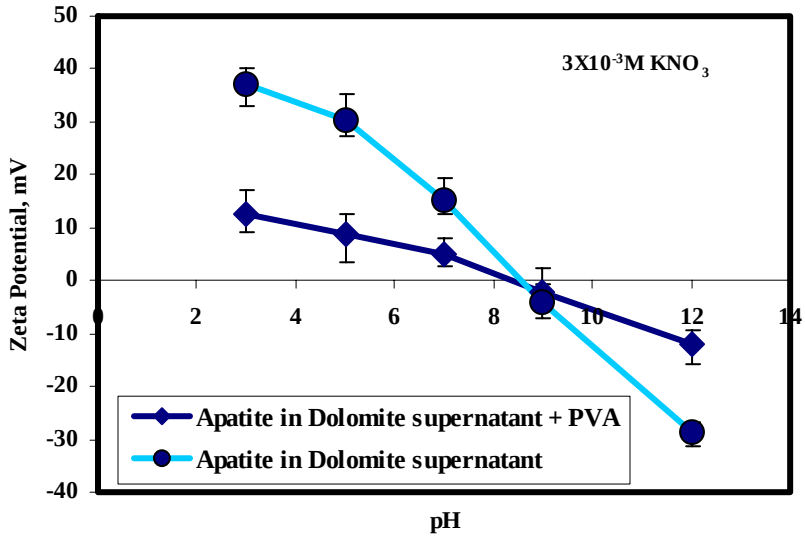

Figure 5-16. Zeta potential of apatite in dolomite supernatant before and after PVA adsorption

Infrared (FTIR)

The FTIR spectra of the powders, both with and without polymer adsorbed to them, were compared in order to obtain the mechanism of adsorption of PVA on dolomite and apatite surfaces. This method was applied in previous studies [Kiselev and Rygin, 1972;

Paradip and Moudgil, 1991; Howard, and McConnel, 1967; Behl and Moudgil, 1993; Bjelopavlic et al., 2000; Zaman et al., 2002; Mathur and Moudgil, 1997; Moudgil and Prakash, 1998] to explain polymer–solid interactions. The major peaks for dolomite and apatite are identified according to Ince et al. [1991] and Farmer [1974].

FTIR spectroscopic studies were carried out on the dolomite and apatite and polymer samples both before and after adsorption. The assignments of the various bands and peaks made in this study are in reasonable agreement with those reported in the literature for similar functional groups [Finch, 1973; Chanchani, 1986; Ince, 1987].

The FTIR spectrum of PVA is shown in Figure 5-17. A broad-band, is displayed at 3450 cm^{-1}, which may be attributed to hydrogen-bonded surface hydroxyl groups. The sharp band at 2930 cm^{-1} is attributed to strong C-H stretching. The band at 2860 cm^{-1} is attributed to shoulder C-H stretching. The transmission band at 1650 cm^{-1} is due to the presence of moisture in the sample. The band at 1460 cm^{-1} can be attributed to O–H and C-H bending. These results are in good agreement with the spectra of PVA reported by other workers [Finch, 1973; 1992].

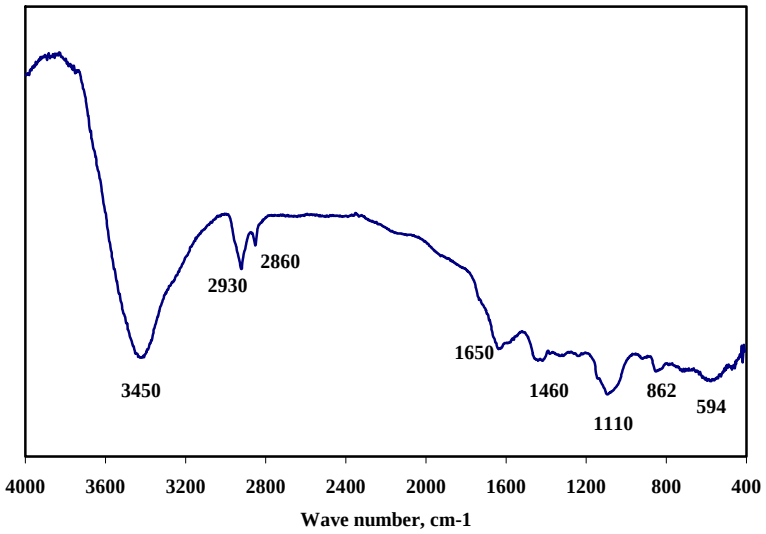

Figure 5-17. Infrared transmittance spectra (FTIR) of poly vinyl alcohol (PVA)

The FTIR spectrum of the bare-dolomite sample as well as those that had previously interacted with PVA is shown in Figure 5-18. The isolated hydroxyl group peak is present in dolomite powder without polymer, but the spectra with polymer shows the disappearance of this peak. Moreover, the peak intensity of the hydrogen-bonded hydroxyl groups is smaller in case of the powder with the polymer than without. These observations indicate that the adsorption of PVA on dolomite occurs by hydrogen bonding involving –OH groups of the polymer. This finding is in concurrence with earlier studies on silica-PEO [Rubio and Kitchener, 1976; Cheng, 1985] and silica-Polyacrylic acid PAA [Tadros, 1978], which showed that the presence of isolated OH-groups on the surface is responsible for the adsorption of polymer molecules by hydrogen bonding.

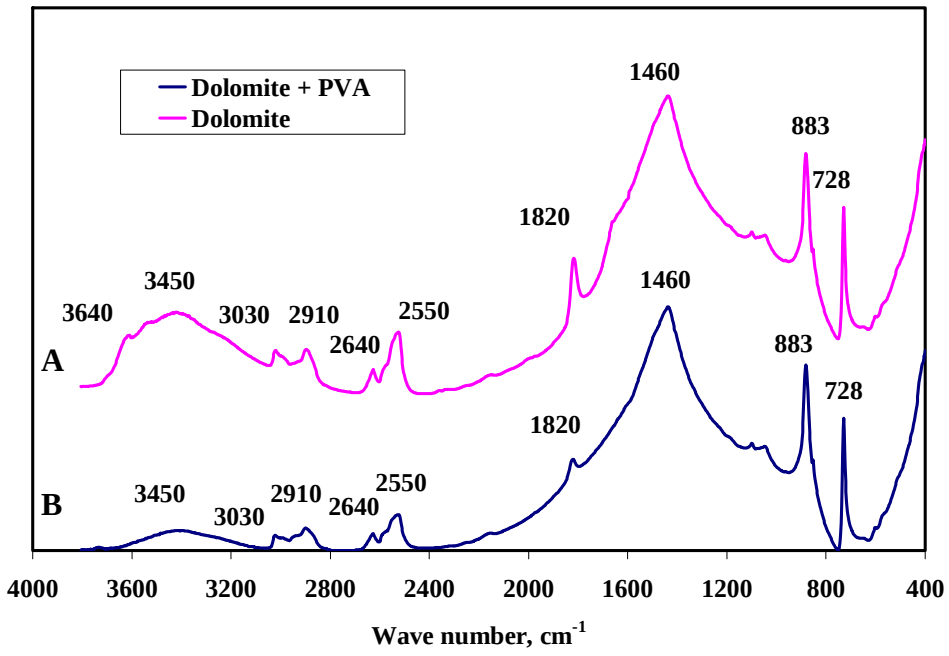

Figure 5-18. Infrared absorbance spectra (FTIR) of A) dolomite alone, and B) dolomite/PVA system.

The FTIR spectrum of the apatite sample after having interacted with PVA is shown in Figure 5-19. However, unlike the case of dolomite, this figure indicates that the adsorption mechanism of the polymer on apatite is not clarified by using FTIR—no change is shown in the bands' intensities or positions, either for bare apatite or apatite with polymer adsorbed on it. This finding is in agreement with the current literature [Chanchani, 1986; Ince, 1987]. It is pertinent to mention that FTIR spectroscopic studies on the dolomite–PVA and apatite-PVA systems revealed the presence of hydrogen bonding only.

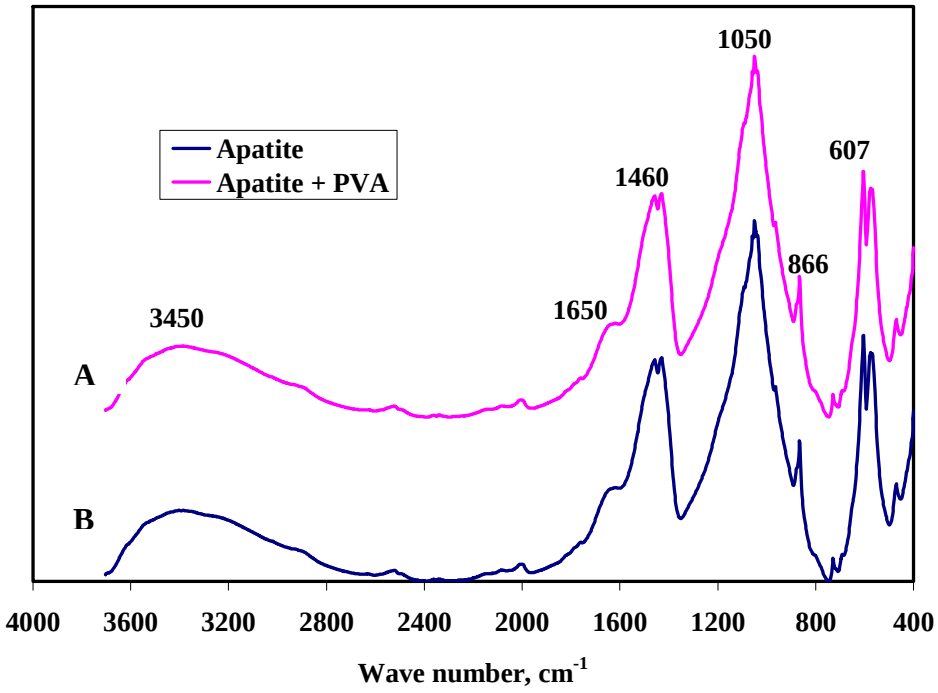

Figure 5-19. Infrared absorbance spectra of A) apatite alone, and B) apatite/PVA system.

Adsorption Study

An adsorption study was used for the purpose of determining PVA adsorption on both dolomite and apatite. The calibration curve for PVA concentration was determined colometrically. Figure 5-20 shows the calibration curve and its equation, which was used in this study to calculate the residual concentration of PVA in adsorption experiments.

The limitation of the PVA concentration to create this curve is 40 ppm [Finch, 1973; 1992].

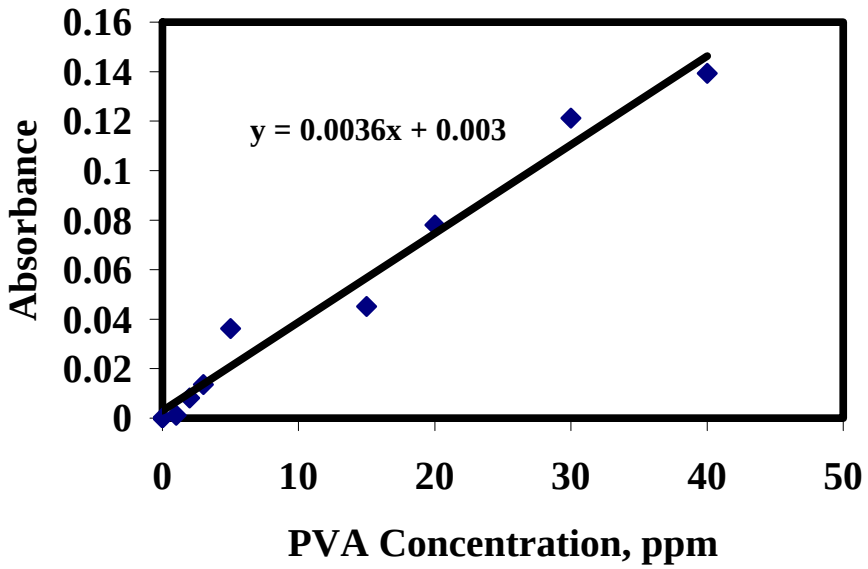

Figure 5-20. Calibration curve for PVA concentration measurements

Kinetics of adsorption

A study of the kinetics of adsorption is mainly to determine the equilibrium time of adsorption. The rate by which equilibrium is established during adsorption depends on the chemical nature of the polymer and its molecular weight, the solvent, and the type of adsorbent. In most cases, the kinetic curves indicate an increase in the amount of adsorbed polymer over time, with an asymptotic approximation of the equilibrium value [Lipatov and Sergeeva, 1974]

The adsorption of a polymer on solid surfaces occurs by a three-step mechanism [Dijit et al., 1990; Somasundaran and Ramachandran, 1988]. First, the polymer is diffused from the bulk to the interface. Second, adsorption of the polymer molecules occurs on the initially bare solid surface. Finally, polymer conformation and orientation changes in the surface layer to accommodate the adsorption of more polymer molecules.

To ascertain the time required for the adsorption equilibrium to be attained, kinetic tests were carried out at a natural pH of 7 for a period of 24 hours; PVA concentration was 100 ppm ($6.7X10^{-7}$ M). Figure 5-21 shows results on the adsorption of PVA onto dolomite and apatite as a function of time. It is evident that the equilibrium is attained at about one hour. The equilibrium values are $0.04X10^{-6}$ and $0.011X10^{-6}$ mole/m^2 for dolomite and apatite respectively. In consideration of these findings, a 2-hour conditioning time was selected for the adsorption studies.

It was observed that the adsorption followed a typical second-order adsorption process. The second-order model predicts the behavior over the whole range of adsorption and is in agreement with an adsorption mechanism being the rate-controlling step. The second-order rate expression [Ozacar, 2003] based on solid capacity is generally expressed as follows:

$$\frac{d\Gamma}{dt} = k(\Gamma eq - \Gamma)^2 \text{ ……..……. (5.4).}$$

Or, by integration

$$\Gamma = \frac{t}{\frac{1}{k\Gamma_{eq}^2} + \frac{t}{\Gamma_{eq}}} \text{ ……..(5.5)}$$

Where Γ is adsorption density (mole/m^2) and Γ_{eq} is equilibrium adsorption density (mole/m^2), K is second-order adsorption rate constant (hr^{-1}), and t is time (hr). By fitting the experimental data to Equation 5.5, the parameters Γeq and K were determined. These are listed in Table 5-2.

Table 5-2. Fitting parameters of second-order kinetic model

	Γ_{eq} X 10^{-6} mole/m^2	K, hr^{-1}
Dolomite	0.04	361.6
Apatite	0.011	200

It can be seen that the Γ_{eq} values for dolomite and apatite match the experimental values. The higher Γ_{eq} value of dolomite indicates the presence of more sites available for PVA adsorption than on apatite. Moreover, the K_{ad} for dolomite is higher than the K_{ad} for apatite, which indicates the higher adsorption rate on dolomite. However, the plateau was reached almost at the same time for both minerals.

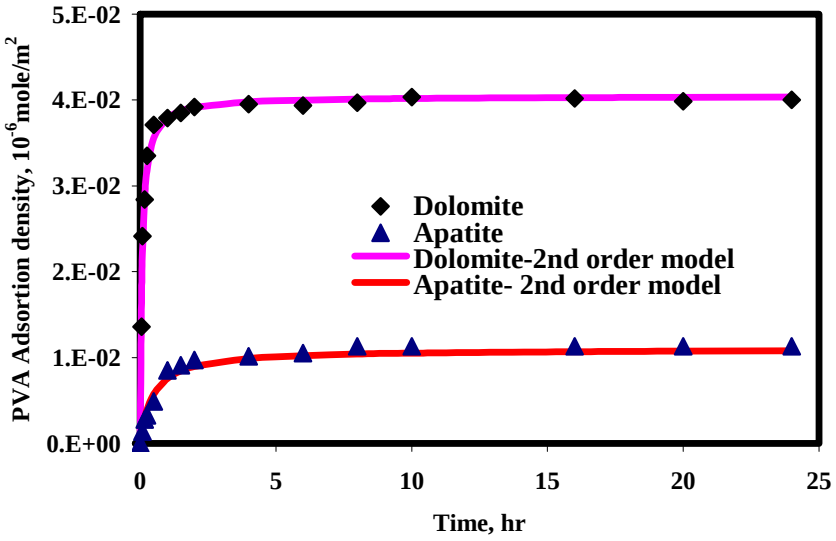

Figure 5-21. Kinetics of PVA adsorption on dolomite and Apatite
(Initial PVA concentration $6.7X10^{-7}$ M, pH 7, $2X10^{-3}$ M KNO_3 and 23°C).

Explanation of the higher adsorption rate on dolomite: The higher adsorption rate on dolomite may be explained by: (1) The higher solubility of dolomite and production of more ions in the solution, which affects the solution's property as a solvent (effectively converting it to poorer solvent). This property also affects the polymer's conformation, which will either be flat on the solid surface—greater tendency for molecules of polymer to be adsorbed on the solid surface or attach to each other, (2) The neutrality of apatite (pH 7) while having an IEP of 6.8, which means less ions in the solution are available to act as additional driving force for PVA to adsorb on the apatite

surface. This is especially significant as there is high competition between the interaction of PVA with water molecules and interaction of PVA with the apatite surface, and (3) OH-groups on dolomite surface (isolated and hydrogen-bonded hydroxyls) are greater than those on apatite surface (hydrogen-bonded hydroxyls). In other words, the isolated OH is exclusive to the dolomite surface, which is confirmed with FTIR spectra measurement.

Adsorption isotherm

Most isotherms of the adsorption of polymers from dilute solutions can be visually represented as curves that reach saturation at specific concentrations [Lipatov and Sergeeva, 1974]. It is important to note that polymers may adsorb on surfaces in various conformations depending on bulk (solvent) and surface chemical properties of the substrate, as well as other physical conditions of the system [Hong et al., 2001].

At low concentrations, the polymer chain behaves like isolated coil. If the concentration of the polymer in the solution is raised, the chains become close to each other, which allows polymer-polymer intermolecular interactions to influence the motion of the polymer chains. The effects may be expected to be cumulative until the point of chain-overlapping concentration, which is the close packing of the polymer coils in solution. Once the overlapping concentration has been reached, the polymer motion will be dominated by the presence of direct polymer-polymer interaction. As polymer concentration is increased, the polymer diffusivity decreases. If the concentration increases even further, a pseudo-matrix-gel will be formed. The resulting viscosity is governed mainly by intermolecular interaction, which is related to polymer chains overlap [Izmailova et al., 1975; Gotze and Sonntag, 1987; Andreyeva et al, 1973; Babayevskii et al., 1986; Koopal et al., 1988].

For PVA, –OH is the only functional group [Koopal and Lyklema, 1979; Chibowski and Paszkiewicz, 1995; Chibowski et al., 2000]. Increasing the degree of hydrolysis reduces acetate groups, which usually show preferential adsorption. Thus, the conformation of the polymer chain at the solid–polymer solution interface will depend on the number of acetate groups in a PVA macromolecule. The lower the degree of hydrolysis, the flatter the polymer chains; conversely, at high degree of hydrolysis, the polymer chains should be oriented perpendicularly to the surface [Santhiya et al., 1999; Sjöberg et al., 1999; Bajpai and Vishwakarma, 2003; Koopal and Lyklema, 1979]. This conformation of the PVA macromolecule will favor the adsorption of the polymer on the surfaces of dolomite and apatite, which is shown in Figures 5-22 and 5-23.

Chibowski [2000] reported that the adsorption of PVA on alumina increases with an increase in the degree of hydrolysis. This is also confirmed by previous experimental results and polymer screening experiments. In this work, it was found that the fully hydrolysed PVA was the best among different degrees of hydrolysis PVAs' (Chapter 3 in this thesis).

The adsorption density (mol/m^2) of fully hydrolyzed PVA (acetate groups < 1 %) on the minerals' surface as a function of the initial polymer concentration (0 to $4X10^{-6}$ mole) was determined at 23° Celsius and a pH 7 for dolomite and apatite. The results obtained are presented in an adsorption isotherm plot (Figures 5-22 and 5-23 for dolomite and apatite, respectively).

The analysis of these adsorption isotherms shows formation of a plateau for both apatite and dolomite. Such behavior of the macromolecules comes from a different adsorption affinity towards different surfaces. This result suggests that the observed

increase in PVA adsorption is mainly caused by the change in conformation of the polymer chain at the minerals' surface. Following this change, a number of active sites on the surface become available for further adsorption of polymer molecules. As mentioned previously, the greater porosity of apatite leads to high number of adsorption sites available and the horizontal stretching of the polymer to cover these sites. This, in turn, explains the lower adsorption layer thickness and higher parking area of apatite.

The shape of the adsorption isotherms shown in Figures 5-22 and 5-23 is typical for physical adsorption and is an acceptable shape for that range of polymer molecular weight. [Adamson and Gast, 1997]. The measurements were repeated three times and error bars were plotted on each graph. From the figures we can see that the adsorption isotherm is S-shaped, which suggests a physical adsorption of PVA onto the dolomite and apatite surfaces.

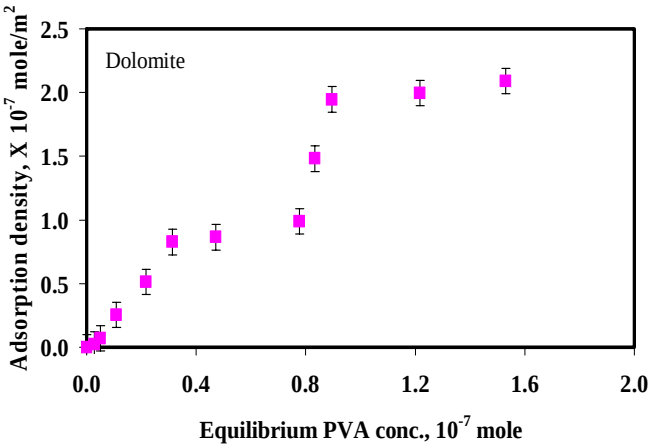

Figure 5-22. Adsorption isotherm of PVA on dolomite at 23°C

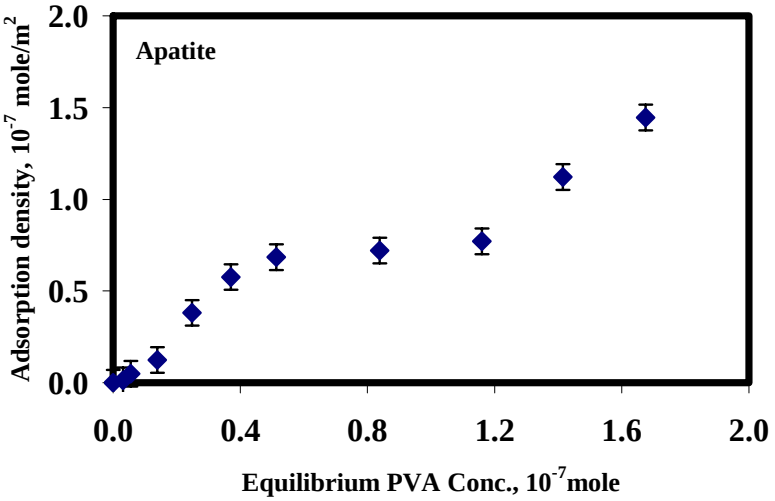

Figure 5-23. Adsorption isotherm of PVA on apatite at 23°C

Calculation of PVA adsorption and parking area

The amount of PVA adsorption was calculated using the following formula:

$$\Gamma = \frac{(C_i - C_r) * V}{m * SA} \qquad (5.6)$$

Where, Γ is the amount of PVA adsorption (mole/m^2), (C_i-C_r) is PVA concentration on the particle (mole/ml), C_i is initial PVA concentration, C_r is residual PVA concentration, V is the volume of solution (ml), m is the mass of dolomite or apatite particles (g), and SA is the specific surface area of particles (dolomite 0.9 and apatite 1.48 m^2/g).

The parking area of PVA molecules was calculated using the following formula:

$$\text{Parking area} = \frac{\left(\frac{1\times10^{18}\times Mw}{\Gamma}\right)}{Av} \qquad (5.7)$$

Where MW = 150,000 g/mole, Av is Avogadro's number (6.023 x 10^{23} #/mol) and parking area is nm^2/#. The calculated parking areas for dolomite and apatite at the first plateau are (23.72 nm^2) and (75.47 nm^2) respectively. Taking into account that the

parking area per stretched molecule is 0.2 nm^2 [Koopal and Lyklema, 1979], it was observed that PVA-molecule forms a wavy or zigzag shape on the solid particles with the higher thickness on the dolomite particles. Moreover, this conformation on dolomite appears at lower relative concentration range. It is worth noting that in the case of dolomite the adsorption isotherm is both steeper and reaches a plateau at lower concentrations than in case of apatite.

The observed results may be explained based on the following hypothesis, which is Schematically illustrated in Figure 5-24: macromolecules are generally more tightly bound to surfaces due to the multiple points of attachment. The figure shows the conformation of single polymer chain (5-24A) and/ or several chains (5-24B). It may be concluded that without intermolecular H-bonds, spiral conformations of PVA are favorable and with intermolecular H-bonds, zigzag conformations is expected.

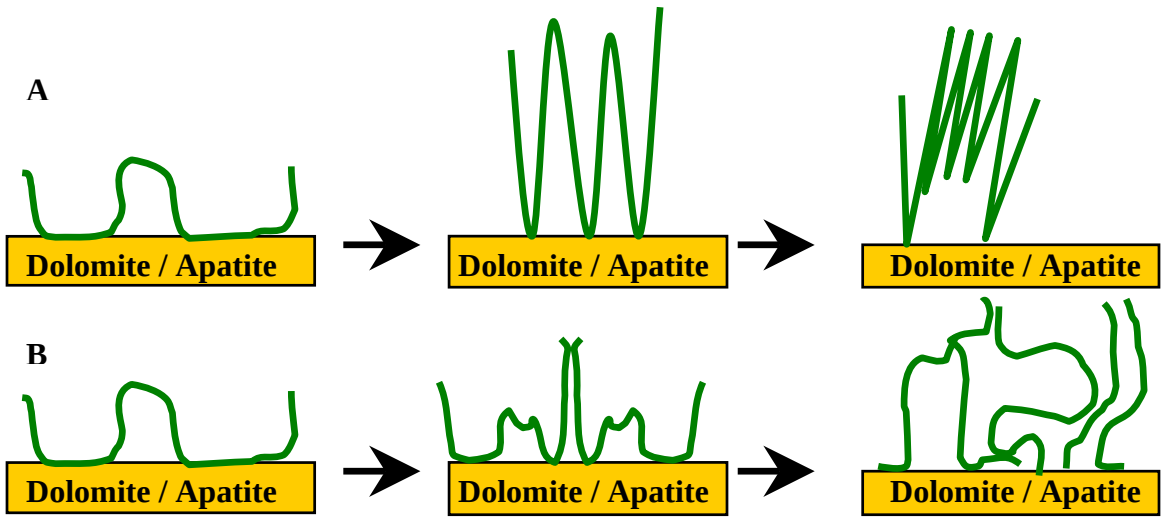

Figure 5-24. Polymer-conformation changes with increase the concentration: A) conformation of a single molecule, B) conformation of more than one molecule.

Adsorbed layer thickness

The thickness of PVA layer adsorbed on dolomite and/or apatite can be calculated from the adsorption isotherm by using the following relationship:

$$h = \frac{\Gamma}{\rho} \qquad (5.8)$$

Where, h is the adsorbed layer thickness, m; Γ is adsorption density, g/m^2, and ρ is PVA density, g/m^3.

Using this relationship, the thickness of the adsorbed layer was found to be 27 nm on dolomite and 9 nm on apatite, which indicates that the vertical polymer chains are stretched three times longer in the case of the dolomite than in the case of the apatite. This explains the greater adsorption on dolomite; since, according to their conformation, the polymer chains occupy smaller number of sites. In addition, more sites are available on dolomite than on apatite.

Note: The length of the PVA molecule of this molecular weight is about 600 nm, which indicates that the polymer conformation would be like Figure 24B.

Effects of pH

Ionic sites at the surface generally control the surface charges, on salt-type minerals such as apatite and dolomite. Specifically, for dolomite are: Mg^{++}, Ca^{++}, CO_3^{--}, HCO_3^{-}, OH^{-}, $MgHCO_3^{+}$, $MgOH^{+}$, $Mg(OH)_2$, $CaHCO_3^{+}$, $CaOH^{+}$, $Ca(OH)_2$ and for apatite are: Ca^{++}, HPO_4^{--}, $CaOH^{+}$, $Ca(OH)_2$, $H_2PO_4^{-}$, $CaH_2PO_4^{+}$. The nature of the mineral surface, pH, the presence of solutes, and the functional group of the polymer all affect the adsorption behavior. Previous studies on different minerals (i.e., alumina, silica, kaolin, clays) showed that the OH group of PVA is mainly responsible for adsorption on the

surface of a mineral [Santhiya et al., 1999; Sjöberg et al., 1999; Bajpai and Vishwakarma, 2003]. The effect of pH on the adsorption of PVA onto dolomite and apatite is shown in Figure 5-25. It can be seen that adsorption is pH-dependent in the studied range of 2 to 12.

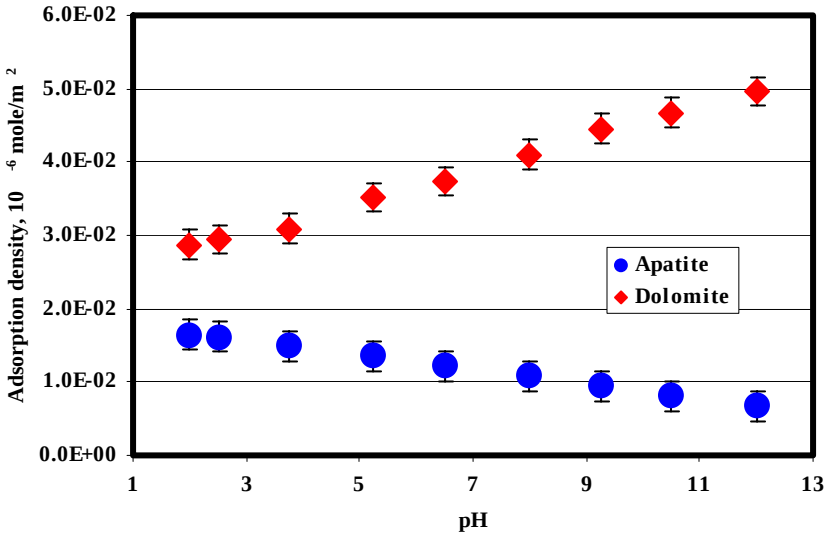

Figure 5-25. Effect of pH on adsorption of PVA on apatite and dolomite

Studying the adsorption of PVA on both minerals gives evidence that, due to fluctuations in pH, the adsorption is due to formation of hydrogen bonding between the dolomite or apatite surface from one side and OH- polymer functional group from another side.

Effects of pH on Apatite: It is evident from Figure 5-25 that the adsorption density decreases with an increase of pH. The decrease in the adsorption density as a function of pH may be explained by taking into consideration the surface charge of the apatite particles as well as the surface species, both of which are dependent on pH. It is interesting to note that the decrease of $CaH_2PO_4^+$ and $H_2PO_4^-$ species, according to the apatite activity chart [Attia and Fuerstenau, 1989] in entire pH range, are responsible for

formation of hydrogen bonding. In addition, there is a presence of about 5 % silica in this sample, which also leads to decrease in adsorption with increasing pH.

Moreover, it has been reported, as in the case of silica, that adsorption behaves the same way as pH due to a reduction in the number of undissociated silanol groups [Rachas et al., 2000].

On the other hand, the reaction of Ca^{+2} or Mg^{+2} ions with four OH groups occurs at pH > 7 and is accompanied by compacting of the macromolecules. The degree of crystallization of the film sharply decreased (evidently because of water) after formation of a calcium or magnesium complex.

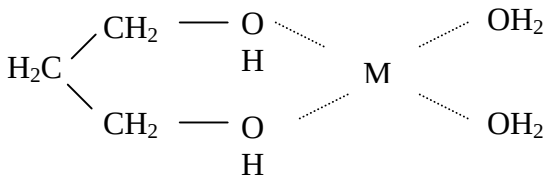

Where M is Ca^{+2} or Mg^{+2} ions

Effects of pH on dolomite: It can also be seen in Figure 5-25, that the adsorption density of dolomite increases with an increase of pH. This increase of adsorption with pH can be attributed to the hydroxylation of dolomite's surface, which enhances its hydrogen-bonding capacity. It was noticed that the increase of OH^- species and formation of metal (Ca and Mg) hydroxides with increasing pH are responsible for this increase in adsorption. Additionally, it has been reported in some cases that, at acidic pH, the decrease in PVA adsorption, can be caused by some or all of the following factors: loss of the most active binding sites for PVA bonding, reduction of the affinity for nonionic compounds by a salting-out effect, the screening effect of hydrated counter-ions, or preferential adsorption of water molecules at those ionized sites [Barker and

Garvey, 1980; Bonekamp et al., 1989; Platonov et al., 1979; Zhang et al, 1996; Hidber et al., 1995; Santhiya et al, 1998]. The adsorption of PVA on both minerals gives evidence that the adsorption is due to formation of hydrogen bonding between the dolomite or apatite surface from one side and OH- polymer functional group from another side.

Adsorption in supernatants

The results of adsorption of PVA on apatite in dolomite supernatant solution and dolomite in apatite supernatant solution are given in Figure 5-26. The adsorption density is lower than when the medium was just water, possibly due to the presence of several ionic species, which may affect the polymer aggregation. The increase in dolomite, on the other hand, is due to the presence of more sites, as mentioned previously. After reaching certain concentrations, both a curve become parallel, which means the same amount of the polymer has adsorbed on both surfaces.

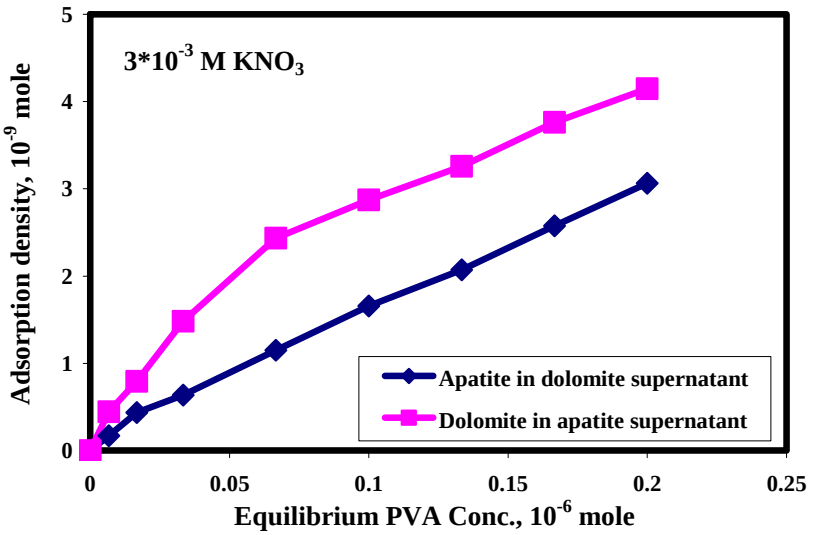

Figure 5-26. Adsorption isotherm of apatite in dolomite supernatant solution, and dolomite in apatite supernatant solution

This can be attributed to adsorption of the newly introduced polymer to the polymer already adsorbed to the surface and the ensuing formation of an aggregate at the solid/liquid interface.

Desorption

To ascertain whether the adsorption process is reversible, desorption tests were carried out by interacting the sample containing the adsorbed polymer with distilled water for a specified period and analyzing the supernatant solution for residual polymer content. The results are shown in Figures 5-27 and 5-28. From Figures 5-27 and 5-28 it is evident that, in the case of PVA, desorption characteristics follow a trend in reverse of the adsorption behavior. However, only about 20 % of the polymer could be desorbed, confirming the relatively weaker nature of this particular interaction with dolomite and apatite.

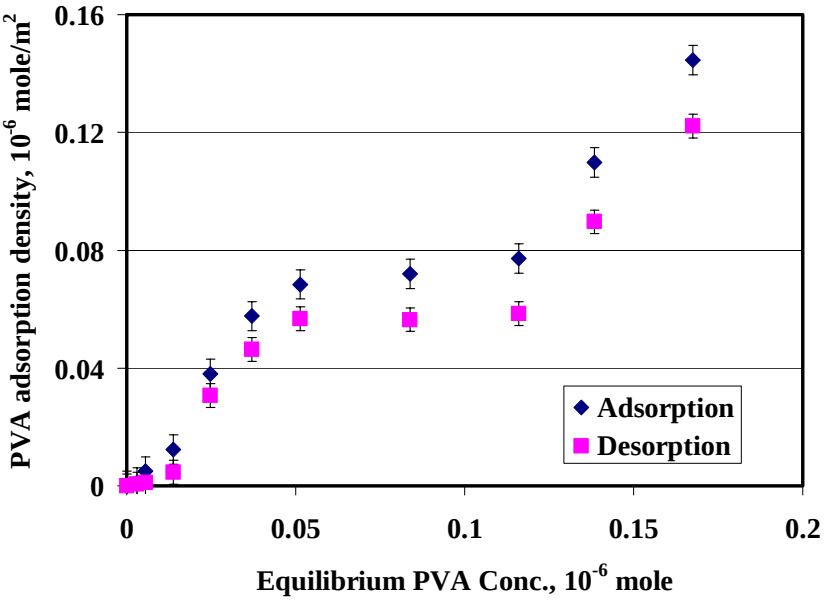

Figure 5-27. Desorption of PVA from apatite surface

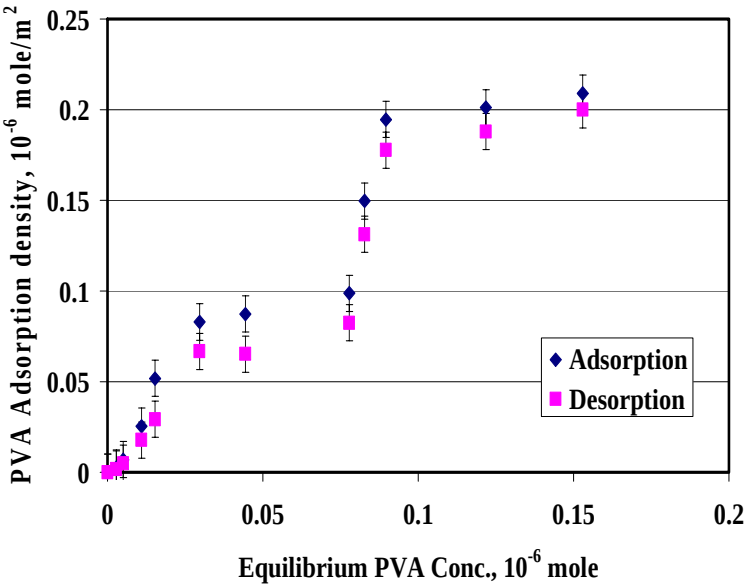

Figure 5-28. Desorption of PVA from dolomite surface

Desorption in Acidic Solution

Since the RF process requires adding PVA coated particles to an acidic media, desorption of PVA in an acidic solution was studied to simulate the RF process.

Desorption tests show almost no desorption in both the cases of dolomite and apatite. This behavior confirms that the formation of polymer cluster at the particle/ solution interface is due to the presence of SO_4^{-2} ions, which is one of the most ionic species leading to cross-linking of the polymer chains [Finch, 1992; Garba et al., 1996]. Consequently, this increases the viscosity of the polymer-coated layer in addition to strengthening the adhesion forces among polymer molecules thus affecting its viscoelastic properties, its hydrodynamic volume, and its stretching when CO_2 gas is produced as a result of the acid-carbonate reaction. Moreover, it is mentioned in the literature that even H_2SO_4, a strong acid, does not lead to salting out of the PVA; rather, its effect is extremely weak [Finch 1973; 1992].

Bubble Formation and Stability

The reactive flotation (RF) process, as mentioned earlier, includes two main steps: (1) the coating step, which is discussed in detail in the previous chapter and (2) the reaction step. In the second step, the sulfuric acid penetrates the polyvinyl alcohol (PVA) membrane and reacts with the dolomite surface. CO_2 gas is one of the reaction products according to the following reaction:

$$Ca\ Mg\ (CO_3)_2 + 2H_2SO_4 \rightarrow CaSO_4 + MgSO_4 + 2CO_2 + 2H_2O$$

Because PVA is known for its very low permeability by gases (Finch, 1992), especially CO_2, the CO_2 will accumulate between the particle and membrane creating a density difference between the dolomite and phosphate rocks (i.e., lowering the dolomite particle density). A schematic illustration of the mechanism of bubble formation during the reaction and how the particle density changes is given in Figure 5-29.

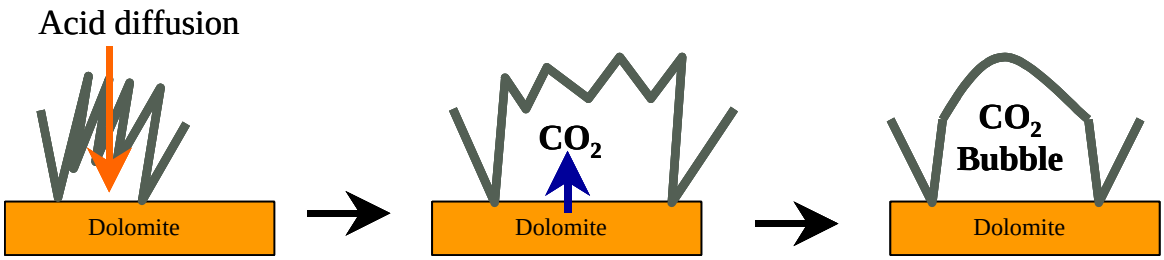

Figure 5-29. The bubble formation mechanism

To predict the required amount of CO_2 to float the particle, the modeling of the acid reaction with the dolomite surface and bubble formation was essential. In this chapter, different modeling efforts are discussed and the CO_2 production rate and the amount of CO_2 required to float the particle are calculated. Furthermore, the results are correlated with dynamic surface tension (DST) measurements to predict the membrane elasticity at

a certain CO_2 flowrate. Figure 5-30 shows a schematic diagram of the requirements to achieve flotation by RF process.

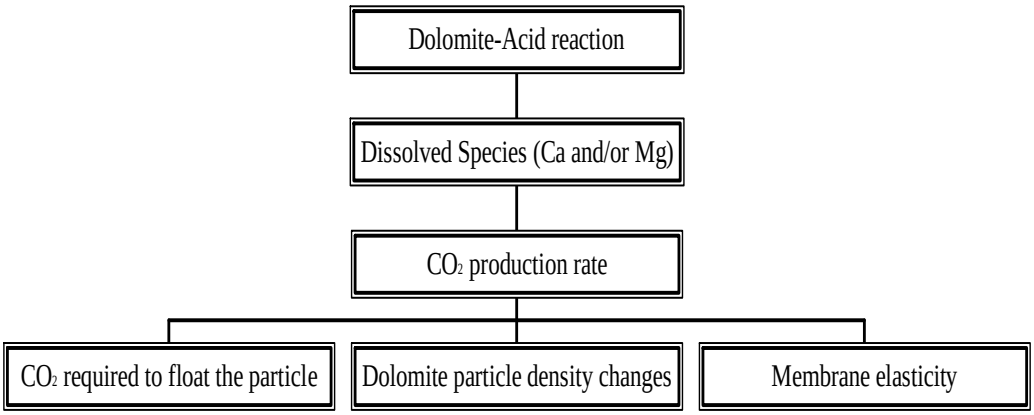

Figure 5-30. Schematic diagram of reaction kinetics of the RF

Chemical Analysis of Samples Used in Kinetic Study: The experiments were carried out with two particle sizes (0.2 – 0.3, and 1-2 mm). The chemical analyses of these two fractions are given in Table 5-3.

Table 5-3. Chemical analysis of the samples used in kinetic tests

Size, mm	MgO%	P_2O_5%	CaO%	Al_2O_3%	Fe_2O_3%	I.R.%	L.O.I. %
-2+1	14.48	2.82	32.6	1.02	1.56	11.2	32.12
-0.3+0.2	15.36	2.45	31.47	0.99	1.34	10.95	34.37

It can be seen from the Table 5-3 that the analysis of the two samples are approximately the same. It is expected that the very small differences, as shown in the analysis, will have a negligible effect on the kinetic tests results.

Effect of Particle Size

Different particle sizes were tested in 3 % sulfuric acid, H_2SO_4, solution (0.33 M). The results of reacting uncoated particles with acid at room temperature (23 ± 1°C), are shown in Figures 5-31 and 5-32 in terms of Ca and Mg dissolved, respectively. In all of the experiments, the solid loading in the reactor was 10 %.

In the course of each dissolution process, concentrations of both the calcium and magnesium ions were determined as a function of time following the reaction between the dolomite and the sulfuric acid. The dissolution process of dolomite in aqueous sulfuric acid was found to depend on the solution acidity, as indicated in statistical design study (Chapter 4). It was also indicated in the literature that the reaction of calcite with sulfuric acid follows first-order kinetics and it depends only on acid concentration at pH< 5 [Booth et al, 1997].

Generally, calcium and magnesium ion concentration in the liquid phase first underwent an exponential increase and then slowly approached an asymptotic value.

For the small particles, 0.2-0.3 mm, the reaction began very rapidly due to the higher surface area available for H^+ ions after which the dissolution reached a plateau (equilibrium) after 30 minutes. In the case of large particles, 1-2 mm, the reaction increased gradually as a result of lower surface area and did not reach equilibrium even after 2 hours.

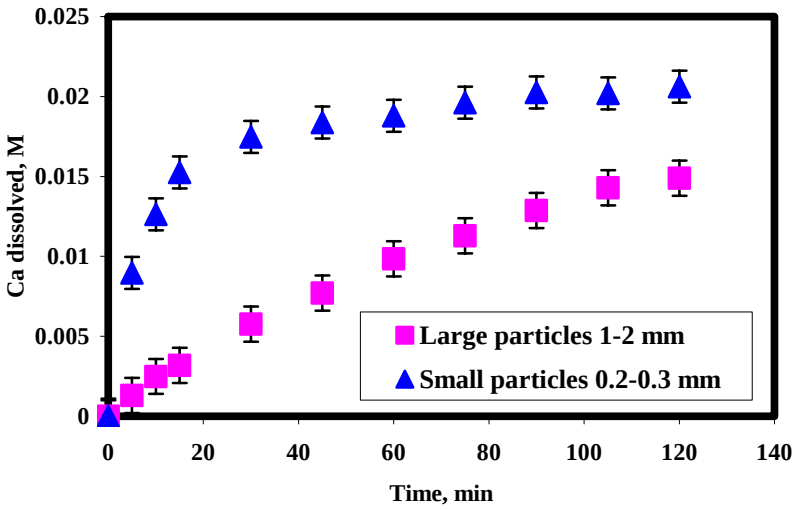

Figure 5-31. Dissolution kinetic of different particle sizes in terms of calcium ions in 3 % sulfuric acid solution at 23°C.

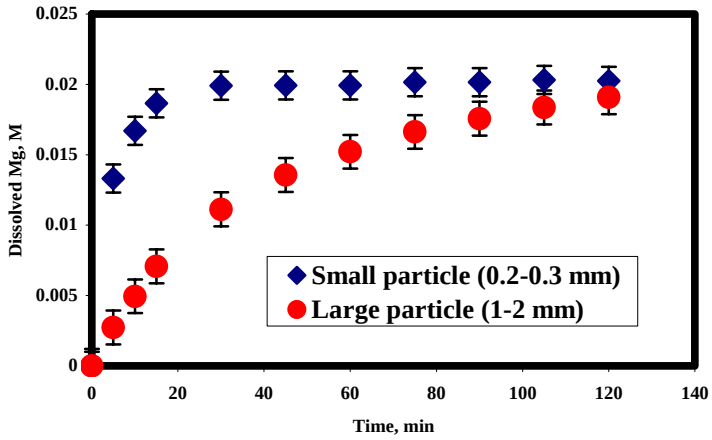

Figure 5-32. Dissolution kinetic of different particle sizes in terms of magnesium ions in 3 % sulfuric acid solution at 23°C.

Formation of an insulating layer: The H^+ transport is perturbed by the presence of the reaction products and since the H^+ has a higher diffusivity, the reaction continued until it reached the point of equilibrium. At this point, the H^+ can no longer reach the surface due to the formation of an insulating layer of reaction products, most probably gypsum, $CaSO_4.2H_2O$ and/or a CO_2 gas layer around the particle. This was especially true in the case of coated particles.

To confirm the formation of a passivation layer of gypsum, a picture of a particle both before and after the reaction was taken (Figure 5-33). The variation of the particle color from yellowish to white is an indication of the formation of the gypsum layer at the surface of the particle.

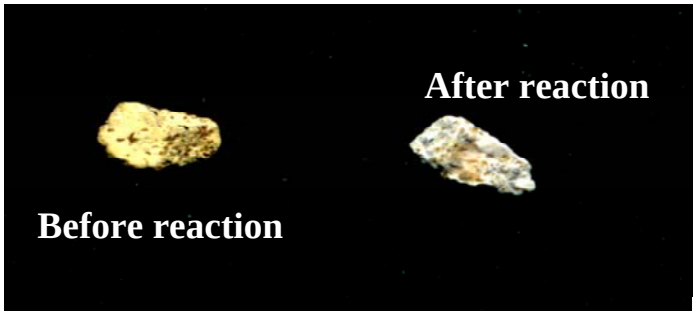

Figure 5-33. Dolomite particle (1-2 mm) before and after the reaction with 3 % H_2SO_4

In the rest of this chapter, the Mg concentration will be taken as the dissolution kinetic indicator since both the calcium and magnesium follow the same trend.

Effect of PVA Coating

The reaction was tested with the particles having been coated with PVA. Figure 5-34 shows the results of both coated and uncoated particles. The curve is steeper in the case of uncoated particles and the curves for both coated and uncoated reach a plateau after 30 and 40 minutes respectively (Figure 5-34). This can be explained by the presence of a polymer, which controls the transfer of ions to and from the boundary layer and then to the bulk solution. In addition, formation of the products occurs in a confined place (between the membrane and the particle surface), which also leads to a decrease in the saturation point and helps in rapid nucleation and growth of hydrated calcium sulfate, gypsum, ($CaSO_2.2H_2O$). Such a possibility exists in the case of a calcite-sulfuric acid system, providing that the solubility products are 2.5×10^{-5} M^2 for ($CaSO_4.2H_2O$) [Culberson et al., 1978] and 4.8×10^{-9} M^2 for ($CaCO_3$) [Stark and Wallace, 1982]. Moreover, the accumulation of CO_2 works as a diffusion barrier as well.

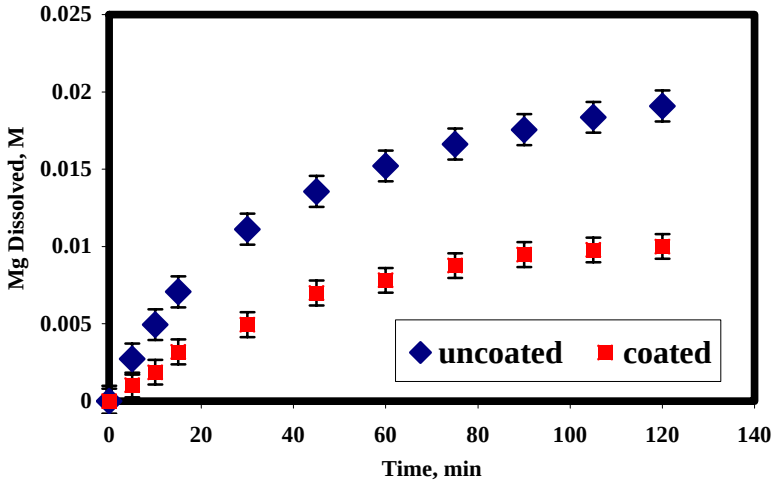

Figure 5-34. Dissolution kinetics of coated and uncoated 0.2-0.3 mm dolomite particle in 3 % sulfuric acid solution at 23°C.

Bubble formation and growth: Figure 5-35 (a-e) shows the growth of bubbles on the dolomite particle surface with time. The reaction starts immediately after adding the particles to the acidic solution. The bubbles then grow as a result of the evolution of CO_2, the impermeability of the PVA membrane, and the stretching of that membrane. If this membrane is not flexible enough, it will rupture and CO_2 gas will be released, leaving the particle without causing any flotation. It is also interesting to notice the rapid growth of bubbles within a few seconds.

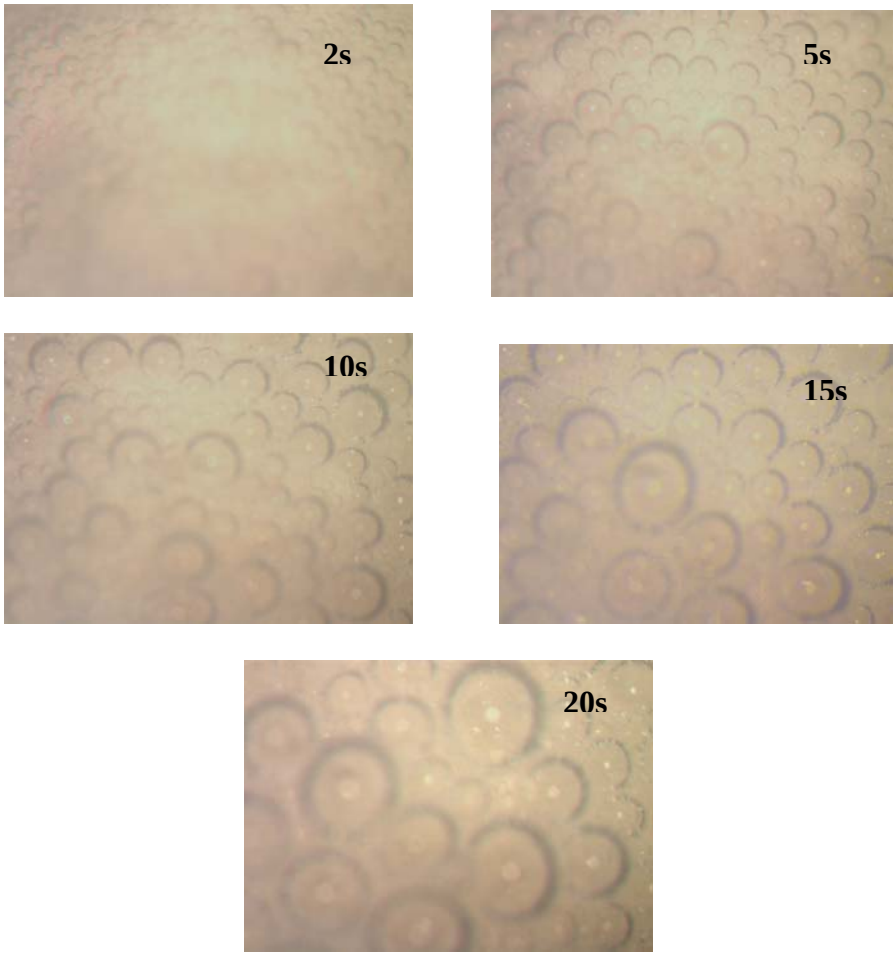

Figure 5-35. Growth of the bubbles with time on the dolomite particle surface, 50 X

Also, Figure 5-35 illustrates that presence of certain sites that can be considered as active sites for reaction to form CO_2 bubbles. In other words, if the entire surface is reacting, the polymer will form a uniform and homogeneous membrane around the particle.

Modeling of Bubble Formation and Dolomite-Particle Separation

In the present study, two models were developed to explain the phenomena associated with the RF process. These models depend on the mechanism(s) controlling the dissolution process. The two mechanisms studied are a) blockage of acid and b) depletion of the active sites. Moreover, two empirical models are given and fitted to experimental data. Those empirical models depend on reaching the saturation concentration in the bulk solution and the depletion of acid as the reaction products are formed. The main purpose of these models is to predict the amount of CO_2 evolved and the consequent density changes of the dolomite particles, which leads to its separation. The details of each model are explained in the following paragraphs.

Blockage of the Acid Model

In this model, the reaction depends on the transfer of the acid to the particle surface; the products of the reaction then diffuse out to the bulk solution. The formation of the reaction products, (i.e., Ca-sulfate and/or CO_2 gas), prevents the acid's accessibility to the surface and stops the reaction.

For simplicity of calculations, the sphericity of the particle, homogeneity of the coating around the particle, and presence of a barrier to CO_2 gas transfer are assumed. The equations of this model are:

$$\frac{dC_{mi}}{dt} = K_r A C_{ai} + K_m A (C_{mi} - C_{mo}) \qquad (5.9)$$

$$\frac{dC_{ai}}{dt} = -K_r AC_{ai} + K_a A(C_{ao} - C_{ai}) \quad (5.10)$$

$$\frac{dC_{mo}}{dt} = \gamma K_m A(C_{mi} - C_{mo}) \quad (5.11)$$

$$\frac{dK_m}{dt} = -\alpha AC_{ai} \quad (5.12)$$

$$\frac{dK_a}{dt} = -\beta AC_{ai} \quad (5.13)$$

Where:

C_{mi} : concentration of Mg at the surface, M

C_{mo} : concentration of Mg in the bulk, M

C_{ai} : concentration of acid at the surface, M

A : surface area, cm^2

K_r : reaction rate coefficient, $cm^{-2}.min^{-1}$

K_a : transfer coefficient, $cm^{-2}.min^{-1}$

K_m : transfer coefficient, $cm^{-2}.min^{-1}$

α and β : coefficients, $M^{-1}\ cm^{-4}\ min^{-2}$

γ : ratio between the boundary layer volume and total solution volume (Vi/Vo)

Fitting of this model to the experimental data is given in Figures 5-36 and 5-37 for both size fractions. The fitting parameters are given in Table 5-4.

Table 5-4. Acid-blockage model parameters

	Large		Small	
	Uncoated	Coated	Uncoated	Coated
*P-1	3	3	8.99	8.99
α	0.67	0.67	9	9
β	0.37	0.46	8.3	8.32
γ	0.00038	0.00085	0.0012	0.002
*K_m'	5.97	5.97	10.04	10.1
*K_a'	3.29	3.29	9.27	9.26

- P-1 = $K_r A$ $K_m' = K_m A$ $K_a' = K_a A$

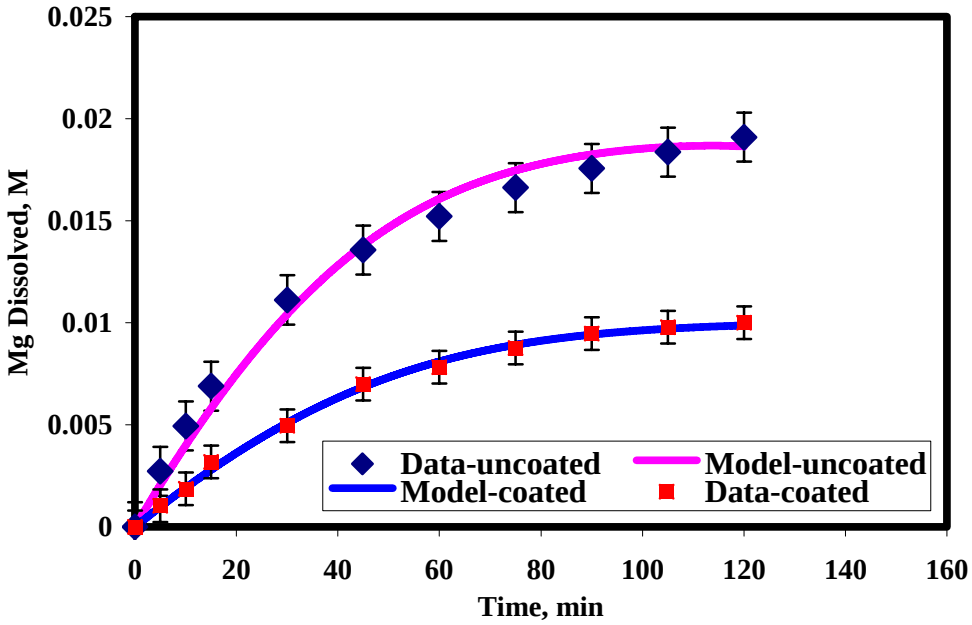

Figure 5-36. Acid blockage model fitting to 1-2 mm experimental data

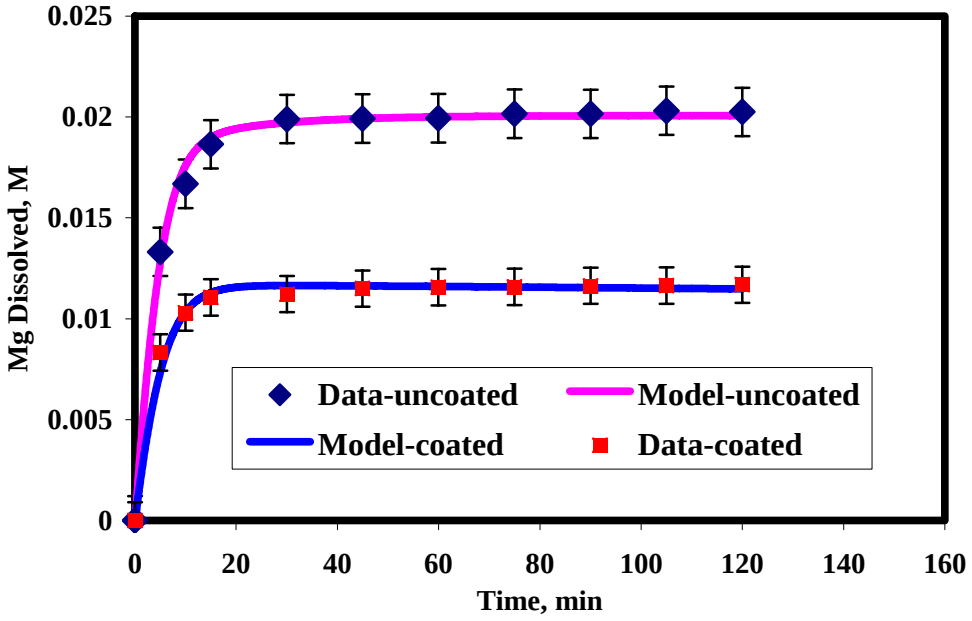

Figure 5-37. Acid blockage model fitting to 0.25-0.35 mm experimental data

This model shows no difference in all its factors between coated and uncoated particles except γ, which increases in the case of coated particles. The γ increase can be explained by the swelling of the membrane due to the formation of CO_2 gas, which

increases the internal boundary layer volume at constant external volume. The increase in P-1 for small particles is due to the increase in the number of sites that the acid can react with.

Disappearance of Active Sites Model

In this model, the reaction depends on the availability of the active sites at the particle surface. The depletion and disappearance of these sites will lead to cessation of the reaction. The disappearance of active sites may be due to formation of a passive layer from the reaction products, (i.e., Ca-sulfate and/or CO_2 gas). In this way the acid is available to react, but there are no active sites to react with.

For simplicity of calculations, the sphericity of the particle, absence of an acid barrier, constancy of acid concentration, homogeneity of the coating around the particle, and presence of a barrier to CO_2 gas transfer are assumed.

$$\frac{dC_{mi}}{dt} = K_r A C_{ao} + K_m A(C_{mo} - C_{mi}) \qquad (5.14)$$

$$\frac{dC_{mo}}{dt} = \gamma K_m A(C_{mi} - C_{mo}) \qquad (5.15)$$

$$\frac{dA}{dt} = -K_r A C_{ao} \qquad (5.16)$$

Where:

C_{mi} : concentration of Mg at the surface, M

C_{ao} : concentration of acid in the bulk, M (assuming $C_i=C_o$)

A : surface area, cm^2 concentration of Mg at the surface, M

C_{mo} : concentration in the bulk, M

K_m : transfer coefficient, $cm^{-2}.min^{-1}$

K_r : reaction rate coefficient, $cm^{-2}.min^{-1}$

γ : ratio of volume of boundary layer to the volume of the bulk (Vi/Vo)

Fitting of this model to the experimental data is given in Figures 5-38 and 5-39 for both size fractions. The fitting parameters are given in Table 5-5.

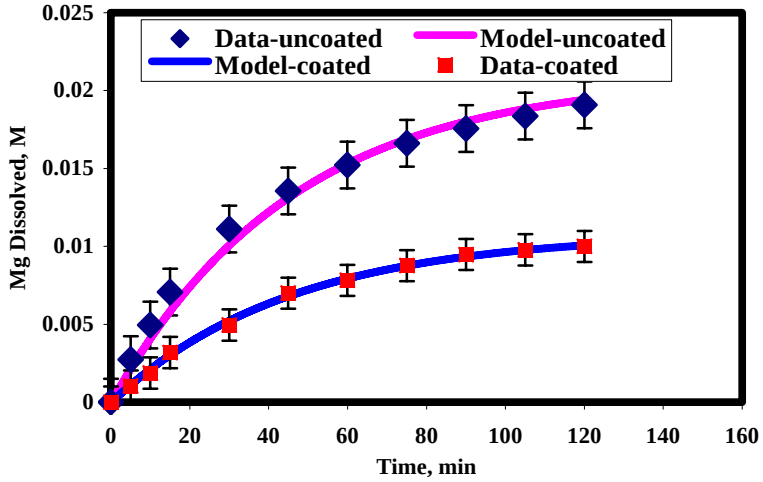

Figure 5-38. Active sites disappearance model fitting to 1-2 mm data

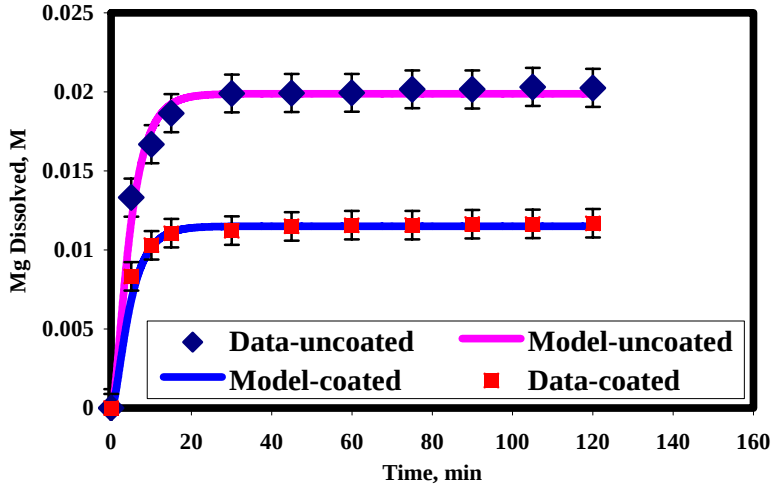

Figure 5-39. Active sites disappearance model fitting to 0.25-0.35 mm data

Table 5-5. Active sites disappearance parameters

	Large		Small	
	Uncoated	Coated	Uncoated	Coated
*P-1	3	3	8.99	8.99
γ	0.00038	0.00085	0.0012	0.002
*K_m'	5.97	5.97	10.04	10.1
Acini	3.29	3.29	9.27	9.26

- P-1 = $K_r A$ $K_m' = K_m A$

This model shows no difference in P-1, K_m, and K_a between coated and uncoated particles. The only difference is in the value of γ, which increases in the case of coated particles. The reason behind this increase is the constant external volume and increase of the internal volume since the polymer does not permeate the CO_2. The increase in P-1 in for small particles is due to the increase in the number of sites that acid can react with.

Empirical Models

There are many models that can fit empirically to experimental data. The Two models chosen to fit the experimental data in this study were widely used in the literature for calcite dissolution [Sjoberg and Rickard, 1984; Sjoberg, 1978; Lund et al., 1973]. These models are the First Order kinetic and Acid Concentration Dependent model. However, these models do not reflect the physics associated with RF process

First-order kinetic model

For the phase of the study involving treatment with Sulfuric acid, a kinetic model [Cameselle et al., 1997; Froment and Bischo, 1979; Blancarte et al., 1987] was employed, the equation of which would be:

$$\frac{dc}{dt} = k(Ceq - C) \qquad (5.17)$$

Where:

C : dissolved Mg concentration, M ;

k : kinetic coefficient, min^{-1} ;

C_{eq} : Equilibrium concentration , M

t : treatment time, min.

By integrating Equation 5.17, the value of the kinetic constant can be deduced:

$$C = Ceq(1 - e^{-kt}) \qquad (5.18)$$

Figures 5-40 and 5-41 show the fitting to this model to the results from experiments with 3 % (0.33 M) sulfuric acid for two different particle sizes. The reaction rate constants are given in Table 5-6. The reaction rate constant, K, is $2.5X10^{-2}$ min^{-1}. The variation in the equilibrium concentration at which the curves are leveling off is the presence of CO_2 as well as the development of a gypsum passivation layer, which prevents the acid from reaching the surface and/or covering the active sites.

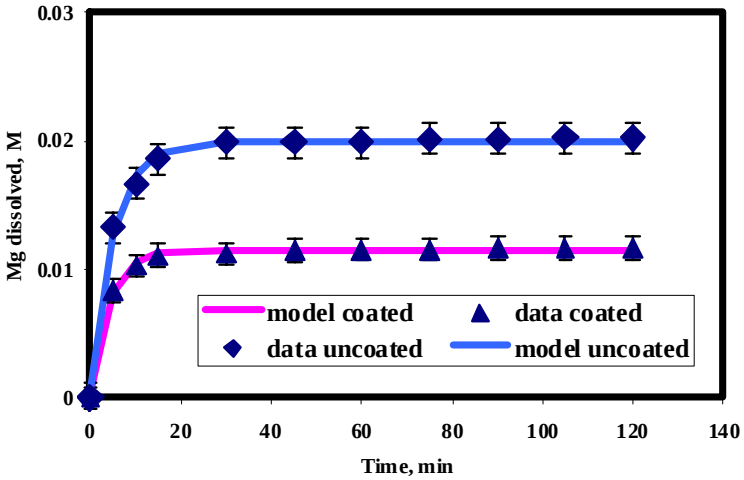

Figure 5-40. First-order model fitting for data of 0.25-0.35 mm particle size

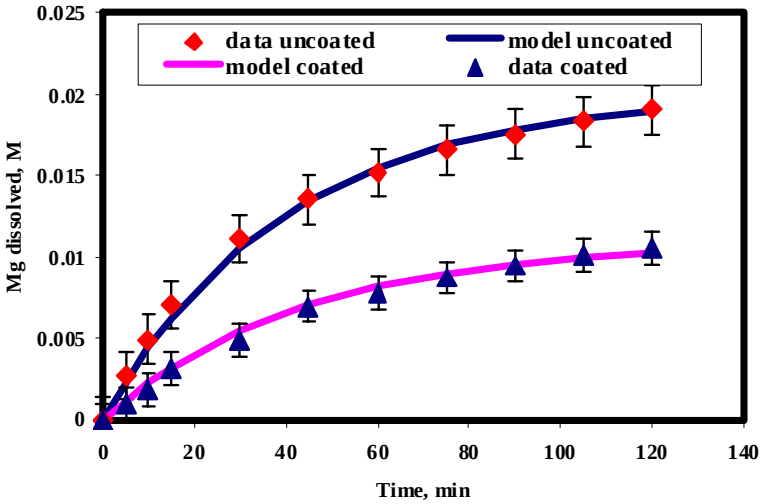

Figure 5-41. First-order model fitting for data of 1-2 mm particle size

Table 5-6. Reaction rate constants of first-order model

		K	Ceq
Large particles	Uncoated	0.025	0.02
(1-2 mm)	Coated		0.0115
Small particles	Uncoated	0.25	0.02
(0.25-0.35 mm)	Coated		0.0115

Acid concentration dependence model

Chemical reaction rate equations are used to define a conversion of the material or change in concentration due to dissolution and involve both a rate constant and a reaction order. However, a third parameter is also included in this model based on fact that the reaction product forms a barrier to acid diffusion. The circumstances under which this barrier is created are as follows: First, the acid concentration decreases with time as an evolution of reaction products. The reaction products then form a barrier between the acid and the particle surface. The thickness of this barrier increases with time until it reaches a certain stage where no acid can diffuse through and/ or the saturation stage is reached.

Compton [1989] found that under very acidic (pH < 4) conditions, dissolution control passed from H^+ diffusion control to a first-order heterogeneous reaction of H^+ at the surface.

This model can be presented by the following equation

$$\frac{dc}{dt} = KC_A{}^m \quad \text{.....(5.19)}$$

But the acid concentration changes with increasing the product concentrations according to the following relationship:

$$C_A = C_{Ao} - nC_i \quad \text{.....(5.20)}$$

By plugging Equation 5.19 into Equation 5.20, we arrive at a differential form, which is:

$$\frac{dc}{dt} = K(C_A - nC_i)^m \quad \text{.....(5.21)}$$

By integrating Equation 5.21, the final expression will be:

$$C_i = \frac{C_A - [n(m-1)Kt + C_A^{1-m}]^{\frac{1}{1-m}}}{n} \quad \text{.....(5.22)}$$

Where,

C_A : acid concentration, M
C_{AO} : initial acid concentration, M
C_i : ions concentration, M
n : number of ions evolved as reaction products
K : reaction rate constant, min^{-1}
t : time, min
m: reaction order

Figures 5-42 and 5-43 show the fitting of this model to experimental data. Its parameters are listed in Table 5-7.

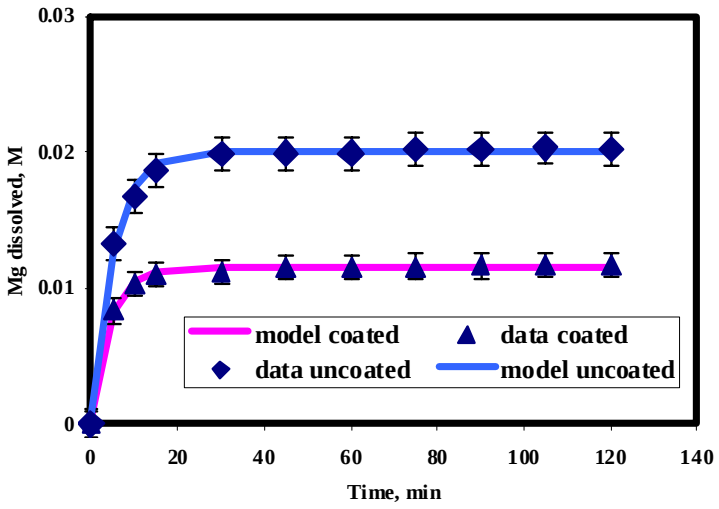

Figure 5-42. Model fitting for data of 0.25-0.35 mm particle size

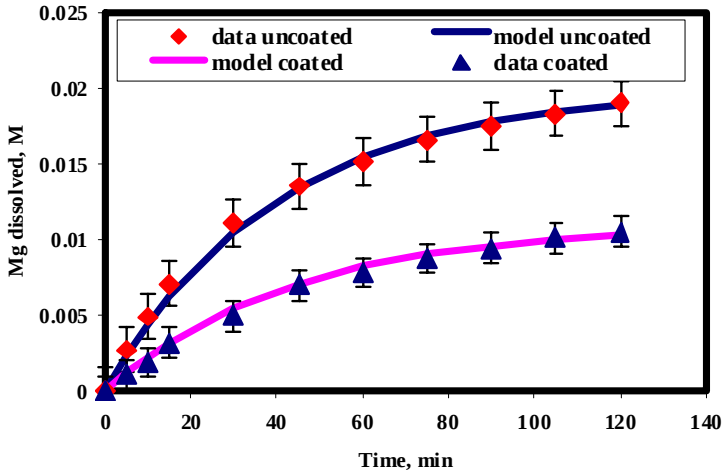

Figure 5-43. Model fitting for data of 1-2 mm particle size

Table 5-7. Acid concentration dependence parameters

Size, mm		K	n	m
1-2	Coated	$1.65X10^{-2}$	11.9	3.97
	Uncoated	$1.65X10^{-2}$	11.9	2.85
0.25-0.35	Coated	$1.65X10^{-2}$	29.0	1.79
	Uncoated	$1.65X10^{-2}$	16.7	1.68

The reaction rate constant, K, is $1.65X10^{-2}$ min^{-1}. For the small particles, the number of ions, n, in the case of coated particles is higher than uncoated because of a lesser volume around each particle in the presence of the polymer. This is not the situation in the case of the large particles—because of the lower surface area, the generation of ions is less and there is no competition among ions to diffuse out. Therefore, the n is the same, 11.9, in both cases.

The order of the reaction, m, is primarily used to express the availability of acid. For uncoated particles m is smaller because there is no barrier for the acid, while for coated particles, the polymer causes the formation of a barrier and limits both the accessibility of acid as well as the outgoing transfer of reaction products. Consequently, a higher m is needed to keep the reaction going at a constant rate.

Estimation of CO_2 Required to Float the Dolomite Particle

Simple calculations were used to predict the size of the particle with its surrounding envelope of gas and to estimate the relation between the radius of the particle before and after the formation of the gas bubbles around the particles. For simplicity, the following conditions were assumed: spherical particle, uniform gas layer around the particle, and at equilibrium condition: The part of the particle dissolved in the reaction was also neglected in the calculations.

As a starting point, we assumed that the particle starts to float when the density of the particle and the gas layer around it is less than the density of acidic solution. The calculations are as follows:

$$\text{density (Dolomite} + CO_2 \text{ gas)} < \text{density (acidic solution)}$$

$$\left(\frac{M_d + M_g}{V_d + V_g}\right) < \frac{M_w}{V_w} = 1\,\text{gm/cm}^3 \quad (M_g \cong 0)$$

$$M_d < V_d + V_g$$

$$\frac{2.9 * 4\pi}{3} r^3 < \frac{4\pi}{3} r^3 + \frac{4\pi}{3}(r_1^3 - r^3)$$

$$\frac{2.9 * 4\pi}{3} r^3 < \frac{4\pi}{3} r_1^3$$

$$(\sqrt[3]{2.9})r < r_1$$

$$r_1 > 1.4\,r$$

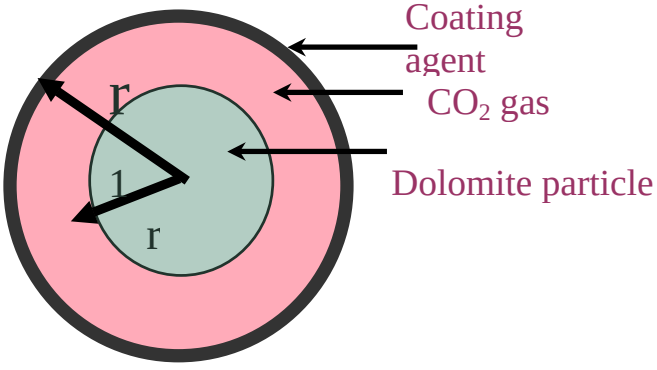

Where:
M_d : mass of dolomite particle
M_g : mass of CO_2 gas
M_w : mass of water
V_d : volume of particle
V_g : volume of CO_2 gas
V_w : volume of water
R: particle radius
R_1 : total radius (particle + gas)
S_d : surface area of the particle

In addition, the ratio between gas volume and particle volume and the ratio between the gas volume and particle surface area were calculated as follows:

Gas volume: *particle volume*

$$\frac{V_g}{V_d} = \frac{\frac{4\pi}{3}(r_1^3 - r^3)}{\frac{4\pi}{3}r^3} \quad \textit{and} \quad r_1 \geq 1.4r$$

$$\frac{V_g}{V_d} = \frac{[(1.4)^3 r^3 - r^3]}{r^3}$$

$$\frac{V_g}{V_d} = (1.4)^3 - 1 = 1.75$$

$$V_g = 1.75 V_d$$

Gas volume: *particle surface area*

$$\frac{V_g}{S_d} = \frac{\frac{4\pi}{3}(r_1^3 - r^3)}{4\pi r^2}$$

$$\frac{V_g}{S_d} = \frac{((1.4)^3 r^3 - r^3)}{3r^2}$$

$$\frac{V_g}{S_d} = \frac{((1.4)^3 - 1)r}{3} = 0.58r$$

From the previous calculations, we can deduce that: The total radius is 140 % of the original radius of the particle (without taking the dissolved part of the particle and the pores volume into account). Also, the volume of gas around the particle is approximately twice the original particle radius. A larger particle needs more volume of gas to float due to its lower surface area.

Change in Density: The density change can be calculated according to the sequence in Figure 5-44. The model will be used to calculate the number of moles of Mg, which consequently will give the number of moles of CO_2 through the equation of chemical reaction. Using the CO_2 density, the volume of CO_2 gas can be calculated. The volume generated in certain period of time can then be used to calculate the average flowrate of CO_2 as it evolves. This flowrate can be used to calculate the change in the density as well as to correlate that change to membrane elasticity at different flow rates.

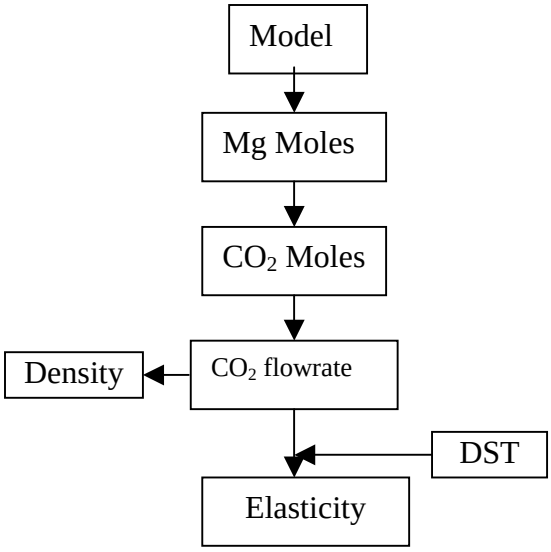

Figure 5-44. Sequence of calculating the particle density and membrane elasticity

Figure 5-45 shows the change in dolomite particle density as a function of reaction time. It is very rapid due to the CO_2 build up in the RF process. The density of the dolomite particles changes rapidly due to intense reaction in the first 20-30 seconds; after that the rate of change decreases dramatically (Figure 5-45). The change is sharper in the case of the smaller particles due to their higher surface area and greater amount of CO_2 generated. The density can be calculated by:

$$\rho_f = \frac{\rho_p \times V_p}{V_p + V_g} \qquad (5.23)$$

Where:

ρ_f : floated particle density, g/cm^3,
ρ_p: particle density, g/cm^3,
V_p: particle volume, cm^3, and
V_g: gas volume, cm^3

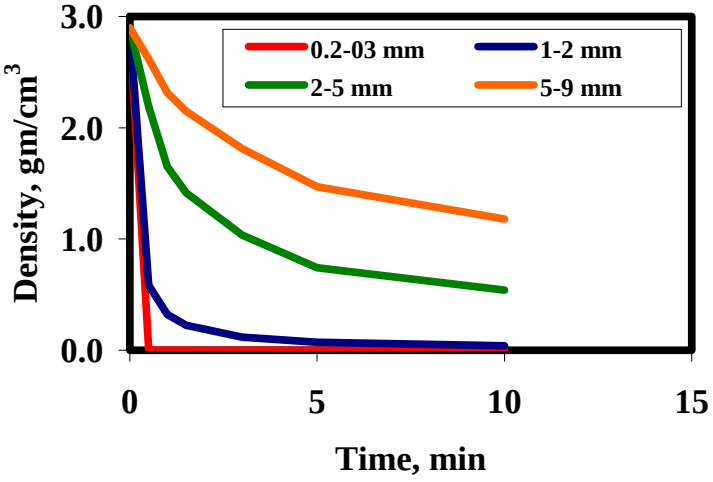

Figure 5-45. Density changes for different particle sizes

Bubbles Stability

As the reaction transpires at the dolomite particle surface, the CO_2 gas produced affects the growing bubbles in terms of their stability, (i.e., the stretching and elasticity of the polymer due to gas-pressure on the adsorbed polymer layer). Presence of the surfactant or polymer adsorbed at either the gas–liquid or liquid–liquid interface leads to the viscoelastic properties of that interface. They may be characterized by a surface dilatational modulus, which is defined according to Gibbs's equation [Johnson and Stebe, 1996; Lunkenheimer et al., 1996; Pikhitsa and Tsargorodskaya, 2000]:

$$E = \frac{d\gamma}{d \ln A} \qquad (5.24)$$

Where

γ is the dynamic surface tension (DST), and

A is the geometric area of the surface.

For that reason, the Dynamic Surface Tension (DST) measurements using the Maximum Bubble Pressure Technique were determined at different gas flow rates: 0.23,

0.47, 0.78, and 1.55 cm^3/min. In Figure 5-46, the experimental data of DST for PVA solutions of different concentrations are given. These results show the change in Dynamic Surface Tension as a function of the increase in polymer concentration. Clearly, at PVA polymer concentrations of up to 1 %, the surface tension significantly decreases as compared to the surface tension of water. Over the concentration range from to 1 % to 3 %, the surface tension decreases gradually but at greater concentration levels the surface tension remains nearly constant.

The decrease in surface tension can be described, according to the Ward and Tordai model [Pefferkorn et al., 1985; Nahringbauer, 1995; Fainerman and Miller, 1996], as a diffusion-controlled adsorption process. For a short time scale (from milliseconds to seconds) the equation can be written as

$$\Gamma(t) = 2c_o\left(\frac{Dt}{\pi}\right)^{\frac{1}{2}} \qquad (5.25)$$

Where,
Γ surface concentration at any time, (g m^{-2}),
C_o bulk concentration, (g m^{-2}),
D monomer diffusion coefficient, (m^2 s^{-1}).
π: commonly used value
t: time, (s)

It is interesting to note that these decreases in surface tension are more pronounced at lower flow rates—the greater the increase in the flowrate, the smaller the variation in the DST. This can be referred to as the time needed for the polymer to get onto the newly formed interfacial region. Therefore, at high flow rates, the bubbles surfaces remain almost clean and the effect of the polymer as an active agent at the interfacial region will be less because the polymer molecules do not have enough time to adsorb onto it. The

lower the flow rate, the higher the chance for the polymer molecules to adsorb onto the interface of the generated bubbles.

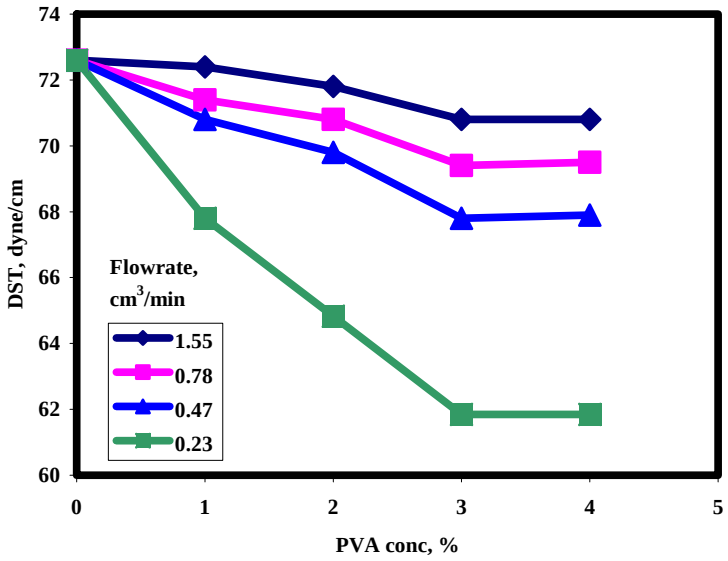

Figure 5-46. Dynamic surface tension of PVA concentration at different CO_2 flowrate

Figure 5-47 shows the results of using Gibbs equation to determine the elasticity in terms of PVA concentration at a different CO_2 gas flowrate. It is interesting to note that the elasticity increases with PVA concentration. This is due to formation of a membrane as a result of increasing the polymer concentration, which is able to resist the pressure exerted by the CO_2 gas generated. However, the higher the bubble formation rate (flowrate), the lower the elasticity. This can be referred to as the lower diffusivity of the polymer to the bubble surface and, consequently, DST at high bubble formation rates. The flow rate of CO_2 generation was found to be very low due to the reaction, which is closer to equilibrium conditions. This also indicates higher membrane elasticity.

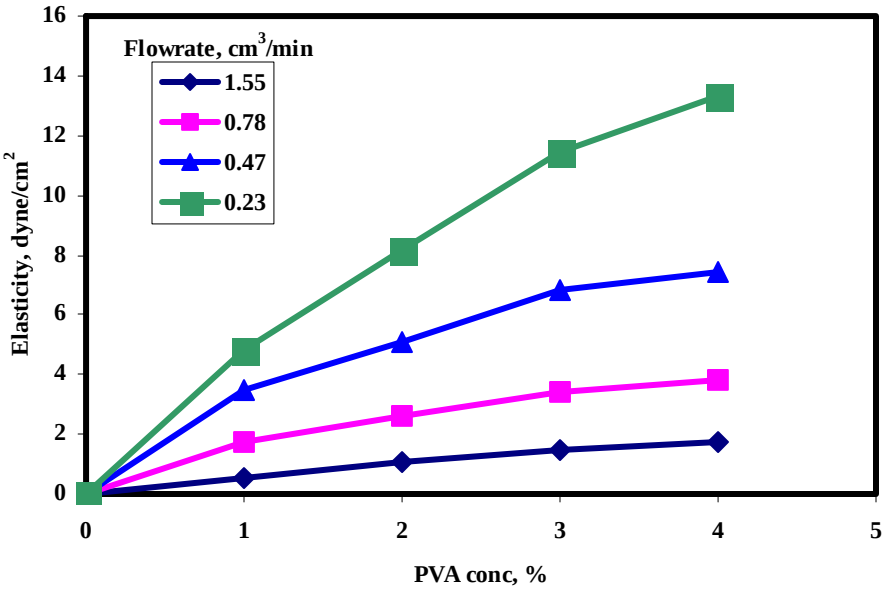

Figure 5-47. Elasticity of PVA membrane in terms of PVA concentration at different CO_2 flowrate.

Validation of the Model Using a Different Carbonate Mineral

The calcite was used as another carbonate material to validate the developed models. The calcite dissolution tests were conducted for coated and uncoated calcite particles in 3 % sulfuric acid solution at room temperature. Figures 5-48 and 5-49 show the results of both coated and uncoated particles. As expected, the curves show similar trends as that obtained in the dolomite dissolution experiments (Figures 5-38 and 5-39). In other words, lower dissolution is obtained in presence of polymer coating. Once again this may be explained on the basis of the presence of a polymer, which controls the transfer of ions to and from the boundary layer and then to the bulk solution.

Fitting of active site model to this experimental data is given in Figures 5-48 and 5-49 for both two different fractions. The fitting parameters are given in Table 5-8. It should be noted that these parameters are different from the dolomite system due to differences in the number of active sites on both cases. Examining the data in Figures 5-

48 and 5-49 indicate an excellent fit of the model to the calcite system, which is a good verification for the model.

Table 5-8. Active sites disappearance parameters for dissolution of calcite

	Large		Small	
	Uncoated	Coated	Uncoated	Coated
*P-1	0.016	0.008	0.06	0.06
γ	0.0051	0.0075	0.0013	0.0026
*K_m'	5.97	5.97	10	10
Acini	5.9	2.5	30	9.3

- P-1 = $K_r A$ $K_m' = K_m A$

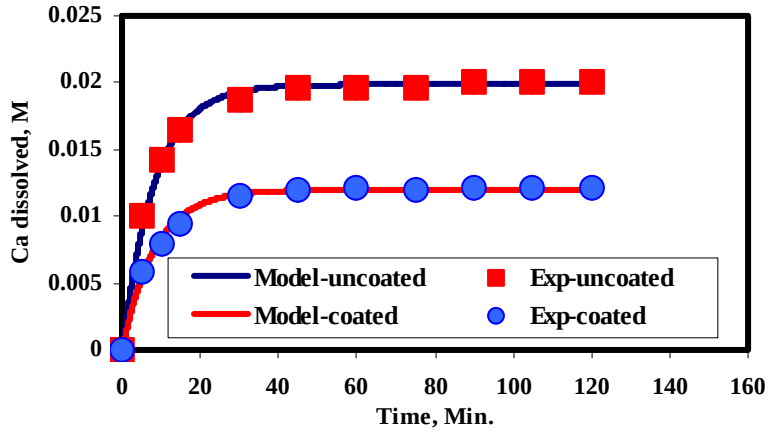

Figure 5-48. Calcite dissolution: model vs. experimental data 0.25-0.35 mm particle size

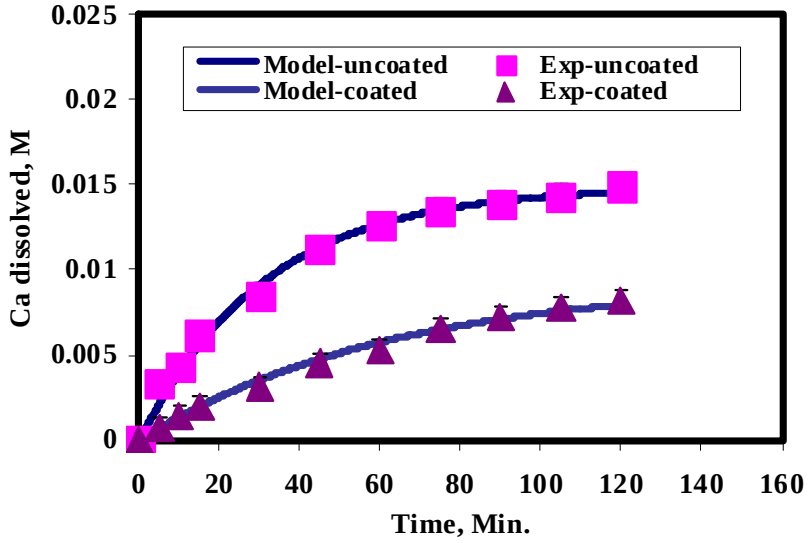

Figure 5-49. Calcite dissolution: model vs. experimental data for 1-2 mm particle size

Summarizing Remarks

It was found that work of adhesion decreases with increasing PVA concentration. Low work of adhesion is favorable for the reactive flotation process—this will create room for bubbles to form and increase the PVA membrane's ability to expand. On the other hand, FTIR shows that the presence of isolated hydroxyl groups is exclusive for dolomite, which can be used evidence that the adsorption or interaction of PVA with dolomite depends mainly on hydrogen bonding. However, the FTIR did not give a clear explanation for the adsorption of PVA on apatite.

As a physical adsorption confirmation, zeta potential measurements indicated that the PVA does not change the IEP for either apatite or dolomite. Also, the adsorption of PVA in the presence of supernatants indicates that the PVA adsorption is not affected by the supernatants even though the PVA may tend to form aggregates in highly ionic strength (as reported in literature). Moreover, The adsorption isotherm is S-Shaped, which means adsorption is physical on both minerals. The adsorption on dolomite is higher than the adsorption on apatite and the conformation of the polymer on dolomite is more stretched than on apatite. Also, the parking area of PVA on dolomite is less than on apatite.

Furthermore the adsorbed layer thickness is higher in the case of dolomite than apatite, desorption tests indicated that the process of PVA adsorption on the minerals surfaces (dolomite and apatite) is a slowly reversible process, and the PVA membrane elasticity was determined using dynamic surface tension. The elasticity modulus increases with PVA concentration and decreases with increasing CO_2 flowrate. More

interestingly, the rate of CO_2 evolution at the particle surface is very low which keeps the membrane at its higher elasticity.

From modeling point of view, two models were developed to predict the CO_2 formation rate and these models agreed well with the experimental data. The density change of the particle was predicted and verified by single particle beaker tests. As another carbonate mineral, calcite was used. Calcite dissolution tests showed similar trends as that obtained in the dolomite dissolution experiments. Moreover, the model showed an excellent fit to experimental data of the calcite system, which is a good verification for the model.

CHAPTER 6
CONCLUSIONS AND RECOMMENDATIONS FOR FUTURE WORK

Conclusions

In this study, the reactive flotation (RF) process was developed with a high potential to separate dolomite from phosphate rock at high recoveries.

The optimization of this process was carried out using screening and central composite designs. The controlling factors were screened using the Placket Burman design and three factors were determined to be significant within a 95 % confidence level. These factors were PVA concentration, acid concentration, and particle size. To further explore the effect of these factors, Central Composite Design (CCD) was used. The surface responses of CCD for different particle sizes indicated that the percentage of MgO could be lowered to less than 1 % with recovery increasing with decreasing the particle size.

Additionally, it was noticed that the PVA consumption in the original RF process was about four to six pounds per ton, which is very high and unfeasible. Many attempts to decrease the PVA consumption were conducted and it was found that using a spray to pre-condition the rock can decrease the consumption to as little as one pound per ton. This was determined by running a factorial design in terms of particle size, conditioning time, and PVA.

The optimized results were applied for process enhancement using a sluice, a gravity concentrator, which separates particles depending on the differences in the gravity

of individual particles. The results were very encouraging and similar to the data obtained in beaker tests.

With the RF process developed and optimized, the next step was understood the mechanisms involved in this process. Consequently, the process was explored in terms of dolomite/PVA and phosphate/PVA interactions as well as bubble formation and stability.

The interactions of both dolomite and phosphate with PVA were studied using several techniques in order to elucidate the mechanism of adsorption of PVA on both minerals. Work of adhesion was determined by measuring the equilibrium surface tension and contact angle. It was found that the work of adhesion decreases with increasing PVA concentration, which indicates film formation on both Dolomite and Phosphate particles. This decrease is due to the decrease in surface tension and increase in contact angle (making the cosine of the contact angle smaller). The final result is an overall decrease in the work of adhesion.

The decrease in surface tension indicates that PVA is a surface-active molecule, which satisfies the water molecules at the water/air interface. Moreover, the surface tension remains at a constant value after 1 % PVA concentration is reached. This indicates the formation of a tight molecular film at the interface, which, consequently, increases the viscosity and contact angle due to the formation of hydrogen bonds between PVA molecules.

Since the hydroxyl (OH) is the functional group in PVA molecules, this polymer (PVA) was expected to adhere to surfaces by hydrogen bonding. To confirm this hypothesis, the FTIR was used to characterize the surface of both minerals. Results of the

FTIR indicated the presence of isolated OH groups on dolomite only and hydrogen bonded OH groups on both minerals.

Secondary evidence, indicating the physical nature of PVA adsorption on Dolomite and/ or Apatite particles, was also considered. By using zeta potential measurements, results indicated no shift in the isoelectric point of PVA.

The adsorption isotherms were determined for both minerals as well. Isotherms were studied as a function of the equilibrium time, which was determined from previous adsorption kinetic studies to be 2 hours. Characteristics of the isotherms were as follows:

- The isotherms were S-shaped
- The adsorption on dolomite is higher than on apatite
- The adsorption process resulted in the formation of multiple layers on dolomite.
- The thickness of the adsorbed layer on dolomite was calculated to be about 3 times thicker than apatite.

The importance of the thickness of adsorbed layer lies in its resistance to the CO_2 formation rate. If the CO_2 formation rate is very high the stability of the PVA membrane will be affected and the bubbles will burst. Accordingly, the low flow rate is required to keep the bubbles at maximum stability.

The previously discussed finding was revealed using measuring dynamic surface tension (DST) - maximum bubble pressure method at different flow rates. It was found that increasing the PVA concentration increases the elasticity modulus. However, increasing the flowrate decreases the elasticity modulus. The actual experimental results showed the CO_2 formation rate to be very slow relative to the data measured by DST.

In the kinetic study, the CO_2 rate was calculated in terms of Mg^{+2} ions dissolved. From the reaction equation, the CO_2 was determined stoichiometrically for two particle size fractions. The results of the kinetics experiments revealed that bare (uncoated)

particles dissolved faster than coated ones. However, both of them reached a constant level of Mg^{+2} dissolved concentration after certain period of time. These observations were attributed to the formation of product layers such as CO_2 or gypsum, which act as barriers.

I was noted that the coated particles had a higher solubility than uncoated particles. In addition, both types of particles reached a plateau of solubility after a certain period of time. This distinct behavior of the particles was explained by two controlling mechanisms. The first is the acid blockage mechanism in which CO_2 formation prevents the acid from reaching the surface of a particle. The second is the disappearance of active sites to which the magnesium carbonate can adsorb. In both cases, the reaction will continue until all active sites have been used or the sites are covered with reaction products.

The modeling of these two mechanisms were carried out and fitted to experimental data, to which they conformed well. The same models used to predict the CO_2 formation rate were used to predict the decrease of particle density—the smaller the particle size, the sharper the change in the density. To validate this model, the predicted values for several size fractions were compared with experimental beaker tests. These showed a good agreement as well.

Recommendations for Future Work

There are several suggestions for future work:

- Investigate a lower polymer dosage with fine fractions
- Test a lower molecular PVA polymer
- Build a new sluice design capable of continuous operation
- Extend the model derived in this work for prediction of gravity separator performance in terms of grade and recovery

LIST OF REFERENCES

Abdel Khalek, N.A., 2000. Evaluation of flotation strategies for sedimentary phosphate with siliceous and carbonates gangues. Journal of Minerals Engineering 13 (7), 789-793.

Abu El-shah, S.I., 1991. Beneficiation of calcareous phosphate rock using dilute acetic acid solution: optimization of operating conditions for Ruseifa (Jordan) phosphate. International Journal of Mineral Processing 31, 115-126.

Adamson, A., Gast, A., 1997. Physical Chemistry of surfaces. Wiley (6^{th} edition), New York

Amankonah, J.O., Somasundaran, P., 1985. Effects of dissolved mineral species on the electrokinetic of calcite and apatite. Colloids and Surfaces 15, 335-353.

Ananthapadmanabhan, K.P., Somasundaran, P., 1985. Surface precipitation of inorganic and surfactants and its role in adsorption and flotation. Colloids and Surfaces 13, 151-167.

Andreyeva, V., Anikeyeva, A., Lirova, B., Tager, A., 1973. Investigation of PVA solutions. Polymer Science USSR 15 (8), 1991-1998.

Atalay, V., 1985. Beneficiation of low grade Tasit phosphate ore from Turkey. World Congress on non-metallic Minerals Proceedings, Belgrade, 389-396.

Attia, Y., Fuerstenau, D.W., 1989. The equilibrium composition of hydroxyapatite and fluorapatite- water interface. Colloids and Surfaces 34, 271-285.

Babayevskii, P.G., Kozlov, N.A., Trostyasnkaya, F., 1986. Effect of water on physical transformations and viscoelastic properties of sparse-network polyvinyl alcohol. Polymer Science USSR 28 (2), 475-482.

Bajpai, A., Vishwakarma, N., 2003. Adsorption of polyvinyl alcohol onto Fuller's earth surfaces. Colloids and Surfaces A: Physicochemical and Engineering Aspects 220 (1-3), 117-130.

Barker, M., Garvey, M., 1980. The effect of solvency on the adsorption of poly(vinyl alcohol) onto polystyrene latex. Journal of Colloids and Interface Science 74 (2), 331-340.

Becker, P.,1989. Phosphates and phosphoric acid: Raw materials technology and economics of the wet process. Fertilizer Science and Technical Series, 2nd ed., 6, Marcel Dekker Inc.

Behl, S., Moudgil, B., 1993. Mechanisms of PEO interactions with dolomite and apatite. Journal of Colloids and Interface Science 161**,** 443–449

Bjelopavlic, M., Singh, P., El-Shall, H., Moudgil, B., 2000. Role of surface molecular architecture and energetics of hydrogen bonding sites in adsorption of polymers and surfactants. Journal of Colloid and Interface Science 226 (1), 159-165.

Blancarte-Zurita, M.A., Branion, R.M., Lawrence, R.W., 1987. Application of a shrinking particle model to the kinetics of microbiological leaching. In Fundamental and Applied Biohydrometallurgy, eds R.W.Lawrence, R.M.R. Branion & H.G.Ebner. Elsevier Science Publishers, Amsterdam, 243-253.

Bonekamp, B., Schoute, M., Veringa, H., 1989. Elsevier Science, London, G. de With, R. A. Terpstra, R. Metselaar, Eds., EuroCeramics 1, 145.

Booth, J., Hong, O., Compton, R., Prout, K., Payne, R., 1997. Gypsum overgrowths passivate calcite to acid attack. Journal of Colloid and Interface Science 192**,** 207–214.

Cameselle, C., Nunez, M.J., Lema, J.M, 1997. Leaching of kaolin iron-oxides with organic acids. Journal of Chemical Technology and Biotechnology 70, 349-354

Chanchani, R., 1986. Selective flotation of dolomite from apatite using sodium oleate as collector. Ph.D. Dissertation, Gainesville, University of Florida.

Chander, S., Furestenau, D., 1982. On the dissolution and interfacial properties of hydroxyapatite. Colloids and Surfaces 4, 101-120.

Cheng, Y.C., 1985. The effect of surface hydration on the adsorption and flocculation of a model silica suspension using polyethylene oxide. M.S.Thesis, Gainesville, University of Florida.

Chibowski, S., Paszkiewicz, M., 1995. Journal of Polymer Chemistry 69, 461.

Chibowski, S., Paszkiewicz, M., Krupa, M., 2000. Investigation of the influence of the polyvinyl alcohol adsorption on the electrical properties of Al_2O_3–solution interface, thickness of the adsorption layers of PVA. Powder Technology 107 (3), 251-255.

Compton, R.G., Pritchard, K.L., Unwin, P.R., Grigg, G., Silvester, S., Lees, M., House, W.A., 1989. Journal of Chemical Society, Faraday Transactions I 85, 4335.

Culberson, C., Latham, G., Bates, R., 1978. Solubilities and activity coefficients of calcium and strontium sulfates in synthetic sea water at 0.5 and 25°C. Journal of Physical Chemistry 82 (25)**,** 2693-2699.

Davis, B.E., Liewellyn, T.O., Smith, C.W, 1984. Continuous beneficiation of dolomitic phosphate rocks. RI 8903, United States Bureau of Mines.

Dho, H, Iwasaki, I., 1990. Role of sodium silicate in phosphate flotation. Minerals and Metallurgical Processing 7, 215-235.

Dijit, J., Stuart, M., Hofman, J., Fleer, G, 1990. Kinetics of polymer adsorption in stagnation point flow. Colloids and Surfaces 51, 141-158.

Elgilani, D.A., Abouzeid, A-Z.M., 1993. Flotation of carbonates from phosphate ores in acidic media. International Journal of Mineral Processing 38, 235-256.

El-Shall, H., Bogan, M., 1990. Characterization of future Florida phosphate resources. 2nd progress report, FIPR Project 89-02-082R.

El-Shall, H., Zhang, P., Abdel Khalek, N., El-Mofty, S., 2004. Beneficiation technology of phosphates: challenges and solutions. Minerals and Metallurgical Processing 21 (1), 17-26.

El-Shall, H., Zhang, P., Snow, R., 1996. Comparative analysis of dolomite/francolite flotation techniques. Minerals and Metallurgical processing 7, 135-140.

Fainerman, V., Miller, R., Joos, P., 1994. Colloid and Polymer Science 272, 731-740.

Fainerman, V.B., Miller, R., 1996. Adsorption kinetics of short-chain alcohols at the water/air interface: diffusion-controlled adsorption under the conditions of a nonequilibrium surface layer. Journal of Colloid and Interface Science 178 (1), 168-175.

Farmer, V., 1974. The layer silicate. The Mineral Society, London.

Fbiehn, G., Erusberger, M., 1951. Industrial Engineering Chemistry 43, 1108.

Finch, C.A., 1973. Polyvinyl alcohol; properties and applications. John Wiley and Sons, New York.

Finch, C.A., 1992. PVA-Developments. John Wiley and Sons, New York.

Froment, G. F., Bischo, K. B., 1979. Chemical Reactor Analysis and Design. John Wiley and Sons, New York, USA.

Fu, E., Somasundaran, P., 1986. Alizarin red S as a flotation modifying agent in calcite-apatite systems. International Journal of Mineral Processing 18 (3-4), 287-296.

Fuerstenau, M.C., 1968. The influence of sodium silicate in non-metallic flotation systems. Transactions of American Institute of Mining, Metallurgical, and Petroleum Engineers 241, 319-323.

Garba, O., Yahya, S., Ali, A., Hamad, E., 1996. Surface and interfacial activities of hydrophobically modified poly (vinyl alcohol) (PVA). Polymer 37 (7), 1183-1188.

Garrett, P., Ward, D., 1989. A reexamination of the measurement of dynamic surface tensions using the maximum bubble pressure method. Journal of Colloids and Interface Sciences 132 (2), 475-490.

Geo, Z., Zheng, S., Gu, Z., 2002. Review of beneficiation technology for Florida high dolomite pebble. In: Beneficiation of Phosphates: Fundamentals and Technology. P.Zhang, H.El-Shall, P.Somasundaran, and R.Stana (Editors), SME, USA, Chapter 21, 235-245.

Gotze, Th., Sonntag, H., 1987. The effect of solvent quality on the interaction between two layers of adsorbed PVA. Colloids and Surfaces 25, 77-90.

Gruber, G.A., Raulerson, J.D, Farias, R.P., 1987. Adapting technology to beneficiate a low-grade phosphate ores. Minerals and Metallurgical Processing 7, 14-18.

Gu, Z., Geo, Z., Hwang, C.L., 1999. Development a new technology for beneficiation of Florida dolomitic phosphate resources. Final Report, FIPR-02-129-167, Florida, USA.

Hanna J., Anazia I., 1990. Selective flotation of dolomitic limestone impurities from Florida phosphates. University of Alabama, FIPR report No. 002-066-089.

Harkins, W., 1928. Surface energy and orientation of the molecules in surfaces are revealed by surface energy relations. Journal of Physical Chemistry 139, 647-691.

Hidber, P., Graule, T., Gauckler, L., 1995. Competitive adsorption of citric acid and poly(vinyl alcohol) onto alumina and its influence on the binder migration during drying. Journal of American Ceramic Society 78 (7), 1775-1780.

Hong, P., Chou, C., He, C., 2001. Solvent effects on aggregation behavior of PVA solutions. Polymer 42 (14), 6105-6112.

Howard, G., McConnel, P., 1967. Adsorption of polymers at the solution-solid interface. I. Polyethers on silica. Journal of Physical Chemistry 71 (9), 2974-2981.

Howard, G., McConnel, P., 1967. Adsorption of polymers at the solution-solid interface. II. Polyethers on carbon. Journal of Physical Chemistry 71 (9), 2981-2990.

Hsieh, S.S., Lehr, J.R., 1985. Beneficiation of dolomite Idaho phosphate rock by the TVA diphosphonic depressant process. Mineral and Metallurgical Processing 2, 10-13.

Ince, D., Johnston, C., Moudgil, B., 1991. Fourier transform infrared spectroscopic study of adsorption of oleic acid/oleate on surfaces of apatite and dolomite. Langmuir 7 (7), 1453-1457.

Ince, D.E., 1987. Effect of sodium chloride on the selective flotation of dolomite from apatite. Ph.D. Dissertation, Gainesville, University of Florida.

Izmailova, V.N., Alekseyeva, I.G., Tulovskaya, Z.D., 1975. Rheological properties of interphase adsorption layers of PVA on liquid boundaries. Polymer Science USSR 17 (9), 2422-2428.

Jho, C., Burke, R., 1983. Drop weight technique for the measurement of dynamic surface tension. Journal of Colloids and Interface Sciences 95 (1), 61-71.

Johnson, D.O., Stebe, K.J., 1996. An oscillating bubble technique to determine surfactant mass transfer kinetics. Colloids and Surfaces A: Physicochemical and Engineering Aspects 114, 41-51.

Kelvin, L., 1871. Physics Magazine 42, 368.

Kim, I.T., Luckham, J.P., 1991. The viscoelastic properties of polystyrene latex-particles bearing an adsorbed layer of poly (vinyl alcohol). Journal of Colloids and Interface Sciences 144 (1), 174-184.

Kiselev, A.V., Rygin, V.I., 1972. Infrared spectra of surface compounds. John Wiley, New York.

Koopal, L., Hlady, V., Lyklema, J., 1988. Electrophoretic study of polymer adsorption: Dextrin, polyethylene oxide and polyvinyl alcohol on silver iodide. Journal of Colloids and Interface Science 121 (1), 49-62.

Koopal, L., Lyklema, J., 1979. Characterization of adsorbed polymers from double layer experiments: The effect of acetate groups in polyvinyl alcohol on its adsorption on silver iodide. Journal of Electroanalytical Chemistry 100, 895-912.

Lawendy, T.A., 1993. Flotation of dolomitic and calcareous phosphate ores. Engineering Foundation Conference. Beneficiation of Phosphate: Theory and Practice, Dec 5-10, Palm Coast, Florida, Chapter 5, 60-72.

Lawver, L.E., Snow, R.E., 1980. Method of beneficiating phosphate ores. U.S. Patent 4,189,103.

Liewellyn, T.D.,1982. Beneficiation of high-magnesium phosphate from southern Florida. RI 8609, United States Bureau of Mines.

Lipatov, Y., Sergeeva, L., 1974. Adsorption of polymers. Halsted Press, John Wiley and Sons Inc., New York.

Lloyd, T.B., 1994. Experimental procedures to characterize acid-base and dispersion force contributions to solid wettability: A Review. Colloids and Surfaces 93, 25-37.

Luckham, P., Vincent, B., Tadros, Th., 1983. The controlled flocculation of particulate dispersions using small particles of opposite charge. IV. Effect of surface coverage of adsorbed polymer on heteroflocculation. Colloids and Surfaces 6 (2), 119-133.

Lund, K., Fogler, H., McCune, C., 1973. Acidization-I: The dissolution of dolomite in hydrochloric acid. Chemical Engineering Science 28, 691-700.

Lunkenheimer, K. Winsel, K., Fruhner, H., Fang, J., Wantke, K.-D., Siegler K., 1996. Dynamic surface tension and surface area elasticity of adsorbed pulmonary surfactant layers. Colloids and Surfaces A: Physicochemical and Engineering Aspects 114, 199-210.

Macleod, C., Radke, C., 1993. A growing drop technique for measuring dynamic interfacial tension. Journal of Colloids and Interface Sciences 160 (2), 435-448.

Mathur, S., Moudgil, B., 1997. Adsorption mechanism(s) of poly(ethylene oxide) on oxide surfaces. Journal of Colloid and Interface Science 196, 92-98.

Miller, R., Sedev, R., Schano, K., Neuman, A., 1993. Relaxation of adsorption layers at solution/air interfaces using axisymmetric drop-shape analysis. Colloids and Surfaces 69 (4), 209-216.

Moudgil, B.M., 1988. Separation of dolomite from the south Florida phosphate rock. University of Florida, FIPR report No. 02-023-066.

Moudgil, B., Prakash, T.S., 1998. Competitive adsorption of polymer and surfactants on solid substrates. Colloids and Surfaces 133, 93-97.

M'pandou, A., Siffert, B., 1987. Polyethyleneglycol adsorption at TiO_2-H_2O interface: Distortion of ionic structure and shear plane position. Colloids and Surfaces 24, 159-172.

M'pandou, A., Siffert, B., 1984. Sodium carboxylate adsorption onto TiO_2: Shortest chain length allowing hemimicelle formation and shear plane position in the electric double layer. Journal of Colloids and Interface Science 102 (1), 138-145.

Mysels, K, 1986. Improvements in the maximum-bubble-pressure method of measuring surface tension. Langmuir 2 (4), 428-432.

Nahringbauer, I, 1995. Dynamic surface tension of aqueous polymer solutions, I: Ethyl (hydroxyethyl) cellulose (BERMOCOLL cst-103). Journal of Colloid and Interface Science 176**,** 318–328.

Ottewill, R., 1967. Nonionic surfactant. In Martin J.Schick (Ed.), Marcel Dekker, New York, 1, 627-682.

Ozacar, M., 2003. Equilibrium and kinetic modeling of adsorption of phosphorus on calcined alunite. Adsorption 9, 125-132.

Paradip, Moudgil, B., 1991. Selective flocculation of tribasic calcium phosphate from mixtures with quartz using polyacrylic acid flocculant. International Journal of Mineral Processing 32 (3-4), 271-281.

Pefferkorn, E., Carroy, A., Varoqui, R., 1985. Adsorption of polyacrylamide on solid surfaces: Kinetics of the establishment of adsorption equilibrium. Macromolecules 18, 2252-2258.

Pikhitsa, P., Tsargorodskaya, A., 2000. Possible mechanism for multistage coalescence of a floating droplet on the air/liquid interface. Colloids and Surfaces A: Physicochemical and Engineering Aspects 167 (3), 287-291.

Platonov, B., Baran, A., Polischuk T., 1979. Acta Physica Chemica 25, 201.

Pugh, R., Stenius, P., 1985. Solution chemistry studies and flotation of apatite, calcite and fluorite minerals with oleate collector. International Journal of Mineral Processing 15, 193-218.

Rachas, I., Tadros, Th.F., Taylor, P., 2000. The displacement of adsorbed polymer from silica surfaces by the addition of a nonionic surfactant. Colloids and Surfaces A: Physicochemical and Engineering Aspects 161, 307-319.

Rao, D.V., 1979. Flotation of low-grade phosphate ore. International Symposium on Resources Engineering and Technology, Jan 8-11, 1-7.

Rao, D.V., 1985. Flotation of calcareous Mussori phosphate ore. International Journal of Mineral Processing 14 (1), 57-66.

Rao H.K., 1989. Flotation of phosphatic material containing carbonatic gangue using sodium oleate as collector and sodium silicates modifier. International Journal of Mineral Processing 26, 123-140.

Rao, H.K., 1988. Mechanism of oleate interaction on salt type minerals, I-Adsorption and electrokinetic studies of calcite in presence of sodium oleate and sodium metasilicate. Colloids and Surfaces 34, 227-239.

Ross, J., Bruce, W., Janna, W., 1992. Surface tension measurements of benzyl benzoate using the Sugden maximum bubble pressure method. Langmuir 8 (11), 2644-2648.

Rubio, J., Kitchener, J.A., 1976. The mechanism of adsorption of poly(ethylene oxide) flocculant on silica. Journal of Colloids and Interface Science 57 (1), 132-142.

Rule, A.R., 1970. Removal of magnesium impurities from phosphate rock concentrates. RI 7362, United States Bureau of Mines.

Rule, A.R., 1982. Application of carbonate-silica flotation techniques to Western phosphate materials. RI 8728, United States Bureau of Mines.

Rule, A.R.,1985. Beneficiation of complex phosphate ores containing carbonate and silica gangue. XV International Mineral Processing Conference proceedings 3, 380-389.

Santhiya, D., Subramanian, S., Natarajan, K.A., Malghan S.G., 1999. Mineral and Metallurgical Processing 16, 51.

Santhiya, D., Subramanian, S., Natarajan, K.A., Malghan S.G., 1999. Surface chemical studies on the competitive adsorption of poly(acrylic acid) and poly(vinyl alcohol) onto alumina. Journal of Colloid and Interface Science 216 (1), 143-153.

Santhiya, D., Nandini, G., Subramanian, S., Natarajan, K., Malghan, S., 1998. Surface chemical studies on the competitive adsorption of PAA and PVA onto alumina. Colloid and Surfaces 133, 157.

Sjöberg, M., Bergström, L., Larsson, A., Sjöström, E., 1999. The effect of polymer and surfactant adsorption on the colloidal stability and rheology of kaolin dispersions. Colloids and Surfaces A: Physicochemical and Engineering Aspects 159 (1), 197-208.

Sjoberg, E.L., Rickard, D.T., 1984, Calcite dissolution kinetics: surface speciation and the origin of the variable pH dependence. Chemical Geology 42, 119-136.

Sjoberg, E.L., 1978. Kinetics and mechanism of calcite dissolution in aqueous solutions at low temperatures. Stockholm Contribution in Geology 32, 1-96.

Smani, S. M., 1973. Beneficiation of sedimentary Moroccan phosphate ore: Part 4 depression of phosphate oolites and calcite flotation. Transactions of American Institute of Mining, Metallurgical, and Petroleum Engineers 258, 181-182.

Smani, S. M., Cases, J.M., Blazy, P., 1975. Beneficiation of sedimentary Moroccan phosphate ore: Part 3 selective flotation and recovery. Transactions of American Institute of Mining, Metallurgical, and Petroleum Engineers 258, 176-180.

Snow, R.E., 1979. Beneficiation of phosphate ore. U.S.Patent 4,144,969.

Snow, R.E., 1982. Flotation of phosphate ore containing dolomite. U.S.Patent 4,364,824.

Somasundaran, P., Ramachandran, R., 1988. Innovative approaches to elucidate floc structure and polymer conformations at interfaces. B.M.Moudgil and B.J.Scheiner, Eds., Engineering Foundation Conference, Palm Coast, Florida.

Stark, G., Wallace, H., 1982. Chemistry Data Book. 2nd ed., John Murray, London.

Sun, S. F., 1994. Physical chemistry of macromolecules: Basic principles and issues. John Wiley and Sons, Inc., New York, 469 p.

Tadros, Th.F., 1978. Adsorption of polyvinyl alcohol on silica at various ph values and its effect on the flocculation of the dispersion. Journal of Colloids and Interface Science 64 (1), 36-47.

Tamura, T., Kaneko, Y., Ohyama, M., 1995. Dynamic surface tension and foaming properties of aqueous polyoxyethylene *n*-dodecyl ether solutions**.** Journal of Colloids and Interface Sciences, 173 (2), 493-499.

Thomas, W., Hall, D., 1975. Solution/air interfaces. II. Adsorption of surfactants in dilute aqueous solutions. Anomalous oscillating jet phenomena. Journal of Colloids and Interface Sciences 51 (2), 328-332.

Wiegel, R.L., Hwang,C.L., 1984. A predictive model for heavy media cyclone separation of phosphate pebble from dolomite. Society of Mining Engineers - American Institute of Mining, Metallurgical, and Petroleum Engineers Meeting, preprint # 84-648.

Xiao, L., Somasundaran, P., 1989. Interaction between oleate collector and Alizarin modifier in dolomite / francolite flotation system. Minerals and Metallurgical Processing 5, 100-103.

Zaman, A., Tsuchiya, R., Moudgil, B., 2002. Adsorption of a low-molecular-weight polyacrylic acid on silica, alumina, and kaolin. Journal of Colloid and Interface Science 256 (1), 73-78.

Zeno, E., Beneventi, D., Carré, B., 2004. Interactions between poly(ethylene oxide) and fatty acids sodium salts studied by surface tension measurements. Journal of Colloid and Interface Science 277 (1), 215-220.

Zhang, Y., Suga, T., Kawasaki, M., Xiao-Xia, T., Uchida, N., Uematsu, K., 1996. Effect of poly(vinyl alcohol) adsorption on binder segregation during drying. Journal of American Ceramic Society 79 (2)**,** 435.

BIOGRAPHICAL SKETCH

Ayman El-Midany was born in Cairo, Egypt, in February 1969. He attended the College of Engineering at Cairo University from 1986 to 1991. He completed a bachelor's degree in mining engineering in 1991. In 1992, he enrolled for graduate studies in mining engineering at Cairo University. He completed master's degree in May 1997. He Joined Central Metallurgical Research and Development Institute (CMRDI), Cairo, Egypt, as researcher assistant in 1993. In 2001, he came to the University of Florida to pursue a Ph.D degree in materials science and engineering. He worked with Professor Hassan El-Shall as a research assistant and performed research on minerals separation and particle science technology.